3 1176 00163 9740

NASA-CR-162795

NASA-CR-162795
19800009793

The Deep Space Network Progress Report 42-55

November and December 1979

FEB 26 1980

February 15, 1980

National Aeronautics and
Space Administration

Jet Propulsion Laboratory
California Institute of Technology
Pasadena, California

NF02045

The Deep Space Network Progress Report 42-55

November and December 1979

February 15, 1980

National Aeronautics and
Space Administration

Jet Propulsion Laboratory
California Institute of Technology
Pasadena, California

80N18058 #

The research described in this publication was carried out by the Jet Propulsion Laboratory, California Institute of Technology, under NASA Contract No NAS7-100

Preface

This report presents DSN progress in flight project support, tracking and data acquisition (TDA) research and technology, network engineering, hardware and software implementation, and operations Each issue presents material in some, but not all, of the following categories in the order indicated

Description of the DSN

Mission Support
- Ongoing Planetary/Interplanetary Flight Projects
- Advanced Flight Projects

Radio Astronomy

Special Projects

Supporting Research and Technology
- Tracking and Ground-Based Navigation
- Communications-Spacecraft/Ground
- Station Control and Operations Technology
- Network Control and Data Processing

Network and Facility Engineering and Implementation
- Network
- Network Operations Control Center
- Ground Communications
- Deep Space Stations
- Quality Assurance

Operations
- Network Operations
- Network Operations Control Center
- Ground Communications
- Deep Space Stations

Program Planning
- TDA Planning

In each issue, the part entitled "Description of the DSN" describes the functions and facilities of the DSN and may report the current configuration of one of the seven DSN systems (Tracking, Telemetry, Command, Monitor & Control, Test & Training, Radio Science, and Very Long Baseline Interferometry)

The work described in this report series is either performed or managed by the Tracking and Data Acquisition organization of JPL for NASA

This Page Intentionally Left Blank

Contents

Communications—Spacecraft/Ground

Network Control and Data Processing

NETWORK AND FACILITY ENGINEERING AND IMPLEMENTATION

Network

Ground Communications

OPERATIONS

Network Operations

PROGRAM PLANNING

TDA Planning

Network Functions and Facilities

N A Renzetti
Office of Tracking and Data Acquisition

The objectives, functions, and organization of the Deep Space Network are summarized, deep space station, ground communication, and network operations control capabilities are described

The Deep Space Network was established by the National Aeronautics and Space Administration (NASA) Office of Space Tracking and Data Systems and is under the system management and technical direction of the Jet Propulsion Laboratory (JPL) The network is designed for two-way communications with unmanned spacecraft traveling approximately 16,000 km (10,000 miles) from Earth to the farthest planets and to the edge of our solar system It has provided tracking and data acquisition support for the following NASA deep space exploration projects Ranger, Surveyor, Mariner Venus 1962, Mariner Mars 1964, Mariner Venus 1967, Mariner Mars 1969, Mariner Mars 1971, and Mariner Venus-Mercury 1973, for which JPL has been responsible for the project management, the development of the spacecraft, and the conduct of mission operations, Lunar Orbiter, for which the Langley Research Center carried out the project management, spacecraft development, and conduct of mission operations, Pioneer, for which Ames Research Center carried out the project management, spacecraft development, and conduct of mission operations, and Apollo, for which the Lyndon B Johnson Space Center was the project center and the Deep Space Network supplemented the Manned Space Flight Network, which was managed by the Goddard Space Flight Center The network is currently providing tracking and data acquisition support for Helios, a joint U S /West German project, Viking, for which Langley Research Center provided the Lander spacecraft and project management until May, 1978, at which time project management and mission operations were transferred to JPL, and for which JPL provided the Orbiter spacecraft, Voyager, for which JPL provides project management, spacecraft development, and is conducting mission operations, and Pioneers, for which the Ames Research Center provides project management, spacecraft development, and conduct of mission operations The network is adding new capability to meet the requirements of the Galileo mission to Jupiter, for which JPL is providing the Orbiter spacecraft, and

the Ames Research Center the probe In addition, JPL will carry out the project management and the conduct of mission operations

The Deep Space Network (DSN) is one of two NASA networks The other, the Spaceflight Tracking and Data Network (STDN), is under the system management and technical direction of the Goddard Space Flight Center (GSFC) Its function is to support manned and unmanned Earth-orbiting satellites The Deep Space Network supports lunar, planetary, and interplanetary flight projects

From its inception, NASA has had the objective of conducting scientific investigations throughout the solar system It was recognized that in order to meet this objective, significant supporting research and advanced technology development must be conducted in order to provide deep space telecommunications for science data return in a cost effective manner Therefore, the Network is continually evolved to keep pace with the state of the art of telecommunications and data handling It was also recognized early that close coordination would be needed between the requirements of the flight projects for data return and the capabilities needed in the Network This close collaboration was effected by the appointment of a Tracking and Data Systems Manager as part of the flight project team from the initiation of the project to the end of the mission By this process, requirements were identified early enough to provide funding and implementation in time for use by the flight project in its flight phase

As of July 1972, NASA undertook a change in the interface between the Network and the flight projects Prior to that time, since 1 January 1964, in addition to consisting of the Deep Space Stations and the Ground Communications Facility, the Network had also included the mission control and computing facilities and provided the equipment in the mission support areas for the conduct of mission operations The latter facilities were housed in a building at JPL known as the Space Flight Operations Facility (SFOF) The interface change was to accommodate a hardware interface between the support of the network operations control functions and those of the mission control and computing functions This resulted in the flight projects assuming the cognizance of the large general-purpose digital computers which were used for both network processing and mission data processing They also assumed cognizance of all of the equipment in the flight operations facility for display and communications necessary for the conduct of mission operations The Network then undertook the development of hardware and computer software necessary to do its network operations control and monitor functions in separate computers A characteristic of the new interface is that the Network provides direct data flow to and from the stations, namely, metric data, science and engineering telemetry, and such network monitor data as are useful to the flight project This is done via appropriate ground communication equipment to mission operations centers, wherever they may be

The principal deliveries to the users of the Network are carried out by data system configurations as follows

(1) The DSN Tracking System generates radio metric data, i e , angles, one- and two-way doppler and range, and transmits raw data to Mission Control

(2) The DSN Telemetry System receives, decodes, records, and retransmits engineering and scientific data generated in the spacecraft to Mission Control

(3) The DSN Command System accepts spacecraft commands from Mission Control and transmits the commands via the Ground Communications Facility to a Deep Space Station The commands are then radiated to the spacecraft in order to initiate spacecraft functions in flight

(4) The DSN Radio Science System generates radio science data, i e , the frequency and amplitude of spacecraft transmitted signals affected by passage through media such as the solar corona, planetary atmospheres, and planetary rings, and transmits these data to Mission Control

(5) The DSN Very Long Baseline Interferometry System generates time and frequency data to synchronize the clocks among the three Deep Space Communications complexes It will generate universal time and polar motion and relative Deep Space Station locations as by-products of the primary data delivery function

The data system configurations supporting testing, training, and network operations control functions are as follows

(1) The DSN Monitor and Control System instruments, transmits, records, and displays those parameters of the DSN necessary to verify configuration and validate the Network It provides the tools necessary for Network Operations personnel to control and monitor the Network and interface with flight project mission control personnel

(2) The DSN Test and Training System generates and controls simulated data to support development, test, training and fault isolation within the DSN It participates in mission simulation with flight projects

The capabilities needed to carry out the above functions have evolved in the following technical areas

(1) The Deep Space Stations, which are distributed around Earth and which, prior to 1964, formed part of the Deep Space Instrumentation Facility The technology involved in equipping these stations is strongly related to the state of the art of telecommunications and flight-ground design considerations, and is almost completely multimission in character

(2) The Ground Communications Facility provides the capability required for the transmission, reception, and monitoring of Earth-based, point-to-point communications between the stations and the Network Operations Control Center at JPL, Pasadena, and to the JPL Mission Operations Centers Four communications disciplines are provided teletype, voice, high-speed, and wideband The Ground Communications Facility uses the capabilities provided by common carriers throughout the world, engineered into an integrated system by Goddard Space Flight Center, and controlled from the communications Center located in the Space Flight Operations Facility (Building 230) at JPL

The Network Operations Control Center is the functional entity for centralized operational control of the Network and interfaces with the users It has two separable functional elements, namely, Network Operations Control and Network Data Processing The functions of the Network Operations Control are

(1) Control and coordination of Network support to meet commitments to Network users

(2) Utilization of the Network data processing computing capability to generate all standards and limits required for Network operations

(3) Utilization of Network data processing computing capability to analyze and validate the performance of all Network systems

The personnel who carry out the above functions are located in the Space Flight Operations Facility, where mission operations functions are carried out by certain flight projects Network personnel are directed by an Operations Control Chief The functions of the Network Data Processing are

(1) Processing of data used by Network Operations Control for control and analysis of the Network

(2) Display in the Network Operations Control Area of data processed in the Network Data Processing Area

(3) Interface with communications circuits for input to and output from the Network Data Processing Area

(4) Data logging and production of the intermediate data records

The personnel who carry out these functions are located approximately 200 meters from the Space Flight Operations Facility The equipment consists of minicomputers for real-time data system monitoring, two XDS Sigma 5s, display, magnetic tape recorders, and appropriate interface equipment with the ground data communications

Viking Orbiter Completion Mission

R L Gillette
Deep Space Network Operations Section

This report covers Viking Spacecraft activities from 1 April 1979 through 30 November 1979 and continues reporting on DSN Viking Tracking support for the same period

I. Viking Operation

A. Orbiters

The Viking Orbiter 1 (VO-1) spacecraft continued to operate normally during this reporting period, collecting and returning to Earth weather data and high-resolution Mars surface photos, as well as relaying to Earth data from the Lander 2 (VL-2) spacecraft Approximately 300 Mars photos a week have been returned to Earth during this reporting period The Viking Orbiter 2 (VO-2) spacecraft ceased operation on 25 July 1978

B. Landers

The Viking Landers also continued to operate as expected during this reporting period All Lander 1 essential subsystems are healthy as the spacecraft collects imaging and meteorology data for weekly transmission to Earth whenever a Deep Space Station (DSS) is available All Lander 2 essential subsystems are healthy, except for the transmitter which supports transmission of telemetry data directly to Earth All data from Lander 2 are transmitted to Orbiter-1 and then relayed to Earth using the Orbiter transmitter

II. Viking Orbiter Completion Mission

On 6 November 1979, a Viking Mars Orbit Trim Maneuver (MOT-20) officially terminated the Viking Survey Mission and moved the Viking Project into a new phase of the Viking Mission termed the Viking Orbiter Completion Mission The Viking Orbiter Completion Mission (VOCM) is the fifth phase of the Viking Mission following the primary mission (terminated 15 November 1976), the Extended Mission (terminated 31 May 1978), the Continuation Mission (terminated 25 March 1979) and the Viking Survey Mission (terminated this reporting period, 6 November 1979) The Orbiter operations in the Completion Mission are currently scheduled to terminate on 1 February 1980 However, a proposal is currently being worked between the Viking Project and NASA to continue support until the Orbiter runs out of attitude control gas sometime in late 1980

The objective of the Orbiter Completion Mission is to obtain moderate resolution photographic coverage of Martian surface areas not previously photographed or inadequately covered during the survey mission

III. Viking Lander Monitor Mission

On 6 November 1979, along with the start of the Orbiter Completion Mission, the Lander 1 Spacecraft became a separate mission of its own, termed the Lander Monitor Mission (LMM) The objectives of the Lander Monitor Mission are to obtain S-band Ranging data from the surface of Mars periodically over a long time span for the conduct of Radio

Science and to obtain meteorology and imaging data from the surface of Mars periodically over a long time span to monitor and disseminate information relative to any significant changes with time

Throughout the Lander Monitor Mission, the Lander 1 Spacecraft will be in an automatic-mission mode, operating autonomously on the programs that have previously been stored in the on-board computers Lander-1 will be repointing its high-gain antenna and acquiring and storing imaging meteorology and engineering data frequently and will be ready to transmit these data to Earth every 7 or 8 days in response to a series of commands transmitted from a Deep Space Station The Viking Lander 1 Spacecraft should be capable of returning Mars data up through 1990

IV. Radio Science

The opportunity has arisen to make new radio occultation measurements of Mars with Viking Orbiter 1 during the Viking Completion Mission Geometrically, the spacecraft as viewed from Earth is occulted by Mars every 24 hours for about 23 minutes Acquisition of data from occultation events in November and December will provide new information on seasonal atmospheric fluctuations at the 5 km level, the correlation of ionospheric plasma temperature with solar activity, and improved characterization of several Martian topographic features

During the period April 1979 through October 1979, the only Radio Science activity has been the near-simultaneous Lander-Orbiter Ranging Experiment

V. Network Support

Table 1 shows the DSN tracking support for the Viking Mission from April 1979 through November 1979 Tracking support started increasing in July, as expected, with the resumption of science acquisition activity on the Orbiter 1 Spacecraft Prior to July, because of pressure from Voyager and Pioneer for Network support, Orbiter 1 was placed in a housekeeping mode with all science instruments powered off at the end of the continuation Mission (25 March 1979) Since August, there has been a continual decrease in the requirements for tracking support This is due to the reduction in overall tracking time required to return science data to Earth at the higher telemetry data rates made possible as Mars approaches opposition on 26 February 1980

References

1 Gillette, R L, "Viking Extended Mission Support", in *The Deep Space Network Progress Report 42-46*, pp 29-32, Jet Propulsion Laboratory, Pasadena, California, August 15, 1978

2 Gillette, R L, "Viking Extended Mission Support", in *The Deep Space Network Progress Report 42-47*, pp 15-20, Jet Propulsion Laboratory, Pasadena, California, October 15, 1978

3 Gillette, R L, "Viking Continuation Mission Support", in *The Deep Space Network Progress Report 42-48*, pp 7-11, Jet Propulsion Laboratory, Pasadena, California, December 15, 1978

4 Gillette, R L, "Viking Continuation Mission Support", in *The Deep Space Network Progress Report 42-51*, pp 14-18, Jet Propulsion Laboratory, Pasadena, California, June 15, 1979

Table 1 DSN Viking Mission tracking support

DSS	1979							
	Apr	May	Jun	Jul	Aug	Sep	Oct	Nov
11	2[a] / 14[b]	4 / 31	2 / 11	3 / 17	–	1 / 6	1 / 3	2 / 11
12	2 / 6	2 / 5	2 / 13	1 / 3	–	–	–	–
14	–	–	–	6 / 33	22 / 91	15 / 65	12 / 62	8 / 64
42	5 / 19	4 / 20	2 / 10	–	1 / 5	2 / 10	–	–
43	6 / 31	–	–	6 / 40	1 / 5	1 / 1	1 / 6	–
44	–	1 / 4	–	1 / 3	4 / 18	–	3 / 12	–
61	–	3 / 10	1 / 4	1 / 4	–	–	–	–
62	1 / 6	–	–	–	2 / 2	1 / 4	–	–
63	1 / 5	2 / 12	1 / 10	13 / 50	29 / 131	27 / 105	19 / 104	15 / 119
Total	17 / 81	16 / 82	8 / 48	31 / 150	59 / 252	47 / 191	36 / 187	25 / 194

[a]Number of tracks, the summation of all Viking spacecraft tracked
[b]Track time scheduled station support in hours

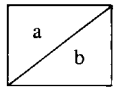

Pioneer Mission Support

G M Rockwell
Deep Space Network Operations Section

This article reports on activities of DSN Operations in support of Pioneers 6 through 11 and Pioneer-Venus (Pioneer 12) for the period October 15 through December 15, 1979

I. Introduction

This article reports on the continuing Deep Space Network support of Pioneer Mission Operations Included in this article is information on the cruise phases of Pioneers 6-9, Pioneer 10, post-encounter coverage of Pioneer 11, Pioneer 12 orbital operations, and other mission-related activities

II. Mission Operations and Status

A. Pioneers 6 through 9

During this period, all Pioneer spacecraft 6 through 9 appear to be healthy and functioning nominally Only Pioneer 9 was tracked during this period over DSS 14 (Goldstone, California) See Table 1 for tracking time A Pioneer 8 track was scheduled, but was cancelled because the required 100-kW transmitter (64-meter station) was not available during the scheduled track time

B. Pioneer 10

The Pioneer 10 spacecraft continues on its course out of the solar system at an asymptote of 2 9 degrees above the ecliptic All onboard systems are functioning nominally The round-trip light time for Pioneer 10 at this time is approximately 5 hours, 24 minutes That would put Pioneer 10's distance from Earth at 2,908,900,000 kilometers (1,807,900,000 miles) Tracking time for September and October is shown in Table 1

C. Pioneer 11

Following its Saturn encounter, the Pioneer 11 spacecraft began its trek out of the ecliptic at an asymptote four times greater than that of Pioneer 10 (12 6 degrees) and in the opposite direction of its sister ship As is the case with Pioneer 10, all systems aboard Pioneer 11 are performing nominally Table 1 shows total tracking time for September and October

D. Pioneer 12

In order to not interfere with Pioneer 11 Saturn Encounter Operations, the Pioneer-Venus Orbiter (Pioneer 12) was configured for a minimum support activity period from 19 August to 8 September 1979 Following this period, normal orbital operations did commence and Radio Science data gathering was reinstituted All occultation and periapsis activities have occurred over the Australian facilities during this reporting period These activities are discussed later in this article

On 11 October, a successful Static Phase Error (SPE) test was performed on the spacecraft's receiver 2, clearing up some doubt as to its condition

Also, during this period, a high-gain antenna (HGA) calibration was successfully performed on 17 October, over DSS 63 (Madrid, Spain) The overall tracking time for Pioneer 12 is shown in Table 1

III. Special Activities

Following Pioneer 11's Saturn Encounter, the DSN began to support the occultation activity of Pioneer 12 again on 9 September This began with 26-meter coverage at DSS 44 (Australia), and 64-meter coverage was reestablished on 5 October over DSS 43 (Australia)

There are three ongoing Radio Science Occultation Experiments

(1) Radio Science Occultation I

(2) Radio Science Corona Turbulence

(3) Radio Science Occultation II

All three were discussed in detail in Reference 1

The last hard occultation occurred on 9 December 1979, but data collection in support of Radio Science requirements will continue until 27 December 1979 The next period of hard occultation will begin in 1980

IV. Summary

At this writing, all Pioneer Spacecraft appear to be in a healthy state with no apparent problems that would hinder nominal operations The period of this report found all Pioneer Spacecraft in a cruise mode, with the exception of Pioneer 12's orbital activity Therefore, no real significant events have occurred outside of normal operational support

Reference

1 Howe, T W, "Pioneer-Venus 1978 Mission Support," in *The Deep Space Network Progress Report 42-51*, pp 19-30, Jet Propulsion Laboratory, Pasadena, California, June 15, 1979

Table 1 Pioneer tracking coverage

Month	Pioneer	Station type	Number of tracks	Tracking time (hour min)
September	6-9	26/34 m	0	00 00
		64 m	(PN 9) 1	03 00
	10	26/34 m	12	48 30
		64 m	51	235 41
	11	26/34 m	21	182 17
		64 m	90	749 35
	12	26/34 m	47	345 49
		64 m	13	48 03
October	6-9	26/34 m	0	00 00
		64 m		00 00
	10	26/34 m	13	60 35
		64 m	48	290 02
	11	26/34 m	36	242 14
		64 m	7	44 32
	12	26/34 m	35	225 07
		64 m	65	523 48

Radio Astronomy

R M Taylor
Deep Space Operations Section

This article reports on the activities of the Deep Space Network in support of Radio Astronomy operations during the period September 1979 to December 1979

I. Introduction

The Deep Space Network 26 meter diameter and 64 meter diameter antennas are used to support experiments in Radio Astronomy

II. Radio Astronomy Operations

During the period of this report, support for radio astronomy operations increased somewhat even though two 26 meter stations, one in Spain and one in Australia, were taken out of service for upgrading to 34 meters and the addition of X-band downlink capability

A. Support for NASA-Office of Space Sciences Activities

Support for activities in this category continued at previous levels except for the Southern Hemisphere Interferometer experiment which requires two stations in Canberra, Australia One of the two stations is temporarily not available due to the upgrade work mentioned above

Pulsar Rotation Constancy observations continue and the latest version of the timing and recording software from Spain is enroute to the Jet Propulsion Laboratory for pre-operational testing at Goldstone, California

Planetary Radio Astronomy activities during this period included observations of Jupiter, Uranus, and the Saturn rings

Microwave Spectroscopy activity recently picked up with five observations, producing a total of 37 hours support from the 64 meter antenna at Goldstone during December

B. Support for Radio Astronomy Experiment Selection Activities

The Radio Astronomy Experiment Selection Panel (RAES) is now chaired by Dr David S DeYoung, replacing Dr Burbridge who resigned recently Dr DeYoung, a scientist with the National Radio Astronomy Observatory, is involved in research into the origin and evolution of extended extragalactic radio sources, physics of galactic nuclei and quasi-stellar objects, evolution of dense stellar systems, solar flares, and interplanetary disturbances The other panel members are Dr Bernard F Burke of the Massachusetts Institute of Technology, Dr W C Erickson of the University of Maryland, Dr Yervant Terzian of Cornell University, Dr Barry Turner of the National Radio Astronomy Observatory, Dr Marshall H Cohen of the California Institute of Technology, and Dr Richard M Goldstein of the Jet Propulsion Laboratory

Currently, twelve experiments have been approved by the RAES Panel All of these experiments require the use of the

64 meter antennas plus the hydrogen maser frequency and timing subsystem The one exception to this is the Quasar Patrol experiment which can on occasion use a 26 meter antenna when the 64 meter antenna is not available

Two experiments were supported during this period

RA 175 This experiment uses the Very Long Baseline Interferometry capability of the Deep Space Network in conjunction with other non-NASA telescopes to observe the galactic object 1909+04, popularly known as SS433

RA 176 The 64 meter diameter antennas in Goldstone and Spain provided nineteen hours each of support to this experiment observing the "twin" quasi-stellar objects, 0957+561 A, B The object of the observations, conducted simultaneously with non-NASA telescopes in Europe and the U S A , is to test the current "gravitational lens" theory about the source

These observations were not successful due to an error in precessed predicts generation and further support has been requested

The early support of RA 175 by the 26 meter antenna at Goldstone and the 64 meter antennas at Goldstone, Spain and Australia resulted in the reduction of support requirements for the monitor phase – only the 26 meter at Goldstone is required for that phase

C. Support of Host Country Activities

1 Australia During this period, host country activity in Australia has been almost exclusively Pulsar observations by the 26 meter station in Canberra These observations are currently being supported at the rate of approximately 10 hours per week

2 Spain In Spain the very long baseline interferometry development activity was supported by both the 26 meter and the 64 meter antennas

Practical Limitations on Noiseless Optical Channel Capacity

S A Butman, J Katz, and J R Lesh
Communications Systems Research Section

Even in noiseless optical channels one must take into account the fact that the time resolution available is finite An optimization scheme under the constraint of a given information rate (in nats/second) and minimum time slot resolution is presented It is shown that system efficiencies in excess of 10's of nats/photon will be extremely difficult to achieve due to fundamental time resolution limitations

In a recent paper (Ref 1) some aspects of the optical channel using an ideal binary quantum detector are considered In particular, it was found that using a quantized PPM modulation scheme, for example, the channel capacity in nats/photon approaches infinity in the noiseless case (except for the unavoidable self-noise due to the Poisson statistics of the photons themselves) However, the final units that are relevant for a communication link design are nats/second The purpose of this article is to show that due to physical limitations on the minimum time-resolution one can achieve, for any given capacity in nats/seconds there is an optimum point which maximizes the capacity in terms of nats/photon, thus minimizing the power requirement of the system

Basically there are three types of time resolution bounds The first and ultimate lower bound comes from the quantum mechanical uncertainty principle

$$\Delta E \cdot \Delta T \geqslant h \tag{1}$$

If the photon source is a laser, ΔE corresponds to the laser transition linewidth, i e , $\Delta T \simeq 1/\Delta\nu$ where $\Delta\nu$ is the transition linewidth (largest $\Delta\nu$ observed is about 10^{13}, which corresponds to $\Delta T \sim 0\ 1$ picoseconds) In any case, it doesn't make much sense to consider for a photon of a certain wavelength ($\lambda = 2\pi\ c/\omega$) time scales that are shorter than the reciprocal of its frequency) Thus, we have the bound

$$\Delta T \gtrsim \frac{1}{\omega} \tag{2}$$

It is true that we actually count photoelectrons, not photons, and the arrival times of the former can be determined with practically arbitrary accuracy However, time accuracies higher than the characteristic time scales of the physical processes associated with the photons (which are the actual information carriers) are meaningless

A second, more practical bound comes from technological limitations, either due to the time response of the photon emitter, photodetector, and electronic circuitry or due to computational complexity The third type of limitation comes from the finite bandwidth of the optical filter

$$\Delta T \gtrsim \frac{2}{B_{\text{opt}}} \tag{3}$$

This limit usually lies between the first two mentioned above

Now let us apply these limits to the optical communications problem A model for the channel is shown in Fig 1 We have a Q-ary alphabet where each letter corresponds to a pulse in a particular time slot out of the possible set of Q slots Although not necessarily the obvious choice, this quantized PPM scheme has the advantage of being an orthogonal signaling in a channel without power and bandwidth constraints This is also the scheme suggested in Ref 2

In any case it is clear that the best coding schemes call for concentrating the power in time slots which are as short as possible (i e , performance is improved by increasing the peak to average power ratio) The transition probability is given by

$$\epsilon = e^{-N_s \Delta T} \tag{4}$$

Here N_s is the source intensity (in photons/second) and ΔT is the time slot The capacity of the channel is

$$C_s = \left(1 - e^{-N_s \Delta T}\right) \ln Q \text{ nats/channel use} \tag{5}$$

In terms of nats/second we obtain

$$C_T = \frac{C_s}{T} = \frac{C_s}{Q \Delta T} \text{ nats/second} \tag{6}$$

or equivalently

$$C_T = \frac{1 - e^{-N_s \Delta T}}{\Delta T} \frac{\ln Q}{Q} \text{ nats/second} \tag{7}$$

In terms of nats/photon we obtain

$$C_{\text{ph}} = \frac{C_s}{\text{number of photons per channel use}} = \frac{C_s}{N_s \Delta T} \tag{8}$$

or equivalently

$$C_{\text{ph}} = \frac{1 - e^{-N_s \Delta T}}{N_s \Delta T} \ln Q \text{ nats/photon} \tag{9}$$

We will now calculate the channel performance in terms of nats/photon under constraints of given minimum time slot (ΔT) and fixed channel throughput rate (in nats/second) In this case $N_s = N_s(Q)$

In Fig 2, results of C_{ph} vs Q are shown for throughput rates of 10^4 and 10^6 nats/second Values of ΔT correspond to the uncertainty principle $\Delta T = 10^{-15}$ sec (= $1/\omega$ for $\lambda \simeq 1\ 8$ μm) and for current technological limitations of $\Delta T \simeq 10^{-9}$ sec It is clearly seen that each curve has an optimum operating point which minimizes the energy consumption of the system (i e , a point where C_{ph} is maximum) For example, the $C_T = 10^6$ nats/second point is $Q \simeq 2\ 10^3$ At this point $C_{\text{ph}} \simeq 6\ 5$ nats/photon

Note also that with a huge improvement in ΔT six orders of magnitude (from 10^{-9} seconds to 10^{-15} seconds) we get a much smaller increase (a factor of two to three) in C_{ph} This shows that pushing the technological limits (i e , decreasing ΔT) would not gain very much in terms of C_{ph}

It is important to note that for fixed C_T and ΔT, as we change Q, N_s (transmitter intensity) also changes, as can be seen from Eq (7) For $Q > Q_{\text{opt}}$, N_s approaches infinity Furthermore, the optimum operating point occurs for $Q\Delta T \simeq 10/C_T$ This implies a PPM block interval (needed for computation of peak to average power ratio) of about 10 bits at all C_T's

References

1 Pierce, J R , "Optical Channels – Practical Limits with Photon Counting," *IEEE Trans Comm* , COM-26 (1978), pp 1819-1821

2 Gagliardi, R M and Karp, S , *Optical Communications*, Wiley, New York, 1976

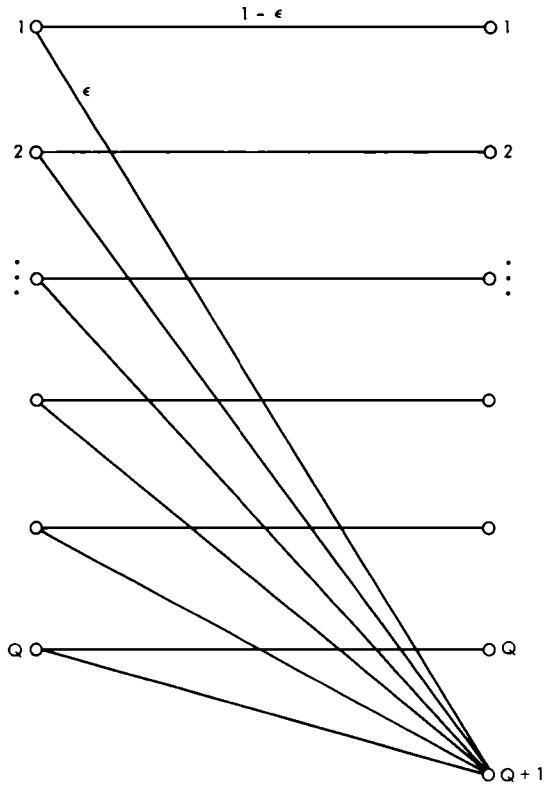

Fig 1 Q-ary PPM channel

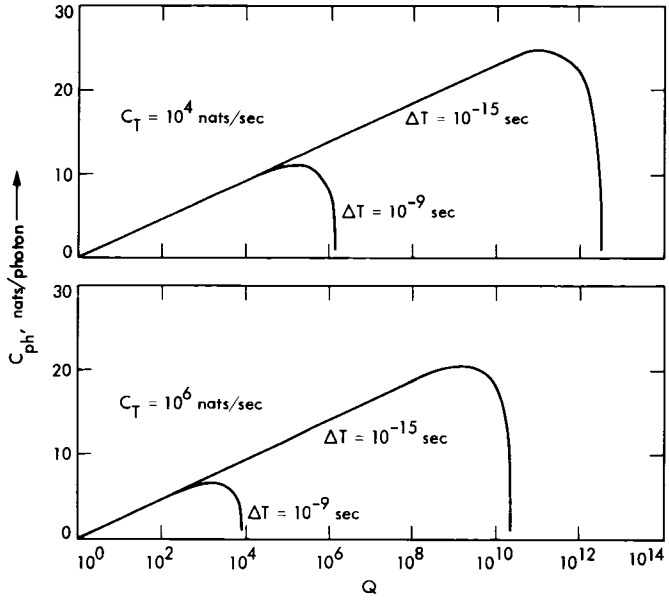

Fig 2 Capacity of noiseless optical channel

Estimating the Angular Position of a Moving Deep Space Vehicle Using Two Rotating Tracking Stations

H H Tan
Communications Systems Research Section

The problem of estimating the angular position of a deep space vehicle moving at a constant velocity using two rotating tracking stations is considered This article reports on an initial phase of analytical studies on the optimal attainable estimation performance and associated receiver design Parametric dependence of the optimum attainable estimation performance is also studied

I. Introduction

Consider the situation in Fig 1 where at a reference time $t = 0$ there is a vehicle at point V and two stations at points S_1 and S_2 relative to Earth geocenter 0 The vehicle is assumed to be at a distance d_0 from the geocenter 0 at time $t = 0$ It is also assumed to be moving at a constant velocity v relative to geocenter 0 for all time in a direction which is at an angle α with respect to OV The stations are both assumed to be rotating at a constant angular velocity ω about 0 At time $t = 0$, station S_1 is at an angle ϵ_0 and the vehicle at an angle γ_0 with respect to a star reference The angle between the stations is denoted by η and the distances of the stations from geocenter by R_1 and R_2, as indicated in Fig 1

We assume that the vehicle is continuously transmitting a signal $s(t)$ Each station receives an additive noise-corrupted version of this transmitted signal The received waveforms from both stations over a given time interval are then used to estimate the unknown vehicle angle γ_0 This article considers this estimation problem based on the assumptions that d_0, v, α, η, ω, and ϵ_0 are known These assumptions are made so that the effect of the rotating stations and the moving target on angular position estimation can be studied Future studies will take into account imprecise knowledge of these parameters

The estimation problem is defined in Section II below along with a discussion of the minimum attainable mean square estimation error performance Since we could not determine the optimal estimator, a suboptimal estimator is derived in Section III The performance of this suboptimal estimator is examined relative to the optimal attainable performance derived in Section II In Section IV we examine the dependence of the optimal attainable performance on angular position, station rotation, station distance from geocenter and observation time duration The specific case of a sinusoidal ranging signal is considered and numerical computations of the optimum attainable angular estimation accuracy are performed for several parameter values Conclusions are given in Section V

II. The Estimation Problem

Let us first derive the equations for the received waveforms at each station The vehicle is assumed to continuously transmit a signal $s(t)$ The received waveform at station S_1 is assumed to be

$$y_1(t) = s[t - \phi_1(t, \gamma_0)] + n_1(t) \tag{1}$$

where $n_1(t)$ is additive white Gaussian noise with power spectral density N_1 and $\phi_1(t, \gamma_0)$ is effectively the signal delay time Similarly, the received waveform at station S_2 is assumed to be

$$y_2(t) = s[t - \phi_2(t, \gamma_0)] + n_2(t) \tag{2}$$

where $n_2(t)$ is additive white Gaussian noise with power spectral density N_2 and $\phi_2(t, \gamma_0)$ is the signal delay time to station S_2 The signal delay times $\phi_1(t, \gamma_0)$ and $\phi_2(t, \gamma_0)$ are both deterministic functions of the unknown vehicle angle γ_0 We assume that γ_0, $n_1(t)$ and $n_2(t)$ are mutually statistically independent In Appendix A, the geometry of Fig 1 is used to derive the following expressions for ϕ_1 and ϕ_2 (c = velocity of light)

$$\begin{aligned}\phi_1(t,\gamma_0) = {} & [1 - (v/c)^2]^{-1} [- (v/c)^2 t - (vd_0 \cos\alpha)/c^2 \\ & + vR_1 \cos(\gamma_0 + \alpha - \epsilon_0 - \omega t)/c^2] \\ & + \{[1 - (v/c)^2]^{-2} [t + (vd_0 \cos\alpha)/c^2 \\ & - vR_1 \cos(\gamma_0 + \alpha - \epsilon_0 - \omega t)/c^2]^2 \\ & + [1 - (v/c)^2]^{-1} [(d_0^2 + R_1^2 - 2R_1 d_0 \cos(\gamma_0 \\ & - \epsilon_0 - \omega t))/c^2 - t^2]\}^{1/2}\end{aligned} \tag{3}$$

$$\begin{aligned}\phi_2(t,\gamma_0) = {} & (1 - (v/c)^2)^{-1} [- (v/c)^2 t - vd_0 \cos\alpha)/c^2 \\ & + VR_2 \cos(\gamma_0 + \alpha \quad \epsilon_0 - \eta - \omega t)/c^2] \\ & + \{(1 - (v/c)^2)^{-2} [t + (vd_0 \cos\alpha)/c^2 \\ & - vR_2 \cos(\gamma_0 + \alpha - \epsilon_0 - \eta - \omega t)/c^2]^2 \\ & + (1 - (v/c)^2)^{-1} [(d_0^2 + R_2^2 - 2R_2 d_0 \cos \\ & - (\gamma_0 - \epsilon_0 - \eta - \omega t))/c^2 - t^2]\}^{1/2}\end{aligned} \tag{4}$$

The receiver's function is to estimate γ_0 based on observations $(y_1(t), y_2(t))$, $- T_1 \leq t \leq T_2$, with a goal of minimizing the mean square estimation error The minimum mean square error (MMSE) estimator is the conditional mean estimator when the prior distribution of γ_0 is known In this case, the conditional mean estimator is nonlinear Moreover, it appears that the problem of determining explicit estimator equations is not tractable An approach to overcome this problem is to derive suboptimum receivers that can be implemented instead In the next section of this paper we consider one method of obtaining a suboptimal receiver by using an extended Kalman filter estimation approach This approach results in a relatively simple receiver structure

It is also of interest to determine the optimum mean square estimation error so that the performance of suboptimal receivers can be evaluated Of course, the minimum attainable mean square estimation error is of interest by itself Unfortunately, it appears in this case that the problem of determining this optimum performance value is also not tractable However, it is possible to obtain lower bounds (Refs 1-3) on the minimum mean square estimation error The Cramer-Rao lower bound (Ref 1, p 275) appears to be the most tractable to use In the case when γ_0 is an unknown but nonrandom parameter, the Cramer-Rao lower bound on the mean square estimation error of any unbiased estimator $\hat{\gamma}_0$ is given by (Ref 1, p 275)

$$E[(\hat{\gamma}_0 - \gamma_0)^2] \geq \left[\sum_{i=1}^{2} (2/N_i) \int_{-T_1}^{T_2} s^2(t - \phi_i(t,\gamma_0)) \left(\frac{\partial \phi_i(t,\gamma_0)}{\partial \gamma_0}\right)^2 dt\right]^{-1} \tag{5}$$

where $s(t) = ds(t)/dt$ In the case when γ_0 is a random parameter with known density $p(\gamma_0)$, the Cramer-Rao lower bound on the mean square estimation error of any estimator $\hat{\gamma}_0$ is given by (Ref 1, p 275)

$$E[(\hat{\gamma}_0 - \gamma_0)^2] \geq \left\{E\left[\left(\sum_{i=1}^{2} (2/N_i) \int_{-T_1}^{T_2} s^2(t - \phi_i(t,\gamma_0)) \left(\frac{\partial \phi_i(t,\gamma_0)}{\partial \gamma_0}\right)^2 dt\right) - \frac{\partial^2 \ln p(\gamma_0)}{\partial \gamma_0^2}\right]\right\}^{-1} \tag{6}$$

where the expectation in the right hand side of Eq (6) is with respect to the prior distribution of γ_0 For a normal γ_0 with variance σ_γ^2, Eq (6) reduces to

$$E[(\hat{\gamma}_0 - \gamma_0)^2]$$

$$\geq \left\{ E\left[\sum_{i=1}^{2} (2/N_i) \int_{-T_1}^{T_2} s^2(t - \phi_i(t,\gamma_0)) \left(\frac{\partial \phi_i(t,\gamma_0)}{\partial \gamma_0} \right)^2 dt + 1/\sigma_\gamma^2 \right] \right\}^{-1} \quad (7)$$

These lower bounds will be used in the remainder of this article to estimate the performance of the suboptimal estimator as well as the optimum theoretically attainable performance

III. The Estimator

Consider the problem of estimating γ_0 in the following equivalent state variable formulation Let $\gamma(t)$ be a variable state satisfying

$$\gamma(t) = 0$$
$$\gamma(-T_1) = \gamma_0 \quad (8)$$

Then $\gamma(t) = \gamma_0$, the parameter to be estimated, for all t Rewrite Eqs (1) and (2) as

$$y(t) = \begin{bmatrix} y_1(t) \\ \\ y_2(t) \end{bmatrix} = \begin{bmatrix} s(t - \phi_1(t,\gamma(t))) + n_1(t) \\ \\ s(t - \phi_2(t,\gamma(t))) + n_2(t) \end{bmatrix} \quad (9)$$

So the equivalent problem is to estimate $\gamma(T_2)$ based on observations of $y(t)$ in the interval $[-T_1, T_2]$

As we noted previously, the problem of determining the MMSE estimator is not tractable An alternative is to derive a suboptimal estimator that approximates the MMSE estimator Another alternative is to abandon the MMSE criterion and to seek estimators based on the maximum likelihood (ML) or maximum a posteriori (MAP) criterion However, it can be shown (Refs 1, 4) that the optimum ML or MAP estimators are also not practically implementable Hence, developing estimators using the ML or MAP criterion will also require consideration of suboptimal estimators Since the ultimate performance measure of interest is still mean square error, it appears more appropriate to seek approximations of the MMSE estimator

There are numerous ways (Refs 4, 5) of determining such suboptimal estimators Our approach will be to adopt one version (Ref 4, p 267) of the extended Kalman filter algorithm This version is the Kalman filter operating on a linearization of the observation equations (9) about the state estimate The reason for adopting this approach over others is its relative simplicity In the nonlinear estimation folklore, the extended Kalman filter is regarded as being capable of performing as well as other suboptimal schemes in most problems So there is a priori no reason to believe that constraining our approach to the extended Kalman filter is overly restrictive

Let $\hat{\gamma}(t)$ denote the extended Kalman filter estimate of $\gamma(t)$ Then a straightforward application of the equations of Ref 4, (p 267) shows that $\hat{\gamma}(t)$ satisfies

$$\frac{d\hat{\gamma}(t)}{dt} = -P(t) \sum_{i=1}^{2} (1/N_i) \left[y_i(t) - s(t - \phi_i(t,\hat{\gamma}(t))) \right] \cdot \left[s(t - \phi_i(t,\hat{\gamma}(t))) \frac{\partial \phi_i(t,\hat{\gamma}(t))}{\partial \hat{\gamma}} \right] \quad (10)$$

$$\frac{dP(t)}{dt} = -P^2(t) \sum_{i=1}^{2} (1/N_i) \left[s(t - \phi_i(t,\hat{\gamma}(t))) \frac{\partial \phi_i(t,\hat{\gamma}(t))}{\partial \hat{\gamma}} \right]^2 \quad (11)$$

with initial conditions

$$\hat{\gamma}(-T_1) = \overline{\gamma}_0 \quad (12)$$

$$P(-T_1) = \sigma_{\gamma_0}^2 \quad (13)$$

where $\overline{\gamma}_0$ and $\sigma_{\gamma_0}^2$ are the prior mean and variance respectively of γ_0 (We shall denote

$$\left. \frac{\partial \phi_i(t,\gamma_0)}{\partial \gamma_0} \right|_{\gamma_0 = \hat{\gamma}(t)} \text{ by } \frac{\partial \phi_i[t,\hat{\gamma}(t)]}{\partial \hat{\gamma}}$$

for simplicity) Also, in Eqs (10), and (11), $P(t)$ represents an approximation of the conditional variance of $\hat{\gamma}(t)$ The solution of Eq (11) can easily be shown to be

$$P(t) = \left\{ 1/\sigma^2_{\gamma_0} + \int_{-T_1}^{t} \sum_{i=1}^{2} (1/N_i) \left[s(\tau - \phi_i(\tau,\hat{\gamma}(\tau))) \frac{\partial \phi_i(\tau,\hat{\gamma}(\tau))}{\partial \hat{\gamma}} \right]^2 d\tau \right\}^{-1} \tag{14}$$

Rewriting Eq (10) as an integral equation gives

$$\hat{\gamma}(t) = \bar{\gamma}_0 - \int_{-T_1}^{t} P(\tau) \sum_{i=1}^{2} (1/N_i) \left[y_i(\tau) - s(\tau - \phi_i(\tau,\hat{\gamma}(\tau))) \cdot \left[s(\tau - \phi_i(\tau,\hat{\gamma}(\tau))) \frac{\partial \phi_i(\tau,\hat{\gamma}(\tau))}{\partial \hat{\gamma}} \right] d\tau \right. \tag{15}$$

Thus, Eqs (14) and (15) give the estimator structure with $\hat{\gamma}(T_2)$, the desired estimate of γ_0 The only prior statistical knowledge of γ_0 required is its mean and variance A block diagram of the implementation of the estimator is given in Fig 3 The expression for $\partial \phi_i[t, \hat{\gamma}(t)]/\partial \hat{\gamma}$ is given in Eqs (B-2) and (B-3) of Appendix B These waveforms are implemented in the receiver of Fig 3 by adjusting the $\hat{\gamma}(t)$ phase contributions in the sinusoidal terms given in Eqs (B-2) and (B-3) The structure of the estimator is somewhat similar to the MAP estimator with normal prior distribution for γ_0 (Ref 1, p 453) One substantial difference of the estimator here with the MAP estimator is that the gain term $P(\tau)$ in the integral in Eq (15) is replaced by $2\sigma^2{}_{\gamma_0}$ in the MAP estimator This is because the gain is updated to account for the change in the a posteriori variance of γ_0 based on the observations This is not performed in the MAP estimator

In Eqs (14) and (15), $\phi_i(t, \gamma)$ is given by Eq (3) and $\partial \phi_i(t, \gamma)/\partial \gamma$ by Eqs (B-2) and (B-3) in Appendix B Further simplification of Eqs (14) and (15) can result from using the simpler approximations in Eqs (24) to (27) given in section IV for ϕ_i and $\partial \phi_i/\partial \gamma$ Simplification of the basic estimator structure depicted in Fig 3 apparently cannot be done without specific assumptions on the signal structure

The performance of this algorithm unfortunately cannot be determined analytically In evaluating extended Kalman filters, $P(t)$ is often regarded as a measure of the mean square error However, care must be taken to adopt this conclusion since $P(t)$ is only an approximation to the conditional variance of $\hat{\gamma}(t)$ (Refs 4, 5) Moreover, $P(t)$ depends on the observations and so cannot be determined other than from simulation runs of the filter In spite of these pitfalls, let us examine Eq (14) to obtain a heuristic estimate of the best possible performance of the estimator

Assume that the estimator is performing well Thus, $\hat{\gamma}(t)$ will be close to $\gamma(t) = \gamma_0$ Assume also that $P(T_2)$ is a good approximation of the mean square estimation error Then, from Eq (14) we have

$$P(T_2) = \frac{\left[\sum_{i=1}^{2} (1/N_i) \int_{-T_1}^{T_2} s^2(t - \phi_i(t,\hat{\gamma}(t))) \left(\frac{\partial \phi_i(t,\hat{\gamma}(t))}{\partial \hat{\gamma}} \right)^2 dt \right]^{-1}}{1 + \left[\sum_{i=1}^{2} (1/N_i) \int_{-T_1}^{T_2} s^2(t - \phi_i(t,\hat{\gamma}(t))) \left(\frac{\partial \phi_i(t,\hat{\gamma}(t))}{\partial \hat{\gamma}} \right)^2 dt \right]^{-1} \Big/ \sigma^2_{\gamma_0}}$$

$$\leq \left[\sum_{i=1}^{2} (1/N_i) \int_{-T_1}^{T_2} s^2(t - \phi_i(t,\hat{\gamma}(t))) \left(\frac{\partial \phi_i(t,\hat{\gamma}(t))}{\partial \hat{\gamma}} \right)^2 dt \right]^{-1} \tag{16}$$

Let γ_0 be the true value of the unknown angle So, if $\hat{\gamma}(t) \cong \gamma_0$, replacing $\hat{\gamma}(t)$ by γ_0 in Eq (16) shows that the upper bound on $P(T_2)$ is roughly twice the Cramer-Rao lower bound (Eq (5)) on the optimum mean square error Thus from the above heuristic point of view, the best possible performance of the estimator is roughly within a factor of 2 from the Cramer-Rao lower bound of Eq (5)

IV. Optimum Theoretically Attainable Estimation Performance

As we noted previously the Cramer-Rao lower bound gives a lower bound on the optimum attainable angle mean square estimation error In this section we shall examine the Cramer-Rao lower bound in a special case In particular, we shall assume the following set of parameters

$$\begin{aligned} d_0 &= 8 \times 10^8 \text{ km} \\ R_1 = R_2 &= 6.5 \times 10^3 \text{ km} \\ v &= 10 \text{ km/sec} \\ T_1 = T_2 &= 30 \text{ min} \end{aligned} \tag{17}$$

This set of parameters is consistent with the distances encountered in a Jupiter mission We assume in addition that $N_1 = N_2$ for simplicity We shall first analyze the effects of the relative angular positions and the rotation of the Earth on the Cramer-Rao lower bound (Eq (5)) This, then, gives the dependence of the optimum attainable performance on these effects

We first consider the effect of the angular positions γ_0, ϵ_0 and η given in Fig 1 Since the problem of estimating γ_0 is nonlinear, the minimum attainable estimation error would generally depend on γ_0 Consider first the case when $\omega = \nu = 0$ for insight into this dependence Using the parameters in Eq (17) we have from Eqs (3) and (4) that

$$\phi_1(t,\gamma_0) = \left[d_0^2 + R_1^2 - 2d_0R_1 \cos(\gamma_0 - \epsilon_0)\right]^{1/2}/c \cong \left[(d_0^2 + R_1^2)^{1/2}/c\right]\left[1 - (R_1 d_0/(d_0^2 + R_1^2)) \cos(\gamma_0 - \epsilon_0)\right] \quad (18)$$

$$\phi_2(t,\gamma_0) = \left[d_0^2 + R_2^2 - 2d_0R_2 \cos(\gamma_0 - \epsilon_0 - \eta)\right]^{1/2}/c \cong \left[(d_0^2 + R_2^2)^{1/2}/c\right]\left[1 - (R_2 d_0/(d_0^2 + R_2^2)) \cos(\gamma_0 - \epsilon_0 - \eta)\right] \quad (19)$$

so

$$\frac{\partial\phi_i(t,\gamma_0)}{\partial\gamma_0} \cong \left[R_1 d_0/c\,(d_0^2 + R_1^2)^{1/2}\right] \sin(\gamma_0 - \epsilon_0) \quad (20)$$

$$\frac{\partial\phi_2(t,\gamma_0)}{\partial\gamma_0} \cong \left[R_2 d_0/c\,(d_0^2 + R_2^2)^{1/2}\right] \sin(\gamma_0 - \epsilon_0 - \eta) \quad (21)$$

Since $[R_i d_0/c(d_0^2 + R_i^2)^{1/2}] = 2.17 \times 10^{-2}$, $\phi_i(t,\gamma_0)$ is relatively independent of γ_0 Thus an approximation of the Cramer-Rao lower bound (Eq (5)) in the case when $\omega = \nu = 0$ is

$$E[(\hat{\gamma}_0 - \gamma_0)^2] \geqslant \left[\frac{2R_1^2 d_0^2}{N_1 c^2 (d_0^2 + R_1^2)} \int_{-T_1}^{T_2} s^2\left(t - \frac{(d_0^2 + R_1^2)^{1/2}}{c}\right) \sin^2(\gamma_0 - \epsilon_0)\,dt + \frac{2R_2^2 d_0^2}{N_2 c^2 (d_0^2 + R_2^2)} \int_{-T_1}^{T_2} s^2\left(t - \frac{(d_0^2 + R_2^2)^{1/2}}{c}\right) \sin^2(\gamma_0 - \epsilon_0 - \eta)\,dt\right]^{-1} \quad (22)$$

Hence under the assumption that $R_1 = R_2$ and $N_1 = N_2$, Eq (23) depends inversely on

$$f(\delta) = \sin^2\delta + \sin^2(\delta - \eta) = 1 - \cos\eta\cos(2\delta - \eta) \quad (23)$$

where $\delta = \gamma_0 - \epsilon_0$ Note that $f(\delta)$ is symmetric about $\delta = \eta/2$, which corresponds to when the vehicle is halfway between the two stations (see Fig 1) When $0 < \eta < 90°$, $f(\delta)$ increases as δ deviates from $\eta/2$, or when the vehicle moves toward either station from the midpoint So, when $0 < \eta < 90°$, the worst performance is when the vehicle is exactly halfway between the two stations This is shown in Fig 4 When $\eta > 90°$, the converse is true and the best performance is when the vehicle is exactly halfway between the two stations Since $f(\delta)$ is independent of δ when $\eta = 90°$, this is the best value of η from the viewpoint of uniformity of performance over a range of γ_0 An examination of Eq (23) shows that for $80° \leqslant \eta \leqslant 100°$, the variation of performance is less than 20% for δ from 0 to η

The above considerations are when $\omega = \nu = 0$ Let us now consider when $\omega \neq 0$ and $\nu \neq 0$ In Appendix B, it is shown that approximate expressions for ϕ_1, ϕ_2, $\partial\phi_1/\partial\gamma_0$ and $\partial\phi_2/\partial\gamma_0$ are

$$\phi_1(t,\gamma_0) \cong -\left(1 - \left(\frac{\nu}{c}\right)^2\right)^{-1}\left[\left(\frac{\nu}{c}\right)^2 + \frac{\nu d_0 \cos\alpha}{[(d_0^2 + R_1^2)(c^2 - \nu^2)]^{1/2}}\right] t + \left(\frac{d_0^2 + R_1^2}{c^2 - \nu^2}\right)^{1/2} - \frac{\nu d_0 \cos\alpha}{c^2 - \nu^2}$$

$$- \frac{R_1 d_0}{[(d_0^2 + R_1^2)(c^2 - v^2)]^{1/2}} \cos(\gamma_0 - \epsilon_0 - \omega t) \quad (24)$$

$$\phi_2(t,\gamma_0)$$

$$\cong - \left(1 - \left(\frac{v}{c}\right)^2\right)^{-1} \left[\left(\frac{v}{c}\right)^2 + \frac{v d_0 \cos a}{[(d_0^2 + R_2^2)(c^2 - v^2)]^{1/2}}\right] t$$

$$+ \left(\frac{d_0^2 + R_2^2}{c^2 - v^2}\right)^{1/2} - \frac{v d_0 \cos \alpha}{c^2 - v^2}$$

$$- \frac{R_2 d_0}{[(d_0^2 + R_2^2)(c^2 - v^2)]^{1/2}} \cos(\gamma_0 - \epsilon_0 - \eta - \omega t) \quad (25)$$

$$\frac{\partial \phi_i(t,\gamma_0)}{\partial \gamma_0}$$

$$\cong \frac{R_1 d_0}{[(d_0^2 + R_1^2)(c^2 - v^2)]^{1/2}} \sin(\gamma_0 - \epsilon_0 - \omega t)$$

$$- \frac{v R_1}{c^2 - v^2} \left[1 - \left(\frac{d_0^2 + R_1^2}{c^2 - v^2}\right)^{-1/2} \left(1 - \left(\frac{v}{c}\right)^2\right)^{-1} t\right]$$

$$\cdot \sin(\gamma_0 - \epsilon_0 + \alpha - \omega t) \quad (26)$$

$$\frac{\partial \phi_2(t,\gamma_0)}{\partial \gamma_0}$$

$$\cong \frac{R_2 d_0}{[(d_0^2 + R_2^2)(c^2 - v^2)]^{1/2}} \sin(\gamma_0 - \epsilon_0 - \eta - \omega t)$$

$$- \frac{v R_2}{c^2 - v^2} \left[1 - \left(\frac{d_0^2 + R_2^2}{c^2 - v^2}\right)^{-1/2} \left(1 - \left(\frac{v}{c}\right)^2\right)^{-1} t\right]$$

$$\cdot \sin(\gamma_0 - \epsilon_0 + \alpha - \eta - \omega t) \quad (27)$$

In Eq (26), the factor in front of $\sin(\gamma_0 - \epsilon_0 + \alpha - \omega t)$ is of the order 10^{-7} while the factor in front of $\sin(\gamma_0 - \epsilon_0 - \omega t)$ is of the order 10^{-2} Hence, the second term in Eq (26) can be neglected except when $\sin(\gamma_0 - \epsilon_0 + \alpha - \omega t)$ is sufficiently larger than $\sin(\gamma_0 - \epsilon_0 - \omega t)$ In an extreme case when $\gamma_0 - \epsilon_0 = 0^\circ$ and $\alpha = 90^\circ$, the first term in Eq (26) is zero at $t = 0$ However, as t deviates sufficiently from 0, the first term will again dominate the second term For example, if $|t| = 10$ sec, the first term is 10 times the second in Eq (26) So, in instances when the observation time interval $T_1 + T_2$ is much larger than 10 sec, the contribution of the second term in Eq (26) to the Cramer-Rao lower bound will be negligibly small The same conclusion can be drawn for the second term in Eq (29) Hence, neglecting these terms results in the following approximation to the Cramer-Rao lower bound (Eq (5))

$$E[(\hat{\gamma}_0 - \gamma_0)^2] \geqslant \left[\frac{2R_1^2 d_0^2}{N_1(c^2 - v^2)(d_0^2 + R_1^2)} \int_{-T_1}^{T_2} s^2(t - \phi_1(t,\gamma_0)) \sin^2(\gamma_0 - \epsilon_0 - \omega t)\, dt + \frac{2R_2^2 d_0^2}{N_2(c^2 - v^2)(d_0^2 + R_2^2)} \int_{-T_1}^{T_2} s^2(t - \phi_2(t,\gamma_0)) \sin^2(\gamma_0 - \epsilon_0 - \eta - \omega t)\, dt\right]^{-1} \quad (28)$$

where ϕ_1 and ϕ_2 are given by Eqs (24) and (25) respectively

Let us now compare Eq (28) with Eq (22) when $\omega = v = 0$ From Eqs (24) and (25) it can be seen that the dependence of ϕ_1 and ϕ_2 on γ_0 is small We may assume that ϕ_1 and ϕ_2 are both essentially independent of γ_0 in Eq (28) So from the viewpoint of dependence on γ_0, the essential difference in the structure of Eq (28) to the structure of Eq (22) is the $\sin^2(\gamma_0 - \epsilon_0 - \omega t)$ and $\sin^2(\gamma_0 - \epsilon_0 - \eta - \omega t)$ factors in the integrands in Eq (28) versus the corresponding $\sin^2(\gamma_0 - \epsilon_0)$ and $\sin^2(\gamma_0 - \epsilon_0 - \eta)$ factors in Eq (22) Although the earth rotational angular velocity $\omega = 7.27 \times 10^{-5}$ rad/sec, for $t = 30$ minutes $\omega t = 7.5^\circ$ Hence this difference is certainly not

negligible This points out a significant contribution to the estimation performance due to the rotation of the stations

To assess the dependence of Eq (28) on the angular position γ_0 we assume that ϕ_1 and ϕ_2 are essentially independent of γ_0 in Eq (28) Under the assumption that $N_1 = N_2$ and $R_1 = R_2$, the integrand in Eq (28) is directly proportional to

$$\sin^2 (\gamma_0 - \epsilon_0 - \omega t) + \sin^2 (\gamma_0 - \epsilon_0 - \eta - \omega t)$$

$$= 1 - \cos \eta \cos [2(\gamma_0 - \epsilon_0 - \omega t) - \eta] \qquad (29)$$

Comparing Eq (29) to Eq (23), we see that to a first order approximation, the conclusions regarding the dependence of performance on angular position $\gamma_0 - \epsilon_0$ in the case $\omega = \nu = 0$ still hold here In particular, it is clear from Eq (29) that from a viewpoint of uniformity of performance over a range of γ_0, angular positions near $\eta = 90^\circ$ are desirable

Let us consider next the effect of varying the parameters R_1 and R_2 on the optimum attainable estimation performance Recall that R_1 and R_2 are the distances from the stations to geocenter In Eq (17), the values of R_1 and R_2 are for ground-based stations The other case of interest is when the two stations are in geostationary orbit with $R_1 = R_2$ We shall consider an orbital radius of up to 10^5 km Hence we need to examine the dependence of Eq (5) on $R_1 = R_2$ for a range of these parameters from $6\,5 \times 10^3$ km to 10^5 km We still take d_0, the distance of the vehicle to geocenter, to be as in Eq (17) Hence d_0 is still much larger than R_1 and R_2 In this case, an examination of the derivation in Appendix B shows that we can still use the approximation in Eq (28) to Eq (5) with the expressions in Eqs (24) and (25) for ϕ_1 and ϕ_2, respectively Since d_0 is much larger than $R_1 = R_2$, an examination of Eqs (24), (25) and (28) shows that the Cramer-Rao lower bound is proportional to $1/R_1^2 = 1/R_2^2$ In other words, the root mean square estimation error is directly proportional to $1/R_1 = 1/R_2$ Increasing, $R_1 = R_2$ from $6\,5 \times 10^3$ km to 10^5 km will decrease the optimum root mean square estimation error by two orders of magnitude

Finally, let us consider the effect of varying the observation duration $T_1 + T_2$ on the optimum attainable estimation performance We assume that $T_1 + T_2$ is large compared to 10 seconds and that the other parameters are given as in Eq (17) Then Eq (28) is again a valid approximation of Eq (5) with ϕ_1 and ϕ_2 approximated by Eqs (24) and (25), respectively We also assume that the frequency of the ranging signal $s(t)$ is much higher than $1/(T_1 + T_2)$ and also much higher than $\omega/2\pi$ (ω = rotational angular velocity of the stations) It is still difficult to assess the dependence of Eq (28) on T_1 and T_2 in general because of the $\sin^2 (\gamma_0 - \epsilon_0 - \omega t)$ and $\sin^2 (\gamma_0 - \epsilon_0 - \eta - \omega t)$ terms in the integrals in Eq (28) These terms change the value of the integrands as T_1 and T_2 are varied To a first order approximation it appears that the right-hand side of Eq (28) is inversely proportional to

$$(T_1 + T_2) [\sin^2 (\gamma_0 - \epsilon_0 - \omega T_2) - \sin^2 (\gamma_0 - \epsilon_0 + \omega T_1)$$

$$+ \sin^2 (\gamma_0 - \epsilon_0 - \eta - \omega T_2) - \sin^2 (\gamma_0 - \epsilon_0 - \eta + \omega T_1)]$$

$$= (T_1 + T_2) \{2 - \cos \eta \cos [2(\gamma_0 - \epsilon_0 - \omega T_2) - \eta)]$$

$$- \cos \eta \cos [2(\gamma_0 - \epsilon_0 + \omega T_1) - \eta]\}$$

In the case when $\eta = 90^\circ$, Eq (30) reduces to $2(T_1 + T_2)$ Thus, when $\eta \cong 90^\circ$, the optimum attainable root mean square error performance is approximately inversely proportional to $\sqrt{(T_1 + T_2)}$

Finally, we consider a specific ranging signal $s(t)$ and perform numerical computations of the Cramer-Rao lower bound

Example

Consider a sinusoidal ranging signal of frequency f_c Hz That is,

$$s(t) = \sqrt{2S} \cos (2\pi f_c t)$$

We assume that for $i = 1, 2$, the demodulated ranging signal power to noise spectral density ratio is

$$\frac{S}{N_t} = 10 \text{ dB}$$

This signal-to-noise ratio is consistent with X-band carrier, 20-dB vehicle antennae gain, 53-dB station antenna gains, receiver noise temperatures of 50°K, 20 W vehicle transmitted power and a 3-dB modulation loss We also assume that

$$d_0 = 8 \times 10^8 \text{ km}$$

$$\nu = 10 \text{ km/sec}$$

$$R_1 = R_2 = 6\,5 \times 10^3 \text{ km}$$

These parameters are consistent with that encountered in a Jupiter mission with ground-based stations We also assume that $T_1 = T_2$ Numerical Monte Carlo integration was used to compute the value of the Cramer-Rao lower bound for various values of signal frequency f_c and observation time duration $T_1 + T_2$ The numerical computations are within a 1% accuracy These numerical results are summarized in Tables 1 and 2 below The listed angle estimation accuracies in these tables are the square root of the Cramer-Rao lower bound

Table 1 shows that the optimum angle estimation accuracy is inversely proportional to the frequency of the sinusoidal ranging signal Although this particular relation between estimation accuracy and signal frequency does not hold in general, it can be easily seen from Eq (5) that signals of higher frequency give a smaller Cramer-Rao lower bound Also note that Table 2 shows that the estimation accuracy is approximately inversely proportional to $T_1 + T_2$, as we would expect, since $\eta = 90^\circ$

We note that the above angle estimation accuracy was obtained using the Cramer-Rao lower bound, Eq (5), which is valid when γ_0 is an unknown but nonrandom parameter Suppose instead that γ_0 is a random parameter and can a priori be assumed to be normally distributed Then the relevant lower bound on mean square estimation error is Eq (7) We claim that if the a priori variance of γ_0 is much larger than the lower bound Eq (5), then the above estimation accuracy calculation is still valid This follows because Eq (5) is essentially independent of γ_0, in this case since $\eta = 90^\circ$ Hence, the expectation term in Eq (7) is 1/(lower bound Eq (5))

V. Conclusion

This work has considered the problem of estimating the angular position of a moving vehicle using two rotating stations The optimum attainable angle mean square estimation error was derived along with an implementable suboptimal estimation algorithm A situation comparable to that encountered in a Jupiter mission was further analyzed In this situation it was shown that the optimum angle between the two stations from a viewpoint of uniformity of estimation performance is 90° It was also shown that the optimum attainable estimation accuracy varies inversely with the distance of the stations from geocenter and approximately inversely with the square root of the observation time duration The optimum attainable angular estimation accuracy was numerically computed for a sinusoidal ranging signal These computations show that the optimum attainable estimation accuracy is 0 02 μrad for a 2 MHz signal and an observation time of one hour

This work has only considered the problem of estimating one angle with the range, velocity and other angles of the vehicle known Further work should be done to include some or all of these parameters as parameters to be estimated along with the angle considered in this work

References

1 H L Van Trees, *Detection, Estimation and Modulation Theory, Part I*, John Wiley and Sons, New York, 1968

2 J I Galdos, "A Lower Bound on Filtering Error with Application to Phase Modulation," *IEEE Trans Inform Theory*, Vol IT-25, No 4, pp 452-462, 1979

3 J Ziv and M Zahai, "On Functionals Satisfying a Data-Processing Theorem," *IEEE Trans Inform Theory*, Vol IT-19, No 3, pp 225-280, 1973

4 T P McGarty, *Stochastic Systems and State Estimation*, John Wiley and Sons, New York, 1974

5 A H Jaswinski, *Stochastic Processes and Filtering Theory*, Academic Press, New York, 1970

Table 1 Estimation accuracy vs signal frequency

Signal frequency fc	Optimum angle estimation accuracy
2 MHz	0 018 μrad
5 MHz	0 0072 μrad
10 MHz	0 0036 μrad
20 MHz	0 0018 μrad

Table 2 Estimation accuracy vs observation time

Observation time duration $(T_1 + T_2)$	Optimum angle estimation accuracy
10 min	0 046 μrad
30 min	0 026 μrad
60 min	0 018 μrad
90 min	0 015 μrad

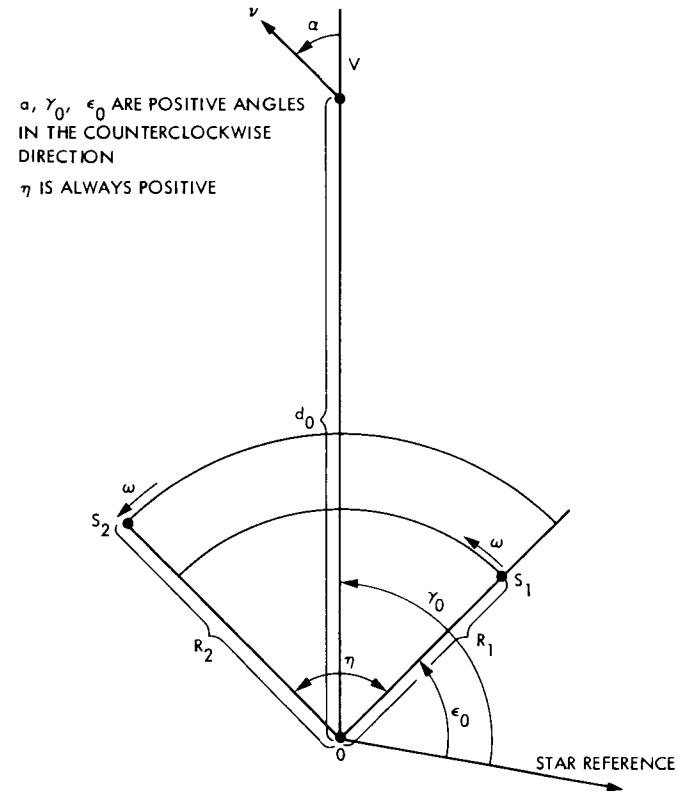

Fig 1 Vehicle and station locations

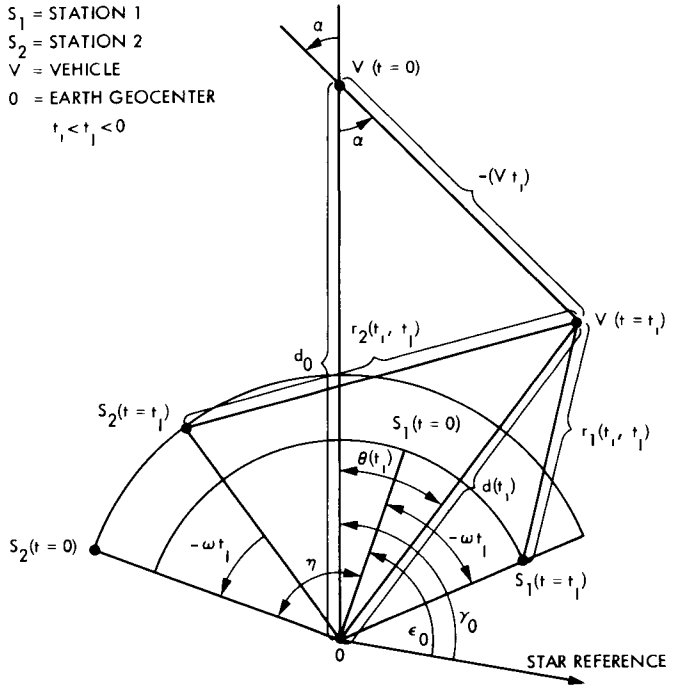

Fig 2 Relative locations for t = 0, t_i, t_j

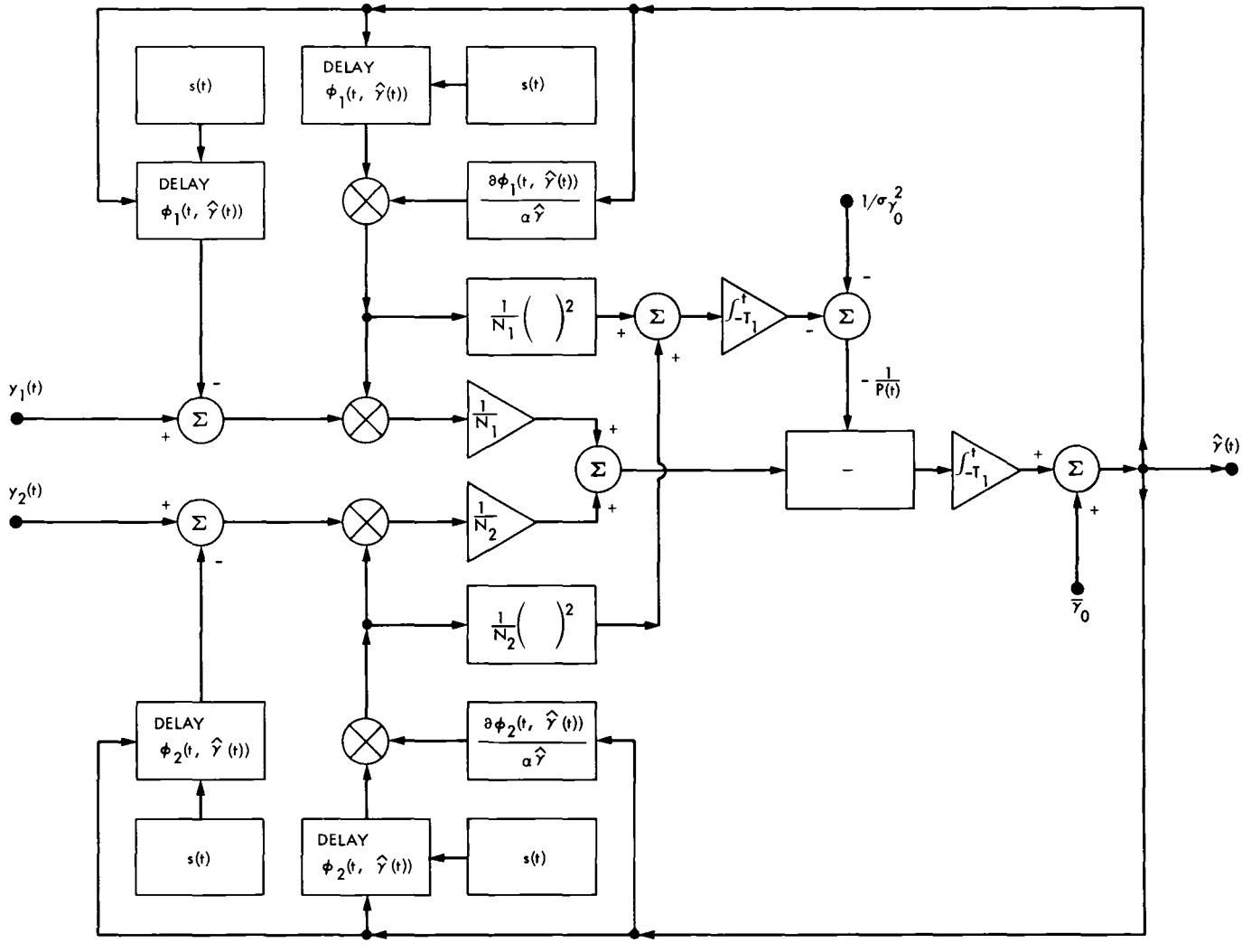

Fig. 3 Estimator block diagram

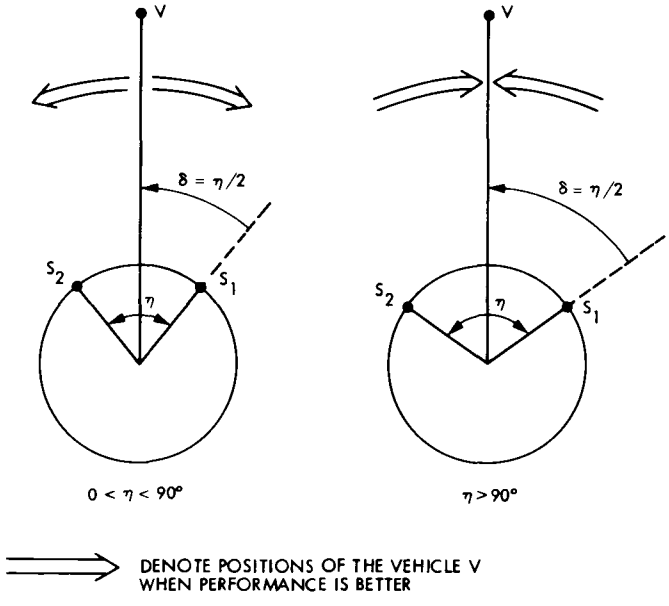

Fig 4 Dependence of estimation performance on the angle between the stations

Appendix A

Derivation of Expressions for ϕ_1 and ϕ_2

It follows from Eqs (1) and (2) that the signal value received at station S_ι at time t is the signal value transmitted by the vehicle at time $t - \phi_\iota(t,\gamma_0)$ for $\iota = 1,2$ Define

$$\tau_\iota(t) = t - \phi_\iota(t,\gamma_0), \quad \iota = 1,2 \tag{A-1}$$

For time instants t_ι and $t_\jmath$ let

$r_1(t_\iota,t_\jmath)$ = distance between the vehicle at time t_ι and station S_1 at time $t_\jmath$

$r_2(t_\iota,t_\jmath)$ = distance between the vehicle at time t_ι and station S_2 at time $t_\jmath$

It is then clear from Eqs (1), (2) and (A-1) that

$$\phi_\iota(t,\gamma_0) = \frac{r_\iota\,[\tau_\iota(t),t]}{c} \tag{A-2}$$

or equivalently,

$$\tau_\iota(t) = t - \frac{r_\iota\,[\tau_\iota(t),t]}{c} \tag{A-3}$$

for $\iota = 1,2$ Hence if Eq (A-3) can be solved for $\tau_\iota(t)$, then $\phi_\iota(t,\gamma_0)$ may be obtained using Eq (A-1) In order to accomplish this we must first obtain expressions for $r_1(t_\iota,t_\jmath)$ and $r_2(t_\iota,t_\jmath)$ Since $\tau_\iota(t) < t$ in (A-3), we are interested in the cases $0 < t_\iota < t_\jmath$, $t_\iota < 0 < t_\jmath$ and $t_\iota < t_\jmath < 0$ only in determining these expressions Consider first the case when $t_\iota < t_\jmath < 0$ as given in Fig 2 Also we shall assume that $0 \leqslant \alpha \leqslant 180^0$ in Fig 2 Let

$d(t_\iota)$ = distance between the vehicle and Earth geocenter at time t_ι

$\theta(t_\iota)$ = relative angle at geocenter between the vehicle positions at $t = 0$ and $t = t_\iota$

From the geometry of Fig 2 we can write the following relations

$$d^2(t_\iota) = v^2t_\iota^2 + d_0^2 + 2d_0vt_\iota\cos\alpha \tag{A-4}$$

$$\frac{d(t_\iota)}{\sin\alpha} = \frac{-(vt_\iota)}{\sin\theta(t_\iota)} \tag{A-5}$$

$$r_1^2(t_\iota,t_\jmath) = d_1^2(t_\iota) + R_1^2 - 2R_1d_1(t_\iota)\cos\,[\gamma_0 - \epsilon_0 - \omega t_\jmath - \theta(t_\iota)] \tag{A-6}$$

$$r_2^2(t_\iota,t_\jmath) = d_1^2(t_\iota) + R_2^2 - 2R_2d_1(t_\iota)\cos\,[\eta + \epsilon_0 - \gamma_0 + \theta(t_\iota) + \omega t_\jmath] \tag{A-7}$$

Next, using Eqs (A-4) and (A-5) we get

$$\cos\theta\,(t_\iota) = [1 - \sin^2\theta(t_\iota)]^{1/2} = \frac{d_0 + vt_\iota\cos\alpha}{d(t_\iota)} \tag{A-8}$$

Now, substitution of Eqs (A-5) and A-8) into Eqs (A-6) and (A-7) yield the following expressions for $r_1^2(t_\iota,t_\jmath)$ and $r_2^2(t_\iota,t_\jmath)$

$$r_1^2\,(t_\iota,t_\jmath) = d^2(t_\iota) + R_1^2 - 2R_1d_0\cos(\gamma_0 - \epsilon_0 - \omega t_\jmath) - 2R_1vt_\iota\cos(\alpha + \gamma_0 - e_0 - \omega t_\jmath) \tag{A-9}$$

$$r_2^2(t_\iota,t_\jmath) = d^2(t_\iota) + R_2^2 - 2R_2d_0\cos(\eta + \epsilon_0 - \gamma_0 + \omega t_\jmath) - 2R_2vt_\iota\cos(\alpha - \eta - \epsilon_0 + \gamma_0 - \omega t_\jmath) \tag{A-9}$$

So, Eqs (A-4), (A-8) and (A-9) define $r_1^2(t_\iota,t_\jmath)$ and $r_2^2(t_\iota,t_\jmath)$ for the case $t_\iota < t_\jmath < 0$ and $0 \leqslant \alpha \leqslant 180^\circ$ Arguments similar to the above can be used to establish Eqs (A-4), (A-8) and (A-9) when $0 < t_\iota < t_\jmath$ or $t_\iota < 0 < t_\jmath$ and also when $180^\circ \leqslant \alpha \leqslant 360^\circ$ Hence, we may conclude that these equations hold for all cases of interest in solving Eq (A-3) for $\tau_\iota(t)$ For simplicity let us denote $\tau_\iota(t)$ by τ_ι for the remainder of the appendix Squaring Eq (A-3) yields

$$c^2(\tau_\iota - t)^2 = r_\iota^2(\tau_\iota,t), \quad \iota = 1,2 \tag{A-10}$$

Next, substitution of Eqs (A-4), (A-8) and (A-9) into Eq (A-10) yields the following quadratic equations satisfied by τ_ι and τ_2

$$(c^2 - v^2)\tau_1^2 - 2[c^2 t + vd_0 \cos\alpha - vR_1 \cos(\alpha + \gamma_0 - \epsilon_0 - \omega t)]\tau_1$$
$$- [d_0^2 + R_1^2 - 2R_1 d_0 \cos(\gamma_0 - \epsilon_0 - \omega t) - c^2 t^2] = 0 \quad \text{(A-11)}$$

$$(c^2 - v^2)\tau_2^2 - 2[c^2 t + vd_0 \cos\alpha - vR_2 \cos(\alpha - \eta - \epsilon_0 + \gamma_0$$
$$- \omega t)]\tau_2$$
$$- [d_0^2 + R_2^2 - 2R_2 d_0 \cos(\eta + \epsilon_0 - \gamma_0 + \omega t)$$
$$- c^2 t^2] = 0 \quad \text{(A-12)}$$

The constraint that $\tau_i < t$ identifies the roots of Eqs (A-11) and (A-12) that give τ_1 and τ_2 respectively These are

$$\tau_1 = (1 - (v/c)^2)^{-1} [t + (vd_0 \cos\alpha)/c^2 - vR_1 \cos(\gamma_0 + \alpha - \epsilon_0$$
$$- \omega t)/c^2] - \{(1 - (v/c)^2)^{-2} [t + (vd_0 \cos\alpha)/c^2$$
$$- vR_1 \cos(\gamma_0 + \alpha - \epsilon_0 - \omega t)/c^2]^2$$
$$+ (1 - (v/c)^2)^{-1} [(d_0^2 + R_1^2 - 2R_1 d_0 \cos(\gamma_0 - \epsilon_0$$
$$- \omega t))/c^2 - t^2]\}^{1/2} \quad \text{(A-13)}$$

$$\tau_2 = (1 - (v/c)^2)^{-1} [t + (vd_0 \cos\alpha)/c^2 - vR_2 \cos(\gamma_0 + \alpha - \epsilon_0$$
$$- \eta - \omega t)/c^2] + \{(1 - (v/c)^2)^{-2} [t + (vd_0 \cos\alpha)/c^2$$
$$- vR_2 \cos(\gamma_0 + \alpha - \epsilon_0 - \eta - \omega t)/c^2]^2$$
$$+ (1 - (v/c)^2)^{-1} [(d_0^2 + R_2^2 - 2R_2 d_0 \cos(\gamma_0 - \epsilon_0 - \eta$$
$$- \omega t))/c^2 - t^2]\}^{1/2} \quad \text{(A-14)}$$

Finally, Eqs (A-1), (A-13) and (A-14) give the expressions in Eqs (3) and (4) for $\phi_1(t,\gamma_0)$ and $\phi_2(t,\gamma_0)$, respectively

Appendix B

Approximations to ϕ_1, ϕ_2, $\frac{\partial\phi_1}{\partial\gamma_0}$ and $\frac{\partial\phi_1}{\partial\gamma_0}$

Consider first ϕ_1 given by Eq (3) Ignoring terms smaller than 10^{-9}, we have

$$\begin{aligned}
&\{(1-(v/c)^2)^{-2}\,[t+(vd_0\cos\alpha)/c - vR_1\cos(\gamma_0+\alpha-\epsilon_0 \\
&\quad -\omega t)/c^2]^2 + (1-(v/c)^2)^{-1}\,[(d_0^2+R_1^2-2R_1d_0 \\
&\quad \cos(\gamma_0-\epsilon_0-\omega t))/c^2 - t^2]\}^{1/2} \\
&\cong \left(\frac{d_0^2+R_1^2}{c^2-v^2}\right)^{1/2}\left[1+\frac{2vd_0\cos\alpha}{(d_0^2+R_1^2)(1-(v/c)^2)}\,t\right. \\
&\quad \left. -\frac{2R_1d_0}{d_0^2+R_1^2}\cos(\gamma_0-\epsilon_0-\omega t)\right]^{1/2} \\
&\cong \left(\frac{d_0^2+R_1^2}{c^2-v^2}\right)^{1/2}\left[1+\frac{2vd_0\cos\alpha}{(d_0^2+R_1^2)(1-(v/c)^2)}\,t\right. \\
&\quad \left. -\frac{R_1d_0}{d_0^2+R_1^2}\cos(\gamma_0-\epsilon_0-\omega t)\right] \qquad \text{(B-1)}
\end{aligned}$$

where the second line in Eq (B-1) is obtained by using the approximation $(1+x)^{1/2} \cong 1+(1/2)x$ with accuracy of the order 10^{-10} Substitution of (B-1) into Eq (3) and ignoring terms of order 10^{-7} and smaller gets Eq (26) A similar argument using Eq (4) gets Eq (27) Consider next $\partial\phi_1/\partial\gamma_0$ and $\partial\phi_2/\partial\gamma_0$ Differentiating Eq (3) and Eq (4) yields

$$\begin{aligned}
\frac{\partial\phi_1(t,\gamma_0)}{\partial\gamma_0} &= -\frac{vR_1}{c^2-v^2}\sin(\gamma_0-\epsilon_0+\alpha-\omega t) \\
&\quad + \{(1-(v/c)^2)^{-2}\,[t+(vd_0\cos\alpha)/c^2 \\
&\quad - vR_1\cos(\gamma_0-\epsilon_0+\alpha-\omega t)/c^2]^2 \\
&\quad + (1-(v/c)^2)^{-1}\,[(d_0^2+R_1^2-2R_1d_0\cos(\gamma_0-\epsilon_0 \\
&\quad -\omega t)/c^2 - t^2]\}^{-1/2} \\
&\quad \cdot\left\{(1-(v/c)^2)^{-2}\,[t+(vd_0\cos\alpha)/c^2\right. \\
&\quad - vR_1\cos(\gamma_0-\epsilon_0+\alpha-\omega t)/c^2] \\
&\quad \cdot (vR_1/c^2)\sin(\gamma_0-\epsilon_0+\alpha-\omega t) \\
&\quad \left. +\frac{R_1d_0}{c^2-v^2}\sin(\gamma_0-\epsilon_0-\omega t)\right\} \qquad \text{(B-2)}
\end{aligned}$$

$$\begin{aligned}
\frac{\partial\phi_2(t,\gamma_0)}{\partial\gamma_0} &= -\frac{vR_2}{c^2-v^2}\sin(\gamma_0-\epsilon_0+\alpha-\eta-\omega t) \\
&\quad + \{(1-(v/c)^2)^{-2}\,[t+vd_0\cos\alpha/c^2 \\
&\quad - vR_2\cos(\gamma_0-\epsilon_0+\alpha-\eta-\omega t)/c^2]^2 \\
&\quad + (1-(v/c)^2)^{-1}\,[(d_0^2+R_2^2-2R_2d_0\cos(\gamma_0-\epsilon_0 \\
&\quad -\eta-\omega t)/c^2 - t^2]\}^{-1/2} \\
&\quad \cdot\left\{(1-(v/c)^2)^{-1}\,[t+(vd_0\cos\alpha)/c^2\right. \\
&\quad - vR_2\cos(\gamma_0-\epsilon_0+\alpha-\eta-\omega t)/c^2] \\
&\quad \cdot (vR_2/c^2)\sin(\gamma_0-\epsilon_0+\alpha-\eta-\omega t) \\
&\quad \left. +\frac{R_2d_0}{c^2-v^2}\sin(\gamma_0-\epsilon_0-\eta-\omega t)\right\} \qquad \text{(B-3)}
\end{aligned}$$

An approximation similar to that used in (B-1) can then be used with (B-2) and (B-3) to establish Eqs (28) and (29)

Validation of Roundtrip Charged-Particle Calibrations Derived From S- and X-Band Doppler Via DRVID Measurements

D W Green
Navigation Systems Section

In this article it is shown that roundtrip signal path calibrations for charged-particle effects can be computed from S- and X-band doppler data The method by which this is done is described, and possible error sources are examined It is shown that roundtrip calibrations computed from S- and X-band doppler compare to direct measurements using DRVID to within the DRVID data noise

I. Introduction

The Tracking Systems Analytic Calibration (TSAC) function provides calibrations for spacecraft radio metric data based on dual frequency (S- and X-band) doppler data These calibrations are based on modeling the charged-particle effects on the uplink portion of the roundtrip path using the downlink only information in the S/X data and certain assumptions about the spatial and temporal distribution of the contributing charged-particle environment

The presence of a low-density plasma along the propagation path of a radio signal causes the group propagation velocity to decrease and the phase velocity to increase The DSN ranging system uses measurement of the roundtrip signal propagation time and the assumption of a constant value for the group velocity to imply the roundtrip distance to the spacecraft The presence of charged particles along the path causes an apparent increase in this range value The doppler measurement system measures the increment in the roundtrip path length by counting cycles of the returning signal and assuming a constant wavelength A positive change in the charged-particle content along the signal path will result in a decrease in the measured range change from counted (integrated) doppler The apparent increase in range inferred from group measurements is equal in magnitude to the apparent decrease inferred from phase measurements taken over the same time period The magnitude of this effect is proportional to the plasma density and inversely proportional to the square of the frequency of the signal involved A comparison of the apparent increase in range from differencing two consecutive range measurements with the apparent decrease in range as measured by doppler data counted over the same interval gives a measurement of the change in the charged particles along the signal path An implementation of this technique has been mechanized in the PLanetary OPerational (PLOP) ranging system and the resulting data type is referred to as Differenced Range Versus Integrated Doppler (DRVID) data (Ref 1) The equivalent range change measured by DRVID is output in PLOP Range Units (RU) An RU is approximately one light nanosecond

On December 1, 1978, a test was run at Deep Space Station 14 to determine the effects of moving the antenna subreflector For this pass of data, range, doppler and DRVID data were taken from the Voyager 1 spacecraft at both S- and X-band DRVID data provide a measurement of the charged-particle environment along the entire signal path Thus, simultaneous acquisition of dual frequency doppler data and DRVID

allows a comparison to be made between a complete roundtrip calibration reconstructed from the doppler data using a model and an actual measurement of the effect by DRVID This in turn allows the modeling technique used to be validated

A similar pass of data during which both dual frequency doppler and DRVID data were taken occurred on April 13, 1977 for the Viking 2 orbiter

In the following sections, the technique used to provide roundtrip signal calibrations from S/X doppler data are described, and several possible error sources are identified For the passes of data processed we find that the roundtrip calibrations derived from S/X doppler data are equivalent to the same data derived from DRVID measurements to within the DRVID measurement noise

II. The TSAC S/X Doppler Model

The model which TSAC uses to compute roundtrip calibrations from downlink S/X data is pictured in Fig 1 Working backward from the reception time, the signal is assumed to pass through Earth's ionosphere at a time negligibly different from the reception time The solar plasma is assumed to affect the signal as if it were concentrated at the point on the ray path closest to the Sun Depending on the Sun-Earth-probe geometry, this can occur anywhere from zero to approximately 500 seconds (light time to Sun) prior to the reception time Prior to this, the signal encounters roughly the same plasma configuration at a time earlier by a roundtrip light time (RTLT) less twice the Earth-to-plasma time Initially, the signal is affected by the Earth's ionosphere at a time negligibly different from the transmission time, i e , the reception time minus one RTLT The reliability of the assumption that the plasma acts as though it were concentrated at the point on the signal path closest to the Sun is examined in Ref 2

The equation for the total effect due to charged particles on a range point received at time t is

$$R(t) = I(t) + P(t) + \lambda P(t - \text{TPLAS}) + \lambda I(t - \text{RTLT}) \quad (1)$$

where

$R(t)$ = total charged particle effect on range at time t

$I(t)$ = ionosphere contribution computed from Faraday rotation data

$P(t)$ = plasma contribution computed by removing ionosphere effect from total downlink effect as measured by S/X doppler data

$P(t - \text{TPLAS})$ = plasma effect evaluated at time corresponding to uplink passage of signal through space where plasma is assumed to be located

$I(t - \text{RTLT})$ = ionosphere contribution at transmission time

$\lambda = (240/221)^2$ = correction factor to account for increased effect on uplink due to lower uplink transmitted frequency

The increment in the S-band cycle count over a particular interval is given by

$$\Delta S|_{t-T}^{t} = fo \int_{t-T}^{t} \left(\frac{r_{s/c}}{c} - \left(\frac{240}{221}\right)^2 \frac{r_{up}}{c} - \frac{r_{dp}}{c} \right) dt \quad (2)$$

and the corresponding X-band cycle count is

$$\Delta X|_{t-T}^{t} = \frac{11}{3} fo \int_{t-T}^{t} \left(\frac{r_{s/c}}{c} - \left(\frac{240}{221}\right)^2 \frac{r_{up}}{c} - \left(\frac{3}{11}\right)^2 \frac{r_{dp}}{c} \right) dt \quad (3)$$

where

ΔS = increment in S-band cycle count

ΔX = increment in X-band cycle count

t = end of count time

T = length of count time interval

fo = S-band downlink carrier frequency

c = speed of light

$r_{s/c}$ = time derivative of roundtrip path length to spacecraft

r_{up} = time derivative of apparent increase in range at received S-band frequency due to charged particles on uplink leg

r_{dp} = time derivative of apparent increase in range at received S-band frequency due to charged particles on downlink leg

Note that

$$\frac{3}{11}\,\Delta X - \Delta S\Big|_{t-T}^{t} = \frac{fo}{c}\left[1 - \left(\frac{3}{11}\right)^2\right]\int_{t-T}^{t} r_{dp}\,dt \tag{4}$$

Hence, the accumulative downlink effect during a time interval $t = nT$ is

$$SX(t) = \sum_{i=1}^{n} \frac{c}{fo}\left[1 - \left(\frac{3}{11}\right)^2\right]^{-1}\left(\frac{3}{11}\right)\Delta X - \Delta S\Big|_{(i-1)T}^{iT}$$

$$= \Delta r_{dp} + K \tag{5}$$

That is, the summation of the appropriate linear combination of S- and X-band doppler counts yields a measurement of the downlink contribution to S-band range due to all charge particles to within a constant of integration

The contribution to the total downlink range change due to the ionosphere is assumed to be known from Faraday rotation measurements Thus, the contribution from space plasma can be computed as

$$P(t) = SX(t) - I(t) \tag{6}$$

and substituting in Eq (1) above

$$R(t) = SX(t) + \lambda[SX(t - \text{TPLAS}) - I(t - \text{TPLAS}) + I(t - \text{RTLT})] \tag{7}$$

III. Error Equation for the Selected Model

We next consider the following possible sources of error in this model

(1) The S/X doppler measurements may be in error, describe the cumulative effect of this error as $\sigma(t)$

(2) The assumed location of the plasma may be in error, call the corresponding error in TPLAS, π

(3) There may be a measurement or modeling error in the Faraday rotation data The cumulative effect of this error is $\eta(t)$

(4) There is a constant of integration K in the S/X data

The equation for the computed range correction becomes

$$R(t) = SX(t) + \sigma(t) + \lambda[SX(t - \text{TPLAS} - \pi) - I(t - \text{TPLAS} - \pi) + I(t - \text{RTLT}) + \sigma(t - \text{TPLAS} - \pi) - \eta(t - \text{TPLAS} - \pi) + \eta(t - \text{RTLT})] \tag{8}$$

The true range correction being removed, the error in the range correction, to first order, is given by

$$ER(t) = \sigma(t) + \lambda\left[(\sigma t - \text{TPLAS}) + \Delta(SX - I)\Big|_{t-\text{TPLAS}-\pi}^{t-\text{TPLAS}} + \Delta\eta\Big|_{t-\text{RTLT}}^{t-\text{TPLAS}}\right] + K \tag{9}$$

Expanding in terms of derivatives

$$ER(t) = \sigma(t) + \lambda\sigma(t - \text{TPLAS}) + \pi(SX - I) - \eta\tau + K \tag{10}$$

where $\tau = \text{RTLT} - \text{TPLAS}$

There are two principle uses for the roundtrip calibration for charged particles derived from S/X doppler data These are

(1) The calibration of doppler observables

(2) The calibration of differenced range data

For both of these phenomena, the quantity of interest is the change in the roundtrip measurement over some period of time For doppler this period is one count time For differenced range it is the time between the last range point taken at one station and the first range point at the next station We are interested in the error in the range change over some period of time ΔT Differencing Eq (10) above yields, to first order

$$\Delta ER = \Delta T\,[\sigma(t) + \lambda\sigma(t - \text{TPLAS}) + \pi(SX - I) - \tau\eta] \tag{11}$$

noting that the constant of integration K in the S/X data has dropped out

IV. Results of Analysis

A. Results of the December 1, 1978 Test

Figure 2 shows the total downlink range change for the December 1, 1978 pass divided into components due to ionosphere and space plasma Figure 3 shows the raw DRVID data points at S-band and a reconstructed S-band DRVID curve based on S/X doppler data and the model described in Section II There is no absolute level information in the S/X doppler data, so the absolute level of the derived DRVID curve has been adjusted to minimize the RMS difference Figure 4 shows the residuals from this adjustment The RMS fit error of the overall fit is comparable to the raw DRVID noise level as determined by linear detrending of short segments of the raw data

Figures 5 and 6 display the corresponding results for X-band DRVID Again, the RMS error over the entire fit is comparable to the data noise level The apparent discontinuity in the residuals at about 12 20 can definitely be ascribed to subreflector motion

B. Initial Results of the April 13, 1977 Test

Figure 7 shows the total downlink range change for the April 13, 1977 pass divided into components due to ionosphere and space plasma Figure 8 shows the raw S-band DRVID and the S/X derived DRVID for the April 13, 1977 Viking 2 pass Figure 9 is a plot of the residuals from this fit There is an obvious linear trend in the entire pass of residuals which a linear least squares fit gives as −3 98 RU/hr In terms of the allowable time gap of six hours between differenced range points specified in the Voyager SIRD, this amounts to a contribution of about 1 75 meters out of a total error budget of 6 4 meters The SIRD allocates only 0 5 meters for this error

C. A Detective Story

What are the possible sources of such an error? Some likely candidates are

(1) An error in setting the night time level for the ionosphere

(2) Errors in the S/X data Possibly frequency offset between S-band and X-band synthesizer frequencies

(3) An error in modeling location of plasma

In order to test item 3, a series of fits was made, assuming locations for the plasma ranging from near Earth to near spacecraft

Figure 10 shows the RMS residuals from these fits In none of these runs was there any substantial reduction in the apparent linear trend in the residuals

The measurements of ionospheric electron density from which the assumed ionosphere contribution is computed are derived from data taken by a Faraday rotation polarimeter These rotation data are supplied modulo 180 degrees of rotation As a result, the absolute electron density level may be in error by an amount corresponding to one or more 180° rotation mods

Re-examination of Section III, Eq (11) shows that the contribution to range change from an error in the ionosphere model is of the order of

$$\Delta R = \eta\,(\mathrm{TPLAS} - \mathrm{RTLT})$$

The second derivative of the ionosphere error due to setting the night time level incorrectly amounts to 0 049 m/hr^2 per mod For this case, TPLAS − RTLT is −825 seconds, resulting in a contribution of

$$\Delta R = \frac{0\,049\ \mathrm{m}}{\mathrm{hr}^2} \cdot -825\ \mathrm{sec} \cdot \frac{1\ \mathrm{hr}}{3600\ \mathrm{sec}}\ \mathrm{per\ mod} \cdot \frac{7\,05\ \mathrm{RU}}{\mathrm{m}}$$

or

$$\Delta R = -0\,079\ \frac{\mathrm{RU}}{\mathrm{hr}}\ \mathrm{per\ mod}$$

Thus an error of −3 98 RU/hr would require about a +50 mod ionosphere error, which is at least an order of magnitude too large

Finally, the minimum settable discrepancy between the S-band and X-band synthesizer frequencies is 10^{-5} Hz The fractional error would then contribute

$$\frac{10^{-5}\ \mathrm{Hz}}{\mathrm{VCO\ Hz}} \cdot \frac{48\ \mathrm{VCO\ RU}}{\mathrm{sec}} \cdot \frac{3600\ \mathrm{sec}}{\mathrm{hr}} \left[1 + \left(\frac{240}{221}\right)^2\right] = 3\ 76\ \mathrm{RU/hr}$$

which is exactly the error we are looking for

D. Final Result for the April 13, 1977 Test

Figures 11 through 14 show the raw DRVID data and the derived DRVID assuming a 1×10^{-5} Hz discrepancy between the S- and X-band synthesizer frequencies and the residuals of the fit between the two at both S- and X-band The residuals are flat to the noise level of the data Figure 15 shows the

RMS fit error as a function of the assumed position of the space plasma

V. Conclusions

For the December 1, 1978 test, the roundtrip calibrations derived from downlink S/X data are equivalent to the measured roundtrip effect at both S- and X-band to the level of observability in the DRVID data A glance at the computed plasma portion of the downlink range change (Fig 2) shows that it is within one or two range units of being a straight line over the entire pass In terms of the error equations derived in Section III, this means that the resulting roundtrip calibration on this particular occasion is quite insensitive to the assumed position along the ray path of such a plasma contribution

For the April 13, 1977 test, the derived data from S/X doppler match the measured DRVID at both S- and X-band to what appears to be the noise level of the DRVID data There is a well-defined minimum in the RMS fit as a function of the assumed plasma location at or near the nominal value (see Fig 15) These results together provide a validation of the assumptions upon which the S/X calibrations are currently based

References

1 MacDoran, P F , "A First-Principles Derivation of the Differenced Range Versus Integrated Doppler (DRVID) Charged-Particle Calibration Method," in *The Deep Space Network, Space Programs Summary 37-62, Vol II*, pp 28-33, Jet Propulsion Laboratory, Pasadena, Calif , Mar 31, 1970

2 Wu, S C and Winn, F B , "A Technique to Determine Uplink Range Calibration Due to Charged Particles," in *The DSN Progress Report 42-41*, pp 57-81, Jet Propulsion Laboratory, Pasadena, Calif , Oct 15, 1977

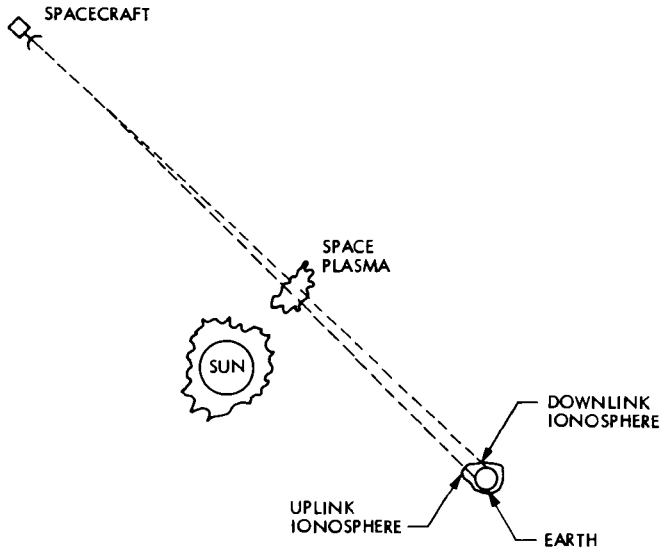

Fig 1 Assumed charged-particle distribution for S/X calibration model

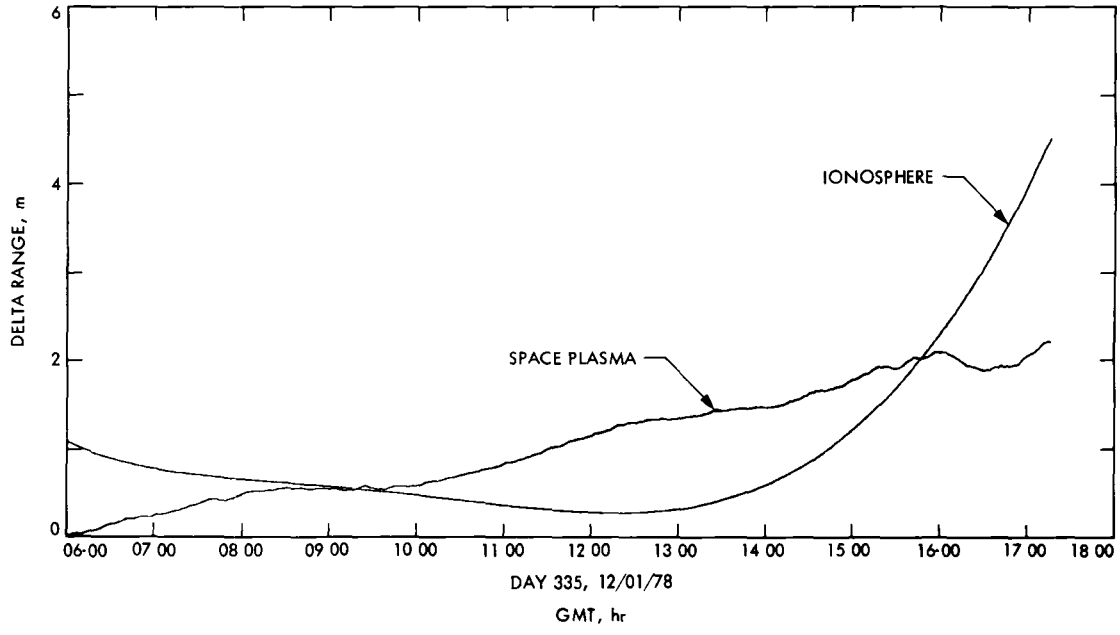

Fig. 2 Ionosphere and space plasma contributions to downlink range change on December 1, 1978

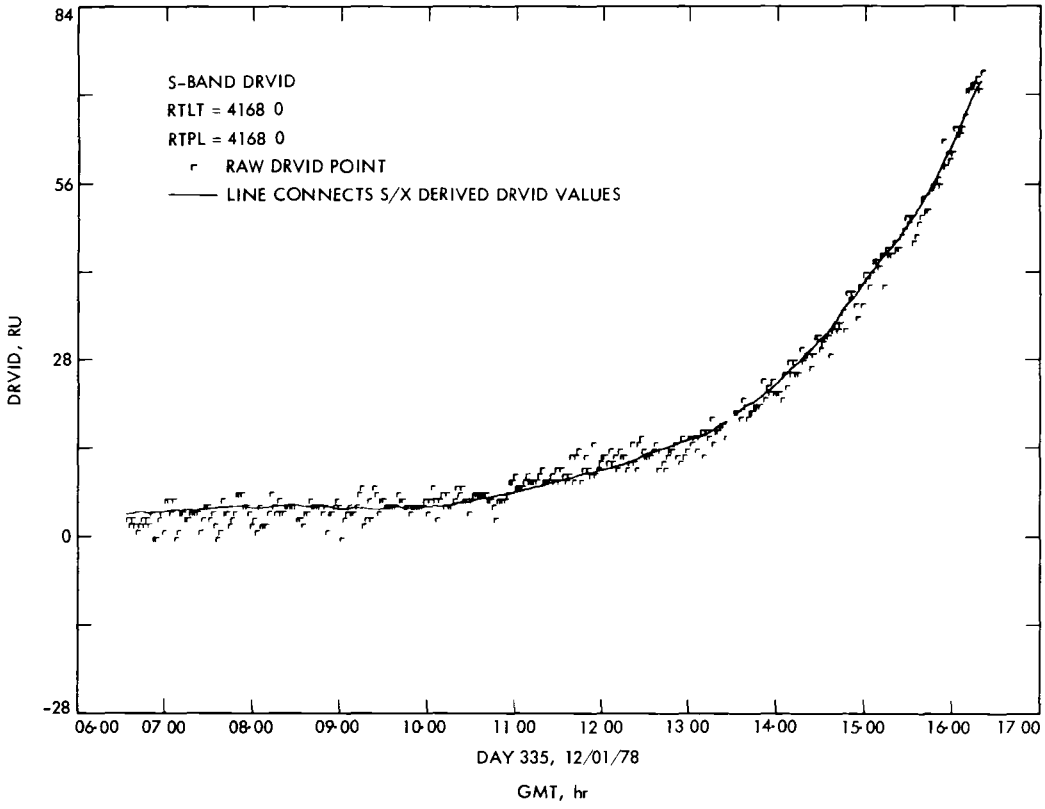

Fig 3 Raw and derived S-band DRVID for December 1, 1978

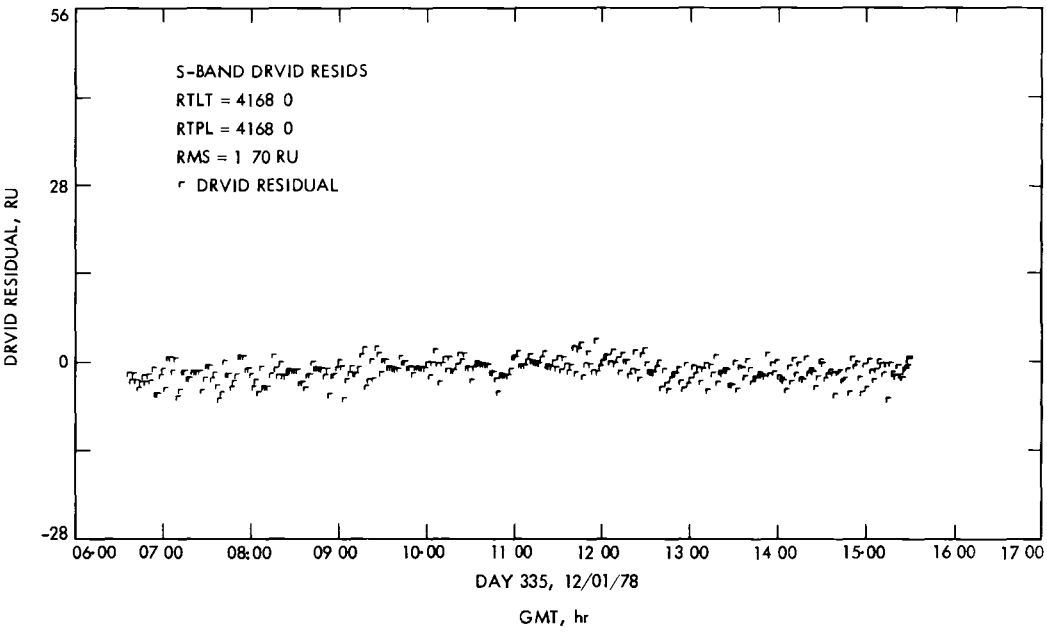

Fig. 4 S-band DRVID residuals (raw-derived) for December 1, 1978

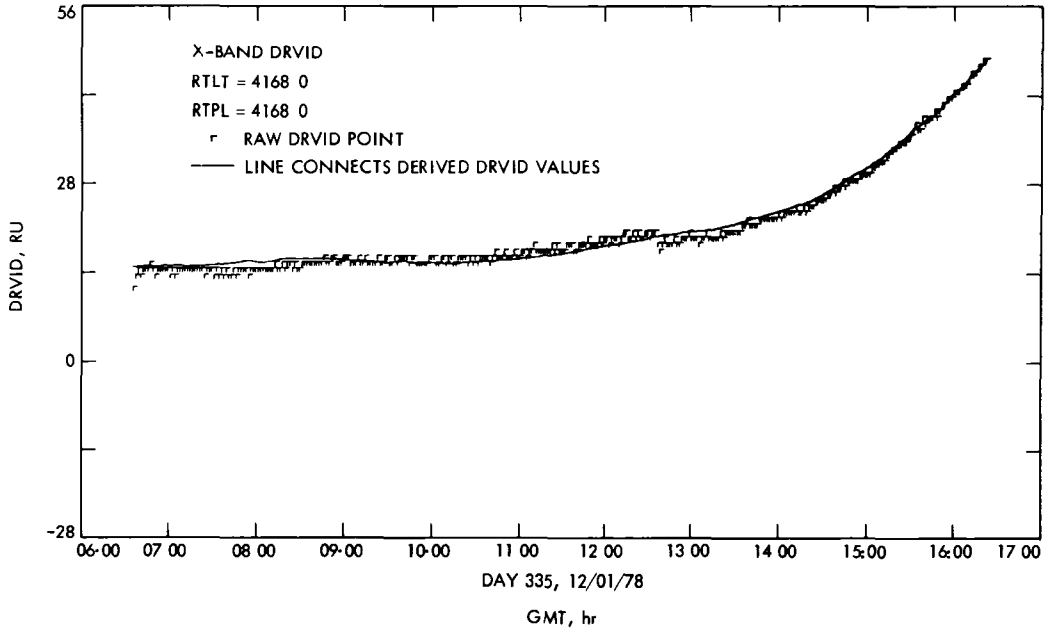

Fig 5. Raw and derived X-band DRVID for December 1, 1978

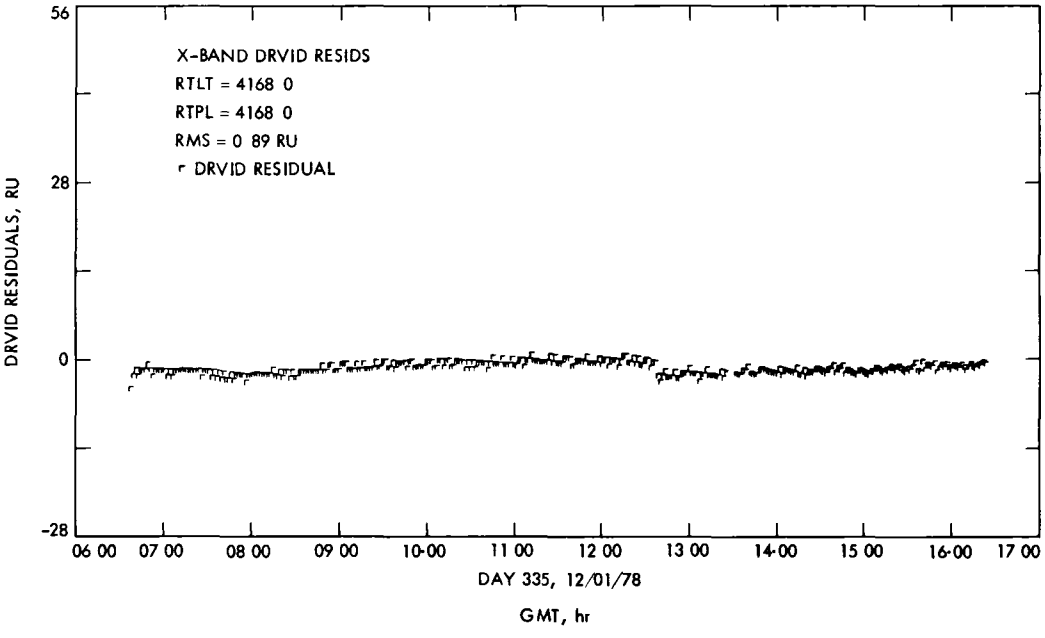

Fig 6 X-band DRVID residuals (raw-derived) for December 1, 1978

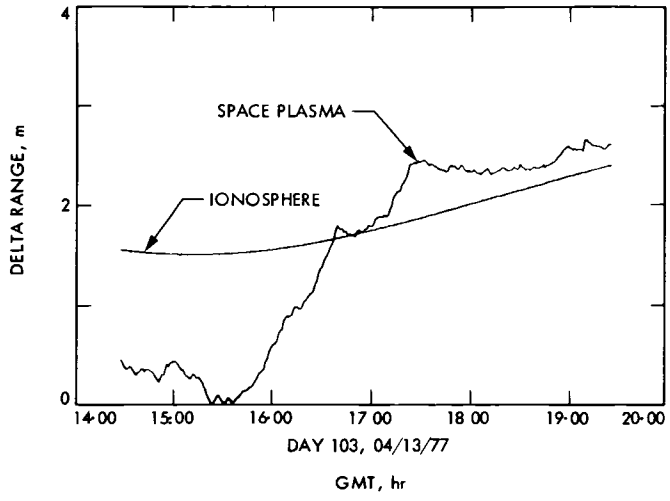

Fig 7 Ionosphere and space plasma contributions to downlink range change on April 13, 1977

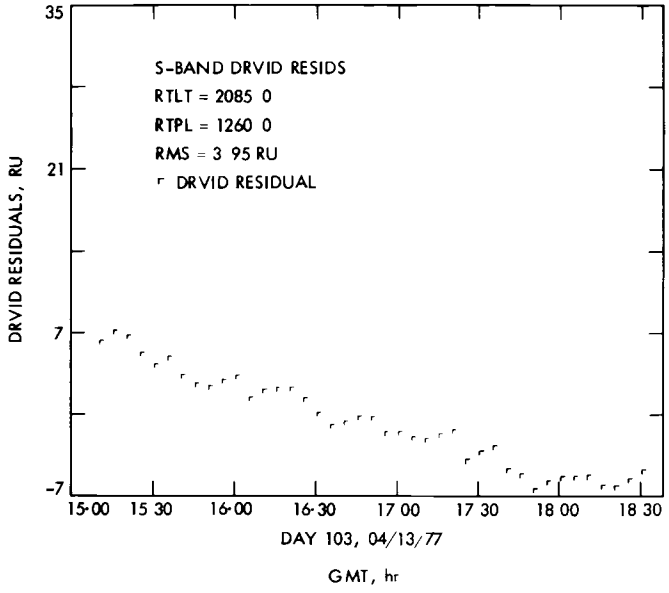

Fig 9 Initial S-band DRVID residuals (raw-derived) for April 13, 1977

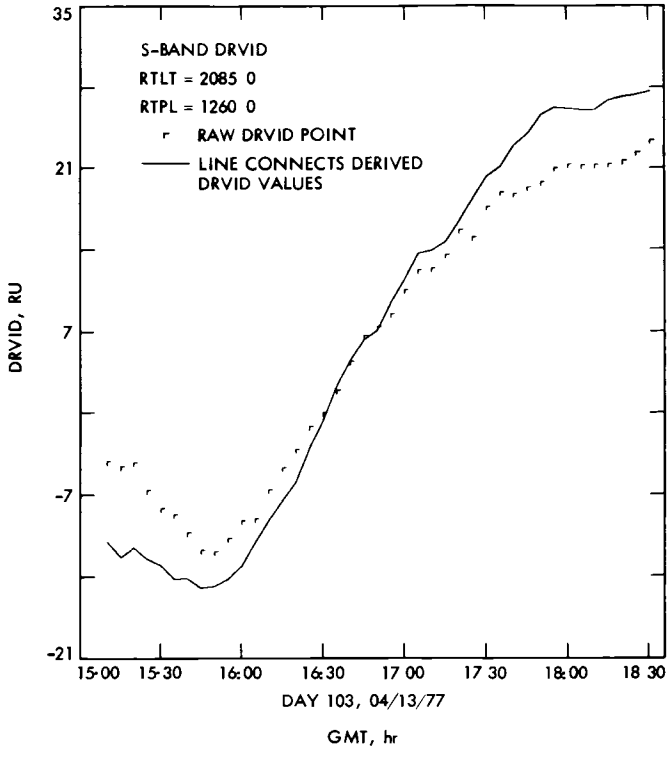

Fig 8 Initial raw and derived S-band DRVID for April 13, 1977

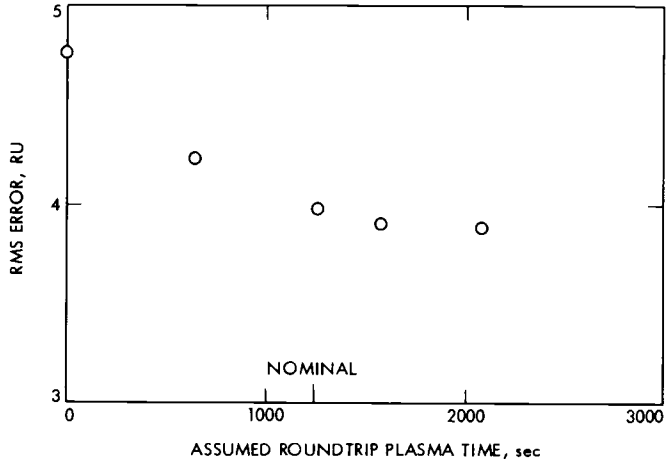

Fig 10 Initial RMS fit error vs assumed plasma location on April 13, 1977

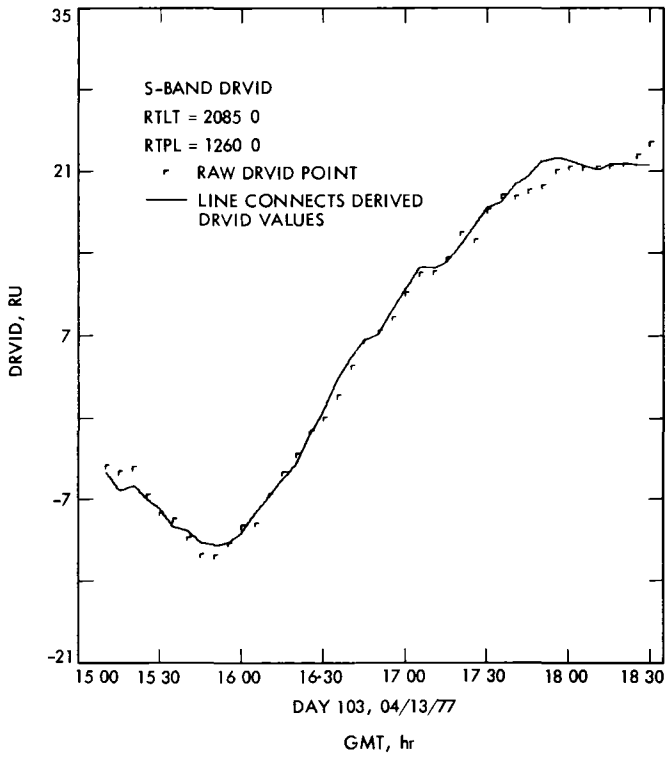

Fig 11 Final raw and derived S-band DRVID for April 13, 1977

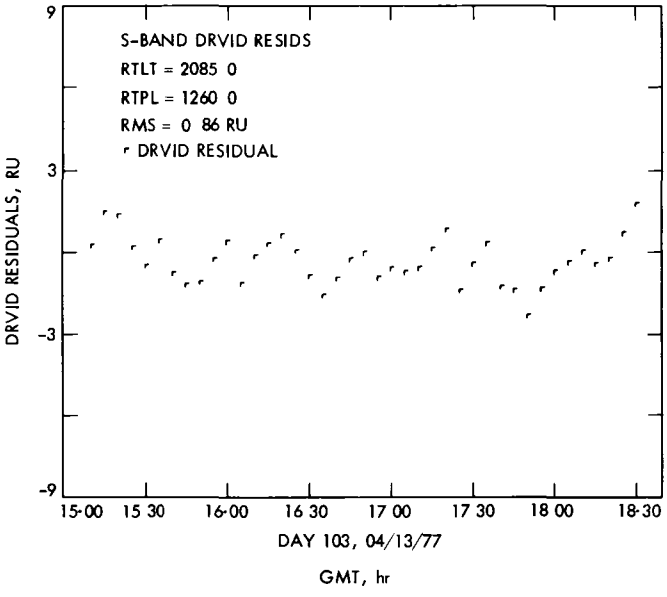

Fig 12 Final S-band DRVID residuals (raw-derived) for April 13, 1977

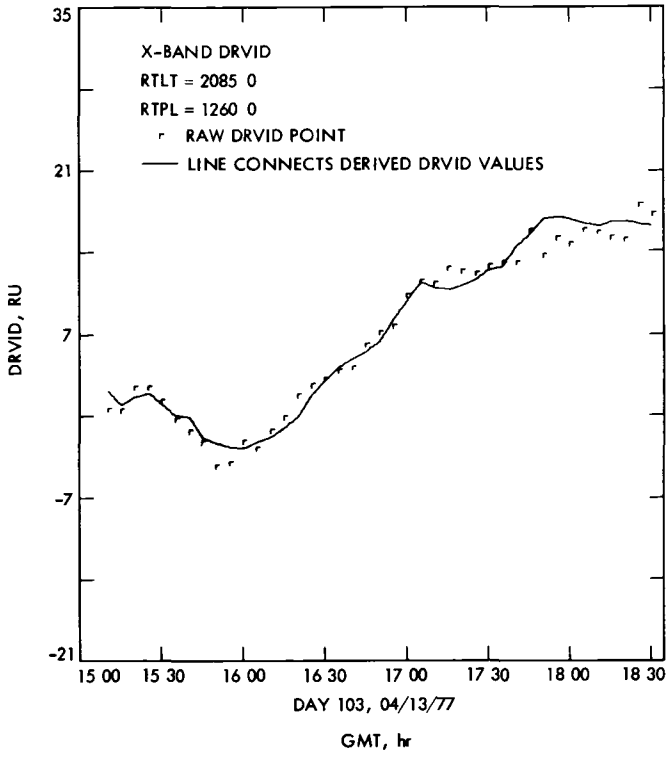

Fig 13 Final raw and derived X-band DRVID for April 13, 1977

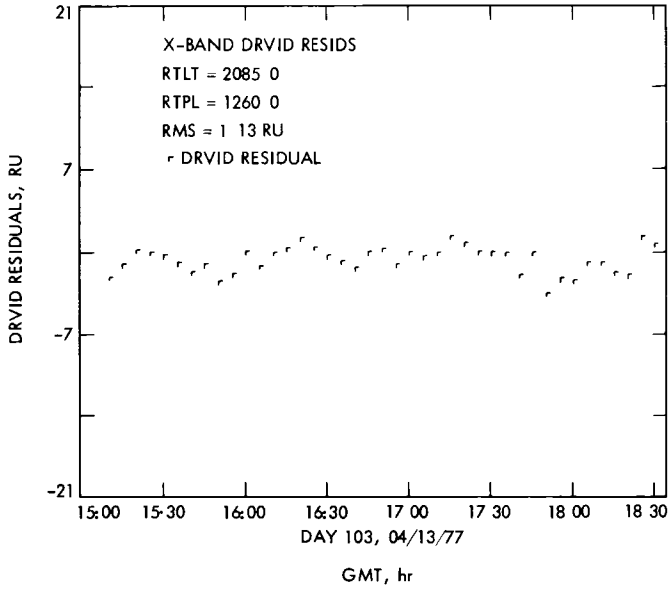

Fig 14 Final X-band DRVID residuals (raw-derived) for April 13, 1977

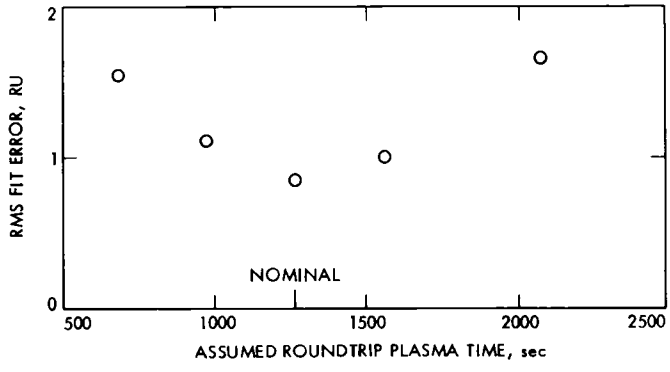

Fig 15 Final RMS fit error vs assumed plasma location on April 13, 1977

Operation of Joule-Thomson Refrigeration Above the Critical Pressure of Helium

D L Johnson
Radio Frequency and Microwave Subsystems Section

Recent emphasis on energy conservation has resulted in new efforts to develop more efficient, long-life refrigeration techniques for the DSN maser As the new techniques are developed, a comparison of their reliability and efficiency to those of the closed-cycle helium refrigerator presently used will have to be made Measurements of the refrigeration capacity have been made on an existing refrigeration system as a function of the supply pressure and the return pressure in the Joule-Thomson circuit The performance of the refrigerator has been calculated and compared to the ideal Carnot-cycle refrigerator

I. Introduction

A new effort has been undertaken to study efficient, long-life refrigeration techniques for the DSN masers Key areas requiring study and development are (1) highly efficient helium compression techniques capable of long unattended operation, (2) long-life seals and bearings, (3) improved system integration to increase the efficiency in the Joule-Thomson cooling process or (4) finding alternatives to the Joule-Thomson process, such as adiabatic demagnetization, to provide liquid helium temperatures at increased efficiencies

The closed-cycle helium refrigerators (CCRs) currently in use in the DSN were developed long before energy conservation became a major concern such that reliability was achieved at the expense of efficiency As a result over one million hours of operation has been logged on some thirty CCRs that have been installed in the DSN since 1967 (Ref 1) However, the CCR operates between room temperature and liquid helium temperatures with only about one percent of Carnot efficiency in producing one watt of refrigeration at 4 5 K

As possible steps to improve upon the efficiency of the CCR, studies and development are presently being undertaken in each of the three basic subsystems of the CCR the compressor unit, the expansion engine, which provides refrigeration down to 15 K, and the Joule-Thomson (J-T) circuit, which provides the final refrigeration between 15 and 4 5 K A schematic diagram of the CCR is shown in Fig 1

In an effort to reduce the electrical input power required to operate the compressor system, a new concept in the mechanical compression of a gas has been under development In the new approach, a centrifugal-reciprocating compressor concept has been developed which utilizes the centrifugal forces produced by the rotating pistons and the housing assembly to assist in the compression of the helium gas The performance of a single stage feasibility model has been demonstrated, and a mathematical analysis of the machine has been published (Ref 2) A patent application has been filed by NASA for the centrifugal-reciprocating compressor

In another area of development the regenerator matrix materials used in the 15 K expansion engine of the CCR are being studied The 15 K expansion engine utilizes the Gifford-McMahon thermodynamic cycle and has proven very reliable It is expected that the efficiency and reliability of the expansion engine may be improved by either improving upon the matrix of the presently used regenerator material or by using a substitute material Lake Shore Cryotronics, Inc , under contract to JPL (Ref 3), has developed a ceramic material which is thermodynamically superior (for $T < 25$ K) to the lead shot presently used as a regenerator material Testing of this ceramic material in an expansion engine will soon be conducted to measure its performance

Adiabatic demagnetization refrigeration (magnetic cooling) is yet another area of study and development The magnetic cooling process is being studied as a possible replacement of the J-T circuit now used in the CCR to provide the final stage of refrigeration Two major advantages of the magnetic cooling process over the J-T process would be its high reliability (since it is a solid state technique) and its high efficiency (60–80 percent of Carnot efficiency between 4 5 K and 15 K, compared with approximately 20 percent of Carnot efficiency for the J-T expansion circuit over the same temperature range) After initial testing of the paramagnetic salts, an experimental magnetic cooling system will be built and tested

The three areas of study and development mentioned above will be the subject of individual reports to be presented at a later time and thus will not be discussed further in this report Rather, the scope of this report has been focused on the operation of the present CCR to determine its refrigeration capacity under various operating conditions It is felt that the study of a more efficient refrigeration system should begin with a complete understanding of the refrigeration system as it presently exists This then provides the baseline for a comparative study as new materials or methods of operation are integrated into the system

The refrigeration capacity for the present CCR was measured in two separate tests First, the capacity was determined for various J-T supply pressures and various refrigerator supply pressures while holding a constant J-T return pressure Second, the capacity was again measured, this time as a function of the J-T return pressure while maintaining constant supply pressures to both the J-T circuit and the expansion engine In the second test particular attention was paid to the capacity measurements for return pressures above the critical pressure of helium ($2\ 27 \times 10^5$ N/m^2 (33 psia)) to determine how well the Joule-Thomson circuit would regulate when no liquid was being produced The performance of the CCR under these conditions was then calculated and compared to the ideal Carnot-cycle refrigerator Before discussing these tests and the test results, the method of thermometry used will first be described

II. Temperature Monitors

Temperature determination at the 4 5 K station was handled by two methods resistance thermometry and vapor pressure/gas thermometry A Lake Shore Cryotronics digital thermometer (Model DRC-70C) provided direct temperature readings using a silicon diode (Model DT-500-Cu) placed at the 4 5 K station (see Fig 1) A vapor pressure transducer, located in close proximity to the diode, connects to a pressure gauge outside the refrigerator and provides the other means of temperature sensing The temperature of this station dictates the pressure of the gas within the gauge At very low temperatures, a portion of the gas within the transducer will liquify In the small range of temperatures for which this liquid and its vapor will exist in equilibrium, the pressure gauge readings may be compared to a known temperature-vapor pressure curve to determine the temperature at the cold station Above this temperature range the device behaves as a gas thermometer, with the pressure readings being proportional to the temperature

The relationship between the two temperature sensing devices at various temperatures was measured by adjusting the J-T return pressure and by applying resistive heating to the 4 5 K station The results are shown in Fig 2 with the resistance thermometer readings plotted on the y-axis and vapor pressure readings plotted along the x-axis Also shown is the curve for the accepted values for the temperature-vapor pressure relationship as tabulated in the *American Institute of Physics Handbook* (Ref 4) The 0 1 K difference between the curves at the low pressures may be attributable to the calibration error of the digital thermometer The measured data were not corrected for this error The diode has been temperature cycled several times and has shown good repeatability in the data The 0 1 K sensitivity limit of the digital readout adds some additional uncertainty to the data at the low pressures The vapor pressure device was unable to maintain a liquid/vapor equilibrium to the $2\ 27 \times 10^5$ N/m^2 (5 2 K) limit as shown by the deviation of the shape of the measured curve from the AIP curve near $1\ 86 \times 10^5$ N/m^2 (27 psia) Thus, the vapor pressure thermometer should not be relied upon for accurate temperature measurements above $1\ 86 \times 10^5$ N/m^2 (4 9 K) where the device changes to a gas thermometer

III. Refrigeration Capacity Measurements

For a fixed pressure operation, the refrigeration capacity at the 4 5 K station of the CCR is determined primarily by the flow rate in the J-T circuit, by the temperature of the

15 K station, and by the efficiency of the heat exchanger between the 15 K station and the J-T valve This capacity is equal to the heat of vaporization of the liquid helium produced by the J-T expansion plus the heat capacity of the cooled gas that had not liquified by the J-T expansion Electrical input power levels below the cooling capacity will vaporize a fraction of the liquid reserve before reaching a new liquid/vapor equilibrium, power levels in excess of this cooling capacity will deplete the liquid reserve and warm the refrigerator It has also been observed that above 5 2 K, the critical temperature at which liquid helium can be maintained, the cooled gas from the expansion process also has a significant cooling capacity This will be discussed shortly

Determination of the refrigeration capacity of the CCR was made by applying an electrical load to the resistive heating element located on the 4 5 K station An electrical power load above the assumed capacity was applied to quickly deplete the reserve liquid in the system, causing the temperature and vapor pressure at this station to rise By incrementally decreasing the input power, the temperature and the vapor pressure were kept from rising above a nominal 4 8 K and $1\ 72 \times 10^5$ N/m^2 (25 psia), respectively (well below the critical temperature and pressure of 5 2 K and $2\ 27 \times 10^5$ N/m^2 (33 psia), respectively), so that the J-T expansion process would continue to produce liquid When the power was decreased to below the cooling capacity, the temperature and the vapor pressure dropped, indicating liquid was being stored This provided a quick method of approximating the capacity A more accurate capacity determination could then be made by applying power levels about this point for periods as long as one hour to determine the highest input power for which the temperature and the vapor pressure would stabilize In this manner the refrigeration capacity has been measured for three J-T supply pressures and two different refrigerator supply pressures while holding the J-T return pressure constant The results are tabulated in Table 1, where the refrigeration capacity has been denoted as Q_{meas} and the temperature of 4 5 K station as T_C (The remainder of the data in the table will be discussed later) The capacity measurements were made throughout the day, during which the ambient temperature surrounding the compressors would change The effect of the daily temperature cycling has been observed to produce up to a 50-mW capacity change on previous CCRs However, temperature changes of 7°C during the measurements on this CCR showed no noticeable change in the refrigeration capacity

The temperature variation as a function of the J-T return pressure and the various heat loads was also monitored The results have been tabulated in Table 2 and are shown in Figs 3 and 4 In Fig 3 the temperature at the 4 5 K station has been plotted as a function of the applied heat loads The values for the constant pressure curves are given for the no load condition since at the higher heater power levels the return pressure will decrease slightly Each pressure curve ends at the highest heater power for which the temperatures and pressures would stabilize, increasing the heater power beyond this point would cause the refrigerator to warm excessively (The power levels could be incremented in approximately 20-mW intervals) The maximum power level at which the stabilization occurs may be considered the cooling capacity for that particular J-T return pressure (or for that particular temperature)

Figure 3 shows that there is a nearly linear degradation in cooling capacity as the temperature is increased from 4 5 to 8 K, and that there is still a significant cooling capacity for temperatures above 5 2 K, the critical temperature above which liquid helium cannot exist Above this critical temperature the refrigeration capacity must be obtained non-isothermally from the sensible heat of the gas rather than from the isothermal heat of vaporization Although temperature and pressure regulation at the 4 5 K station should be difficult to maintain because of the low thermal capacity of the helium gas, the data show very little temperature change with change in heater power for temperatures below 6 K

While the present CCR relies on the liquid helium reserve to insure additional temperature stability, the operation of the CCR at increased J-T return pressures (so that the cold station temperature is above 5 2 K) also provides reasonable temperature stability This depends on the provision that the heat load of the device being cooled is sufficiently less than the refrigeration capacity of the CCR under these operating conditions

For the CCR tested, operating the J-T return pressure as high as $3\ 10 \times 10^5$ N/m^2 (3 atm) increased the temperature by only 1 1 K over the nominal 4 5 K achieved for the normal operating return pressure of just over an atmosphere This result is significant as there are numerous applications (such as cooling superconducting magnets or Josephson devices) that could be satisfied with an efficient and reliable 5 5 K refrigerator Another application could be the cooling of a maser since the refrigeration capacity of the CCR at 5 5 K is much greater than the heatload produced by an operating maser Although it may be desirable to optimize maser performance by operating the maser as cold as possible (Ref 5), there are other factors, such as energy requirements and reliability, which determine the necessary trade-offs to establish the temperature that provides the best overall performance The higher return pressure would permit a reduction in the electrical power requirements by operating with smaller compressors, which may also have the added advantages of prolonged maintenance-free operating times and an increased overall lifetime of the system

Figure 4 shows the temperature at the 4 5 K station as a function of the J-T return pressure Portions of several constant power curves have also been shown The vapor pressure curve has also been placed on the graph to show the similar shape between the vapor pressure curve and the J-T return pressure when no heater power is applied The return pressure curve appears to be a direct extension of the vapor pressure curve showing no discontinuity or change in slope as it extends beyond $2\ 27 \times 10^5$ N/m^2 (33 psia) The pressure differences between the two curves occur because the J-T return pressure gauge monitors the pressure at the room temperature gas line rather than at the 4 5 K station Restriction in the heat exchanger causes the pressure at the external pressure gauge to be lower than indicated by the vapor pressure gauge (It should be noted that the pressure drop due to this restriction has a small effect on the available refrigeration capacity and directly affects the temperature at which the refrigeration takes place (Ref 6)) The appropriate test points for pressure and temperature measurements are shown in Fig 1

IV. Refrigerator Performance Analysis

When a heat load corresponding to the cooling capacity of the machine is applied at the 4 5 K station, the temperatures of the incoming and outgoing streams of gas just above the third exchanger are equal Were they not, the system would either cool down or warm up To determine the performance of the J-T loop below the 15 K station, the remainder of the refrigerator may be thought of as a single compressor operating at 15 K This refrigerator may then be analyzed as if it were a Linde-Hampson refrigerator as shown in Fig 5 The Linde-Hampson refrigerator has been discussed thoroughly elsewhere (e g , see Refs 7, 8, and 9) so only a brief review of the analysis will be presented here

It will be assumed that the final heat exchanger is 100 percent effective, that there are no heat leaks into or out of the system, and that the J-T expansion represents the only irreversible pressure drop throughout the cycle shown in Fig 5 Under these conditions the heat absorbed from the source during one complete cycle may be expressed as

$$\frac{Q_{ref}}{m} = h_1 - h_2$$

that is, the net refrigeration per unit flow rate depends solely on the enthalpies of the incoming and outgoing gases, and is independent of what happens below the top of the heat exchanger If liquid is produced, the net work required by the compressor during one cycle (1-2-3-4-1) is

$$\frac{W_{net}}{m} = T_H (S_1 - S_2) - x(h_g - h_f) + (h_2 - h_3) - (h_1 - h_g)$$

where

$$x = (h_1 - h_2) / (h_1 - h_f)$$

is the fraction of the gas liquified and

$$h_3 = xh_f + (1 - x)h_g$$

If no liquid is produced, the cycle follows path (1-2-3′-4′-1), and the net work required is

$$\frac{W_{net}}{m} = T_H (S_1 - S_2) - (h_1 - h_2)$$

The performance of the refrigerator is expressed as the coefficient of performance by

$$COP = \frac{Q_{ref}}{W_{net}}$$

The efficiency of this refrigerator is determined by using the figure of merit of the refrigerator, defined by

$$FOM = \frac{COP}{COP_c} = \frac{Q_{ref}/W_{net}}{T_C/(T_H - T_C)}$$

where COP_c is the coefficient of performance for a reversible Carnot cycle, and the FOM varies from zero to unity The coefficient of performance and the figure of merit for the measured refrigeration capacity may be evaluated in the same manner

The results for the analysis have been included in Tables 1 and 2 The values for the entropies and the enthalpies used to determine W_{net} and Q_{ref} were estimated from the temperature-entropy diagram given in Ref 10 As the only other non-measured parameter, T_H was assumed to remain constant at 15 K throughout the measurements since there was no provision made to measure the temperature of the 15 K station The 15 K temperature is representative of the temperature of the 15 K station of the CCR when cooling a maser amplifier Heat loads in excess of this amount would raise the temperature of this station by an unknown additional

amount, resulting in a smaller difference between Q_{meas} and Q_{ref} (which depends on this temperature)

The results shown in Table 1 indicate that operating at the higher refrigerator supply pressure increased the refrigeration capacity at the 4 5 K station The increased supply pressure results in a lower temperature at the 15 K station In turn, the temperature of the J-T supply gas, which is in a recuperative heat exchange with the 15 K station, is lowered Expanding the gas at the lower temperature results in the increased cooling capacity The data presented in Table 2 show that the capacity increases with decreasing return pressure This is also consistent with the temperature-entropy diagram However, to insure contaminants will not be drawn into the gas lines, a positive pressure is maintained for the J-T return gas

V. Summary

Several important facts have been established with the testing of this CCR, which may be considered representative of all DSN CCRs First, the vapor pressure gauge worked very well at the extreme low temperatures, but should not be relied upon beyond $1\ 86 \times 10^5$ N/m^2 (27 psia) (4 9 K), where it prematurely begins to function as a gas thermometer In contrast, the resistance thermometer showed a very small but constant error across the 4 through 8 K range, which could be corrected to give accurate temperature readings Second, the maximum cooling capacity of this particular CCR was determined to be 1 00 W when operating with a refrigerator supply pressure of $2\ 20 \times 10^6$ N/m^2 (305 psig), a J-T supply pressure and return pressure of $1\ 82 \times 10^6$ N/m^2 (250 psig) and $1\ 11 \times 10^5$ N/m^2 (16 1 psia), respectively, and a compressor temperature of 25°C Finally, the refrigeration capacity and the temperature stability for J-T regulation above the critical temperature and pressure of 5 2 K and $2\ 27 \times 10^5$ N/m^2 (33 psia) remained quite high for temperatures and return pressures as high as 6 K and $3\ 44 \times 10^5$ N/m^2 (50 psia), respectively This cooling capacity at the increased return pressures is significant and may permit the utilization of smaller compressors with reduced power requirements

References

1 Higa, W H , and Wiebe E , "One Million Hours at 4 5 Kelvin," *Proc App of Closed-Cycle Cryocoolers to Small Superconducting Devices*, pp 99-108, Boulder, Colorado, Oct 1978 (published as NBS Spec Pub 508)

2 Higa, W H , *On the Characteristics of Centrifugal-Reciprocating Machines*, JPL Publication 79-108, Jet Propulsion Laboratory, Pasadena, California, Dec 1979

3 JPL Contract No 955446 entered with Lake Shore Cryotronics Inc , and the Jet Propulsion Laboratory

4 *American Institute of Physics Handbook*, Second Edition, edited by D E Gray, McGraw-Hill Book Company, Inc , New York, 1963

5 Siegman, A E , *Microwave Solid-State Masers*, Chapter 7, McGraw-Hill Book Company, New York, 1964

6 Dean, J W , and Mann, D B , "The Joule-Thomson Process in Cryogenic Refrigeration Systems," NBS Technical Note 227, National Bureau of Standards, Boulder, Colorado, 1965

7 Daunt, J G , "The Production of Low Temperatures Down to Liquid Hydrogen," in *Encyclopedia of Physics, Vol XIV Low Temperature Physics I*, edited by S Flugge, Springer-Verlag, Berlin, Gottingen, Heidelberg, 1956

8 Scott, R B , *Cryogenic Engineering*, D Van Nostrand Company, Inc , Princeton, 1959

9 Barron, R , *Cryogenic Systems*, McGraw-Hill Book Company, New York, 1966

10 McCarty, R D , "Thermodynamic Properties of Helium 4 from 2 to 1500 K at Pressures to 10^8 Pa," *J Phys Chem Ref Data*, Vol 2, p 923, 1973

Table 1 Refrigeration capacity as a function of refrigerator supply pressure and J-T supply pressure

Refrigerator Supply, $N/m^2 \times 10^5$ (psig)	22 04 (305)	22 04 (305)	22 04 (305)	20 31 (280)	20 31 (280)
Refrigerator Return, $N/m^2 \times 10^5$ (psig)	8 60 (110)	8 60 (110)	8 60 (110)	7 91 (100)	7 91 (100)
J-T Supply, $N/m^2 \times 10^5$ (psig)	20 31 (280)	18 25 (250)	16 18 (220)	18 25 (250)	16 18 (220)
J-T Return, $N/m^2 \times 10^5$ (psia)	1 11 (16 1)	1 11 (16 1)	1 11 (16 1)	1 11 (16 1)	1 11 (16 1)
J-T Flow, SCFM	1 48	1 39	1 25	1 38	1 28
T_C, K	4 7	4 6	4 5	4 5	4 5
COP_c	0 456	0 442	0 429	0 429	0 429
W_{net}, W	10 82	9 87	8 61	9 79	8 85
Q_{meas}, W (±0 02 W)	1 037	1 000	0 834	0 896	0 795
COP_{meas}	0 0958	0 101	0 0969	0 0915	0 0898
FOM_{meas}	0 210	0 229	0 226	0 213	0 209
Q_{ref}	1 81	1 60	1 31	1 59	1 35
COP_{ref}	0 168	0 162	0 152	0 162	0 153
FOM_{ref}	0 368	0 367	0 354	0 378	0 357

T_H = 15 K
CCR tested SN 78005

Table 2 Refrigeration capacity as a function of J-T return pressure

P_1, $N/m^2 \times 10^5$ (atm)	1 11 (1 1)	1 82 (1 8)	2 33 (2 3)	2 74 (2 7)	3 24 (3 2)	3 95 (3 9)	4 96 (4 9)	5 98 (5 9)
J-T Flow, SCFM	1 39	1 22	1 20	1 17	1 13	1 05	0 99	0 90
T_C, K	4 6	5 2	5 7	6 0	6 5	7 3	8 1	8 6
COP_c	0 442	0 531	0 613	0 667	0 765	0 948	1 17	1 34
W_{net}, W	9 87	7 11	6 32	5 45	4 81	4 15	3 34	2 58
Q_{meas}, W (±0 02 W)	1 000	0 896	0 803	0 703	0 616	0 489	0 396	0 294
COP_{meas}	0 101	0 126	0 127	0 129	0 128	0 118	0 119	0 114
FOM_{meas}	0 229	0 237	0 207	0 193	0 167	0 124	0 101	0 0851
Q_{ref}, W	1 60	1 31	1 21	1 13	1 05	0 884	0 726	0 606
COP_{ref}	0 162	0 184	0 191	0 207	0 218	0 213	0 217	0 235
FOM_{ref}	0 367	0 347	0 312	0 310	0 285	0 225	0 185	0 175

Refrigerator supply 22 04 × 10^5 N/m^2 (305 psig)	J-T Supply 18 25 × 10^5 N/m^2 (250 psig)
Refrigerator return 8 60 × 10^5 N/m^2 (110 psig)	T_H = 15 K
P_2 = 18 25 × 10^5 N/m^2 (18 atm)	CCR tested SN 78005

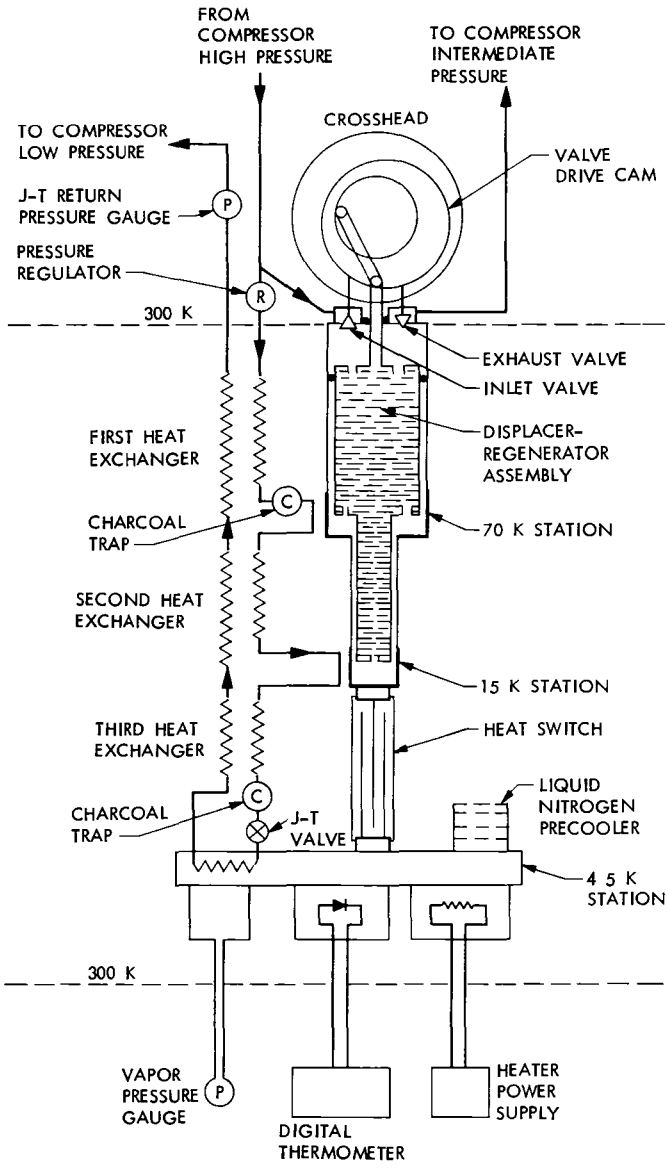

Fig 1 Schematic diagram for CCR

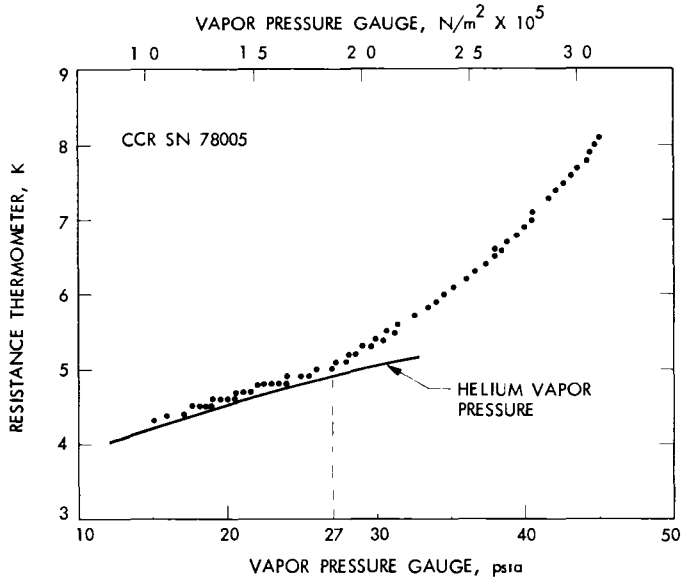

Fig 2 Comparison of temperature sensing devices

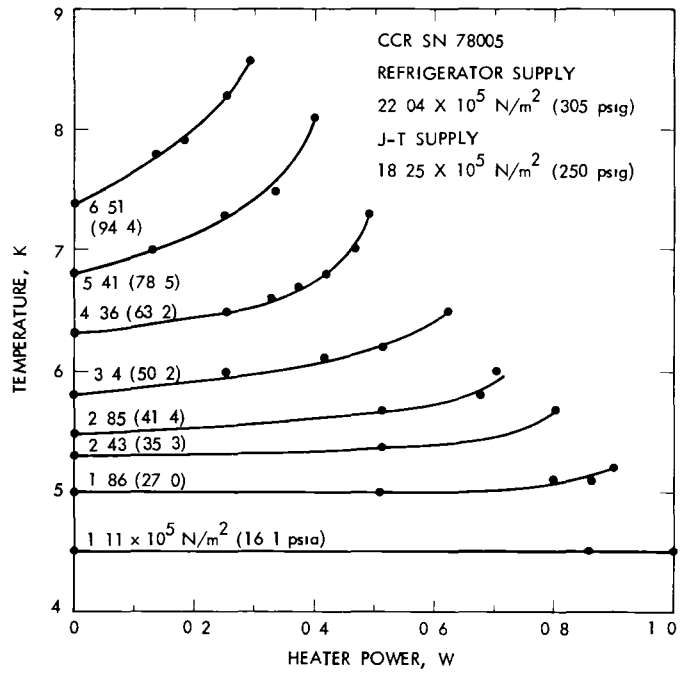

Fig 3 Temperature as a function of the applied heat load for several J-T return pressures

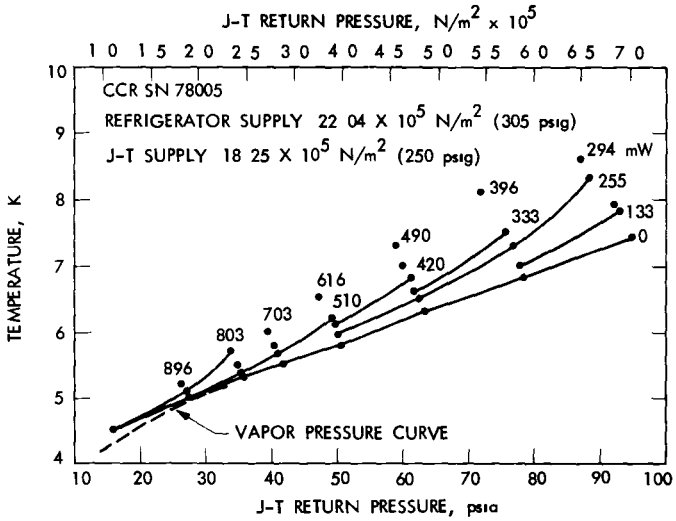

Fig 4 Measured cooling capacity as a function of J-T return pressure

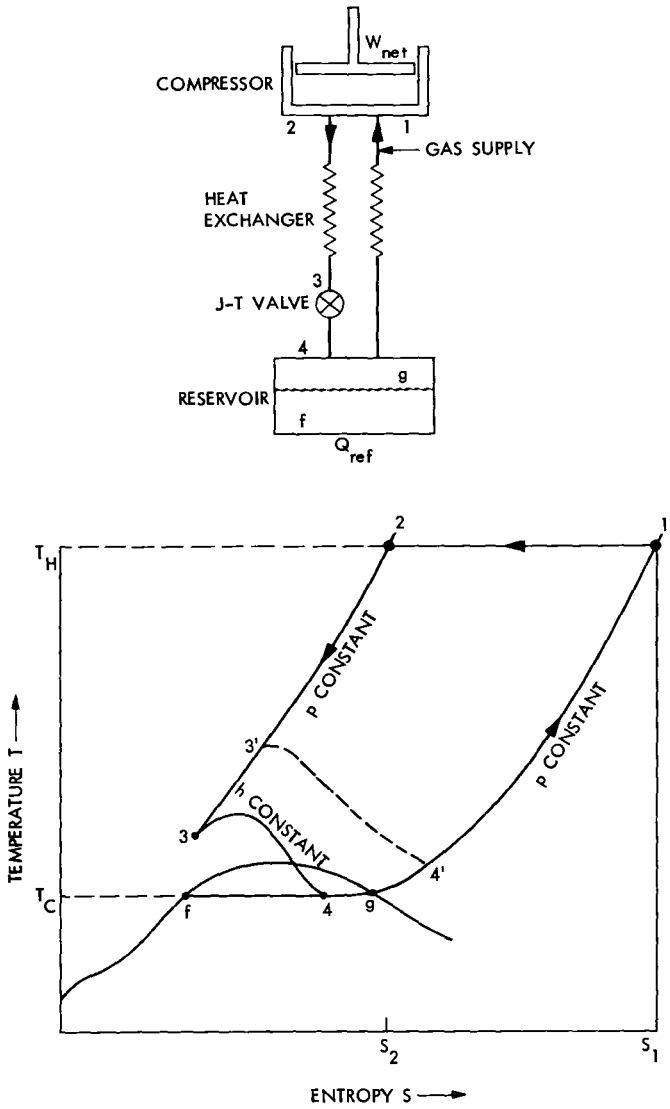

Fig 5 Thermodynamic cycle and flow diagram for Linde-Hampson refrigerator

Feasibility Study of a Spacecraft Surveillance System

C A Greenhall
Communications Systems Research Section

The International Comet Exploration spacecraft will spend 2 4 years in a solar electric propulsion stage (SEPS) cruise mode, during which the health of the spacecraft will be monitored at least once a day Although a daily two-hour DSN pass is now planned, the same surveillance function can be carried out by a much smaller, cheaper system The system studied here uses a commercial fast Fourier transform spectrum analyzer for noncoherent, synchronous detection of an alternating-tone signal received by a small parabolic antenna (0 8 to 3 m in diameter) Integration times vary from 3 7 to 9 5 min

I. Proposed Surveillance Method

The proposed International Comet Exploration (ICE) spacecraft will be capable of monitoring its own health during the solar electric propulsion stage (SEPS) cruise mode It would transmit one of several signals (five, perhaps) whose meanings range from "I'm OK" to "Help!" The signal would be detected by a small, dedicated ground receiving system If the spacecraft says that it has a problem or if no signal is detected, then a regular DSN tracking session would be scheduled

To reduce size, weight, and pointing accuracy requirements we shall try to make the ground antenna as small as possible The data rate can be as low as one word (two or three bits) per hour or per day Under these circumstances we choose noncoherent detection of a multiple frequency shift keyed (MFSK) signal by a spectrum analyzer The main problem is acquisition of the signal, which is corrupted by oscillator phase jitter, displaced by Doppler error, and smeared by Doppler rate error Consequently there is an upper bound on integration time, which in turn puts a lower bound on signal power, no matter how much time is nominally available for detection

Section II and Fig 1 describe the overall surveillance system and set down the assumptions used in the analysis Section III and Table 1 give four numerical examples The rest of the article (up to Section VIII) consists of back-up material Sections IV and V derive certain mission-dependent parameters (signal power and Doppler rate error) needed by the analysis, which is carried out in Sections VI and VII Conclusions are offered in Section VIII

II. Design Assumptions

A conceptual sketch of a surveillance system is given in Fig 1 We list and discuss our assumptions

(1) The *RF signal* consists of alternating *sine-wave tones* with frequencies f_0 and f_1, each held for the *word time* T_d (but see item (8) below) Such a signal is proposed in Refs 1 and 2 for MFSK acquisition The difference $f_1 - f_0$, having one of several possible values, constitutes the message word These values should be much less than *a priori* Doppler uncertainty, discussed below

(2) *Perfect word synchronization* is assumed The word time T_d is long enough (several minutes), the range is known well enough, and spacecraft time is accurate enough for the ground system to know when the transitions between f_0 and f_1 occur Word sync can be refreshed whenever the regular DSN tracks the spacecraft

(3) The *short-term frequency stability* of the spacecraft oscillator that generates the signal is specified by a plot similar to Fig 2, which plots the square root of Allan variance, $\Delta f/f_0$, vs integration time τ The behavior shown is typical of quartz crystal oscillators At τ_1 there is a transition between the behaviors $\Delta f/f_0 = \text{const}/\tau$ and $\Delta f/f_0 = \sigma_y = \text{const}$ To avoid signal power degradations above 1 dB we require

$$f_0 \sigma_y \tau_1 \leqslant 0\ 13 \tag{1}$$

which comes from Eq (13) below Typically, $\tau_1 = 0\ 5$ sec, in which case

$$\sigma_y \leqslant 10^{-10} \qquad \text{S-band}$$

$$\sigma_y \leqslant 3 \times 10^{-11} \qquad \text{X-band}$$

(4) The *transmitter power* is 5 W for S-band, 10 W for X-band All the radiated power goes into the surveillance signal At present, X-band is actually not suitable for this system (which is supposed to reduce the need for DSN tracking) because X-band downlink requires an uplink for pointing the spacecraft antenna Nevertheless, we have provided X-band designs in case a stand-alone X-band downlink is developed

(5) The *ground antenna* is a circular paraboloidal dish This assumption is intended only as a starting point for other designs, a circular beam shape may not be best for this application We shall design both tracking and nontracking systems In a *tracking* system the antenna stays pointed at the spacecraft for the length of time required by the detection process In a *nontracking* system the antenna is pointed at the correct declination on the meridian and the spacecraft sweeps through the beam Thus detection time is limited by the beamwidth The antenna has to be tilted slightly from day to day or week to week

A GaAsFET receiver is used See Table 2 for noise temperatures

(6) *Doppler* and *Doppler rate* uncertainty are critical to a MFSK system The signal must hold still long enough for it to be located Let v be the component of vehicle acceleration provided by the SEPS We assume a Doppler rate *error* f given by

$$f = \frac{2v}{\lambda} \tag{2}$$

where λ is the wavelength This is an upper bound for the error that would occur if the SEPS were to quit entirely or even start blasting in the wrong direction Our Doppler uncertainty bandwidth W is computed by letting f accumulate for one day

$$W = 86400 f \tag{3}$$

We compute a maximum SEPS acceleration of $1\ 8 \times 10^{-4}$ m/sec^2 during the SEPS cruise II, 1986 0 to 1988 4 (Section V below) This gives

$$f = 0\ 0028 \text{ Hz/sec}, W = 240 \text{ Hz at S-band} \tag{4}$$

$$f = 0\ 010 \text{ Hz/sec}, W = 870 \text{ Hz at X-band} \tag{5}$$

It is assumed that the prediction errors of all other contributions to Doppler and Doppler rate are less than these numbers To be conservative we shall make the bandwidth of the detection system at least W Actually, the system might be able to get by with less bandwidth because a large frequency deviation is itself cause for alarm Therefore, a DSN tracking session would be scheduled whether or not the surveillance system finds the signal

(7) A commercial FFT *spectrum analyzer* with 256 channels and a band analysis mode is assumed No time window shaping is used, we found that the uniform window performs better than a hanning window In the system of Fig 1 we use a heterodyne frequency f_h outside the nominal uncertainty band to avoid foldover of the spectrum

(8) The *detection strategy* uses "L-look" spectral analysis and threshold detection (Ref 3) as follows The bandwidth b of an analyzer channel must satisfy $256\ b > W$ Each data segment of duration $1/b$ results in a spectrum, the system sums L of these spectra and declares a signal present if the summed output of some channel exceeds a certain threshold above the average channel noise power Thus $T_d = L/b$ Once f_0 or f_1 is found, the analyzer bandwidth can be reduced for faster detection of the other frequency In fact, the spacecraft

might simply spend less time on f_1 than on f_0 Acquisition would be made on f_0 (perfect word sync assumed), then f_1 would be detected with a narrower bandwidth Other schemes suggest themselves, here we shall examine only the acquisition problem

Other assumptions about the mission appear in Sections IV and V

III. Sample Design Parameters

Table 1 gives the numerical parameters that define four possible surveillance systems For both S-band and X-band we have designed a tracking system and a nontracking system The tracking systems, in which the antenna follows the spacecraft for as long as the detection system needs to see the signal, represent the lowest antenna gains consistent with a detection error probability of 10^{-4} This minimum gain is approximately proportional to the square root of the Doppler rate error f (Eq (29) below) Antenna diameter is 2 3 m for S-band, 0 8 m for X-band The nontracking systems, in which the spacecraft sweeps across the stationary antenna beam, use slightly larger antennas (3 m for S-band, 1 2 m for X-band) because the reduced detection time requires more signal power While the nontracking systems are mechanically less complex than the tracking systems, they are also less flexible and reliable because they have only one brief shot per day at the spacecraft

No margins have been built into these designs except for those created by our approximations (positive, we hope) Actual systems might have to use antennas with higher gains and narrower beams

IV. Power-to-Noise Ratios

Using a design control table format (Table 2), we derive the ratio P/N_0 for an ideal isotropic ground antenna, where

P = carrier power

N_0 = one-sided noise spectral density

Maximum range, $5\,8 \times 10^8$ km (3 9 AU), is assumed

The results are

$$\left(\frac{P}{N_0}\right)_{\text{ISO}} = 5\,4 \times 10^{-4}\ \text{sec}^{-1} \qquad \text{S-band}$$

$$= 6\,0 \times 10^{-4}\ \text{sec}^{-1} \qquad \text{X-band}$$

V. SEPS Acceleration

Standard rocket equations (Ref 4) give

$$v = \frac{2P}{MgI}$$

where

v = vehicle acceleration due to rocket propulsion

P = power expended on propellant

M = vehicle mass

I = specific impulse = V/g, V = exhaust speed

g = Earth gravity, 9 8 m/sec^2

Near the end of the long SEPS cruise, just before the Tempel 2 rendezvous, 3 thrusters will be used with 10 kW available to them We estimate $P = 5630$ W, $M = 2200$ kg, $I = 2940$ sec Therefore,

$$v = 1.8 \times 10^{-4}\ \text{m/sec}^2$$

At the time of greatest range, 1987 7, we estimate

$$v = 6\,3 \times 10^{-5}\ \text{m/sec}^2$$

To be conservative we shall design for a combination of maximum acceleration and maximum range

VI. *L*-Look Spectral Analysis

This section is about threshold detection by a spectrum analyzer of a corrupted sine wave in white Gaussian noise For a pure sine wave, see Ref 3 Here, we attempt to account for the degradations due to (1) position and drift of the signal relative to nearby analyzer channels, and (2) short-term oscillator phase jitter Our analysis is approximate and incomplete, representing the best we have been able to achieve in the time available A rigorous treatment would be a research project Throughout, we neglect the effects of sampling

A. Analyzer Channel Outputs

Let X be the (suitably normalized) sum of L successive outputs of a particular analyzer channel of width b Then X is approximately a scaled version of a noncentral chi-squared random variable with $2L$ degrees of freedom (Ref 3) Its mean and standard deviation are approximately

$$E(X) = N_0 b + P' = N_0 b(1 + r') \tag{6}$$

$$\sigma(X) = \frac{N_0 b}{\sqrt{L}} \sqrt{1 + 2r'} \tag{7}$$

where $r' = P'/(N_0 b)$ and P' is the average signal power in the channel during the L looks If the channel contains only noise then $r' = 0$, else

$$\left.\begin{aligned} r' &= r G_{pd} G_j \\ r &= \frac{P}{N_0 b} \end{aligned}\right\} \tag{8}$$

where G_{pd} is the loss (<1) from position and drift of the signal during the L looks, and G_j is the loss from short-term jitter of the spacecraft oscillator Because these two losses are actually intertwined, they deserve a unified treatment For the present, we simply compute them separately and multiply them

B. Position and Drift Loss G_{pd}

This loss depends on the Doppler rate error f In time L/b the signal frequency drifts by Lf/b, in units of the channel width b the *drift width* is

$$\delta = \frac{Lf}{b^2} \tag{9}$$

Let the frequency origin be centered in the channel Let mb be the signal frequency at the midpoint of the L-look time interval If $m = 0$ the midpoint of the frequency drift is at the center of the channel, if $m = 1/2$ the drift midpoint is at an edge of the channel We call these cases the *center case* and the *edge case* If the drift during a single look is much smaller than b, then G_{pd} is approximately the average of $\mathrm{sinc}^2(\pi f/b)$ over the drift interval, thus

$$G_{pd} = G_{pd}(m, \delta) = \frac{1}{\delta} \int_{m-\delta/2}^{m+\delta/2} \left(\frac{\sin \pi u}{\pi u}\right)^2 du \tag{10}$$

C. Jitter Loss G_j

Using a spectrum analyzer, first observe a perfect sine wave whose frequency is centered in one of the channels Then replace the sine wave by a real oscillator having the same average power Because of short-term phase jitter, the height of the spectral peak will decrease According to Ref 2, measurements of S-band transmitters have placed this "spectral mean loss" between 0 3 dB and 1 5 dB According to Ref 5, it is difficult to include this loss in performance evaluations because little is known about the exact characteristics of phase jitter We shall nevertheless use the information in the Allan variance plot (Fig 2) to obtain a theoretical estimate of the jitter loss G_j The result will put an upper bound on the long-term Allan variance σ_y^2 and a lower bound on the channel bandwidth b

If the oscillator were modulated by either a stationary phase process $\theta(t)$ or a stationary frequency process $\theta(t)$ the situation would be in hand because the oscillator output

$$x(t) = \cos\left[2\pi f_0 t + \theta(t) + \theta_0\right]$$

would be stationary (We assume θ_0 is uniformly distributed and independent of $\theta(t)$) Assuming that $\theta(t)$ is Gaussian, Middleton (Ref 6) and others compute the spectrum of $x(t)$ given the spectrum of $\theta(t)$ or $\theta(t)$

Unfortunately, the typical Allan variance behavior $\Delta f/f_0 = \sigma_y = \text{const}$ for large τ indicates the presence of nonstationary "flicker of frequency" modulation Previous theory does not apply Since the behavior $\Delta f/f_0 = \text{const}/\tau$ for small τ indicates that a stationary phase process is also present, we adopt the following model for $\theta(t)$

$$\theta(t) = \phi(t) + \psi(t)$$

where $\phi(t)$ and $\psi(t)$ are independent Gaussian processes, $\phi(t)$ is stationary, and $\psi(t)$ has stationary second differences The relevant second moment properties of $\phi(t)$ and $\psi(t)$ are characterized from Fig 2 by

$$\sigma^2(\phi) = \frac{1}{3}(2\pi f_0 \sigma_y \tau_1)^2 \tag{11}$$

$$S_{\psi\psi}(2\pi f) = \frac{f_0^2 \sigma_y^2}{(\ln 4) f^3} \tag{12}$$

where $S_{\psi\psi}$ is the one-sided spectral density of $\psi(t)$ The $1/f^3$ spectrum has a rigorous meaning in the theory of processes with stationary nth differences Eq (11) does not depend on the shape of the spectrum of $\phi(t)$ as long as $1/\tau_1$ is much smaller than the bandwidth of $\phi(t)$ One obtains Eqs (11) and (12) from conventional stationary-process formalism by integrating the Allan-variance filter response times the spectral density of $\theta(t)$

In Appendix A we derive the following approximation for the jitter loss

$$\ln\left(\frac{1}{G_j}\right) = (2\pi f_0\sigma_y)^2\left(\frac{\tau_1^2}{3} + \frac{1}{(36\ln 4)b^2}\right) \quad (13)$$

Although the analysis is not rigorous, the author believes that Eq (13) shows the main dependencies of the loss on the Allan-variance turnover point (τ_1, σ_y) and the channel width b The first term on the right comes from the stationary noise $\phi(t)$ and is already well understood The second term comes from the flicker-noise jitter $\psi(t)$, as b gets smaller, the integration time gets longer, and the effect of the low-frequency phase variations predominates

Within the confines of the analysis, Eq (13) actually gives an upper bound for the loss We suggest using it as long as it indicates a loss below about 2 dB

D. Detection Criteria

We set a detection threshold $N_0 b\eta$, where $1 < \eta < r'$ A signal is detected if the outputs of a set of adjacent channels are more than $N_0 b\eta$, and all other channel outputs are less than $N_0 b\eta$

Fix an error probability ϵ Anticipating the discussion below, we define z_0, z_1, and z_2 by

$$Q(z_0) = \frac{\epsilon}{n}, Q(z_1) = \epsilon, Q(z_2) = \sqrt{\epsilon} \quad (14)$$

where n is the number of channels and $Q(z)$ is the probability that a standard Gaussian is more than z

Suppose that no channel has a signal The probability of false detection is approximately

$$P_{FD} = nP\{X > N_0 b\eta | r' = 0\}$$

Setting $P_{FD} = \epsilon$ we obtain from Appendix B that

$$\eta = 1 + \frac{x_0}{\sqrt{L}} \quad (15)$$

where

$$x_0 = z_0\sqrt{1 - 1/(4L)} + \frac{1}{2}(z_0^2 - 1)\sqrt{1/(4L)} \quad (16)$$

Since $N_0 b$ can be estimated as the average channel power, Eq (15) determines the threshold

Suppose that a signal is present The probability that we miss it or that a spurious channel output exceeds the threshold is approximately

$$\prod_k P\{X < N_0 b\eta | r' = r'_k\} + P_{FD} \quad (17)$$

where r'_k is the effective SNR in the kth channel We require the first term of Eq (17) to be at most ϵ This term depends on the drift center m and the drift width $\delta = Lf/b^2$ For a given f, δ is at our disposal but m is not Thus our detection strategy has to work for all m Without loss of generality we can assume $0 \leqslant m \leqslant 1/2$ Lack of time forces us to consider only the center case $m = 0$ and the edge case $m = 1/2$ Also, we assume $\delta \leqslant 2$ so that at most two channels have significant amounts of signal

For the *center case* we consider only one channel in Eq (17) Setting

$$P\{X < N_0 b\eta\} = \epsilon$$

We obtain from Appendix B that

$$\eta = 1 + r' - \frac{x_1\sqrt{1 + 2r'}}{\sqrt{L}} \quad (18)$$

where

$$x_1 = z_1\sqrt{1 - \beta/(4L)} - \frac{1}{2}(z_1^2 - 1)\sqrt{\beta/(4L)} \quad (19)$$

$$\beta = \frac{1 + 2r'}{(1 + r')^2} \quad (20)$$

and r' is calculated using $G_{pd}(0, \delta)$ From Eqs (15) and (18) we get the detection criterion

$$r' = \frac{x_0 + x_1\sqrt{1 + 2r'}}{\sqrt{L}} \quad (21)$$

for the center case

In the *edge case* the two channels on either side of the drift midpoint $m = 1/2$ see an equal amount of signal Therefore we set

$$[P\{X < N_0 b\eta\}]^2 = \epsilon$$

which leads as before to

$$\eta = 1 + r' - \frac{x_2\sqrt{1+2r'}}{\sqrt{L}} \tag{22}$$

where

$$x_2 = z_2\sqrt{1-\beta/(4L)} - \frac{1}{2}(z_2^2 - 1)\sqrt{\beta/(4L)} \tag{23}$$

and r' is calculated using $G_{pd}(1/2, \delta)$ The detection criterion for the edge case is

$$r' = \frac{x_0 + x_2\sqrt{1+2r'}}{\sqrt{L}} \tag{24}$$

Let ϵ, f, and b be fixed Given δ (or L) the right sides of Eqs (21) and (24) depend slowly on r', so they can be iterated to get the required r' for the center and edge cases Computing $G_{pd}(m, \delta)$ ($m = 0$ and $1/2$) and G_l we get the channel SNR

$$r = \frac{P}{N_0 b} = \frac{r'}{G_{pd} G_l}$$

as two functions of δ, say $r_1(\delta)$ (center case) and $r_2(\delta)$ (edge case) Since we don't know which case holds we must choose the worst one by setting

$$r(\delta) = \max\,[r_1(\delta), r_2(\delta)] \tag{25}$$

Finally, we get the optimum values of δ and L, and the minimum required r, by minimizing Eq (25)

$$r_{\min} = r(\delta_{\text{opt}}) = \min_{\delta \leq 2} r(\delta) \tag{26}$$

$$L_{\text{opt}} = \frac{\delta_{\text{opt}} b^2}{f} \tag{27}$$

In the two examples below it turns out that the point (δ_{opt}, $r_{\min}$) is the intersection of the $r = r_1(\delta)$ and $r = r_2(\delta)$ curves (Fig 3) For $\delta < \delta_{\text{opt}}$, $r_2(\delta)$ is larger, for $\delta > \delta_{\text{opt}}$, $r_1(\delta)$ is larger For both examples, $\delta_{\text{opt}} = 1\ 6$ approximately

We can explain this from another point of view For a given r there is a range of L that will support detection with a given error probability If L is too small there is not enough time to build up the signal over the noise If L is too large the drift spreads the signal over several channels The minimum r is the one that shrinks this L-range to a single point

Suppose now that $r > r_{\min}$ Assume that for $\delta < \delta_{\text{opt}}$ the edge case applies $r_2(\delta) > r_1(\delta)$ The required L can be found by iterating

$$L = \left[\frac{x_0 + x_2\sqrt{1+2r'}}{r'}\right]^2 \tag{28}$$

whose right side depends slowly on L

E. Approximations

Put $\epsilon = 10^{-4}$, $\delta_{\text{opt}} = 1\ 6$, $G_{pd} = G_{pd}(1/2, 0) = 0\ 41$, and compute G_l from Eq (13) Then

$$(P/N_0)_{\min} = r_{\min} b = \frac{8}{G_{pd} G_l \sqrt{\delta_{\text{opt}}}}\sqrt{f} \tag{29}$$

$$T_d = \frac{L}{b} = \left[\frac{8}{G_{pd} G_l}\right]^2 \frac{b}{\left(\frac{P}{N_0}\right)^2} \tag{30}$$

for $P/N_0 \geq (P/N_0)_{\min}$

VII. Tracking and Nontracking Systems

A. Design Equations

From Ref 7 we extract some nominal relationships for parabolic antennas Let d = diameter, λ = wavelength, θ = angle off-axis Then

On-axis gain $G_a = (7\pi/4)(d^2/\lambda^2)$

Half-power beamwidth $\theta_a = 63\ \lambda/d$ deg

Off-axis gain $G(\theta) = G_a \exp(-\ln 16\ \theta^2/\theta_a^2)$

We get the weakest possible tracking system by specifying G_a such that

$$G_a r_{\text{iso}} = r_{\min}$$

where $r_{iso} = (P/N_0)_{iso}/b$ The only *a priori* restriction on the word time $T_d = L_{opt}/b = \delta_{opt}\ b^2/f$ is the tracking time available

If the antenna is fixed, the spacecraft simply passing through the center of the beam, then word time is limited We arbitrarily designate the *available antenna time* by

$$T_a = 240\ \theta_a \text{ sec}$$

the time it takes a point on the celestial equator to traverse an angle $\theta_a/2$ If the r_{min} system happens to have $T_d > T_a$ then we must increase G_a until $T_d \leq T_a$ This can always be done because $T_d = L/b$ is roughly proportional to $1/r^2$, whereas T_a is proportional to $1/\sqrt{r}$ We also have to account for the varying gain as the spacecraft sweeps across the beam Since the average value of $G(\theta)/G_a$ for $|\theta| \leq \theta_a/2$ is 0 81, we shall simply insert this extra loss into Eq (8) This is a makeshift adjustment, of course

The system that makes $T_d = T_a$ can be obtained from the following iteration on δ, starting with $\delta = 1$

$$\left.\begin{aligned} L &= \frac{\delta b^2}{f} \\ r &= \frac{17700^2 r_{iso} b^2}{L^2} \\ r' &= 0\,81\ G_J G_{pd}\,(1/2, \delta)\ r \\ \delta &= \frac{f}{b^2}\left[\frac{r' L^2}{x_0 + x_2\sqrt{1+2r'}}\right]^{2/3} \end{aligned}\right\} \quad (31)$$

A $T_d = T_a$ system leaves little room for error, there are at most two chances to acquire the signal We have computed this option simply to find out what can be done with a nontracking parabolic antenna One might design an r_{min} system using a nontracking fan-beam antenna with the wider dimension of the beam oriented east to west The beamwidth would allow the spacecraft to stay in the beam for several word times The antenna would probably have to be adjusted daily in declination

B. Derivation of the Examples

1 S-band Recall that $f = 0\,0028$ Hz/sec, $(P/N_0)_{iso} = 5\,37 \times 10^{-4}$ sec^{-1} From Eq (4) we choose an analyzer bandwidth of 250 Hz (the next bandwidth above 240 Hz for the analyzer we have in mind) Since we assume $n = 256$ channels, we have $b = 1$ Hz Equation (13) with $\sigma_y = 10^{-10}$, $\tau_1 = 0\,5$ sec gives $G_J = 0\,81$

To derive the r_{min} (tracking) system we plot r vs δ for the center and edge cases (Fig 3) The intersection gives $\delta_{opt} = 1\,59$, $r_{min} = 0\,925$ Then $L = \delta_{opt} b^2/f = 568$ looks, $T_d = L/b = 568$ sec The antenna parameters are $G_a = r_{min}/r_{iso} = 1723$, $d = 2\,30$ m, $\theta_a = 3\,56$ deg, and $T_a = 427$ sec

The iteration Eq (31) gives the $T_d = T_a$ (nontracking) system Parameters are $\delta = 0\,909$, $L = 325$ looks, $G_a = 2967$, $d = 3\,02$ m, $\theta_a = 2\,71$ deg, and $T_a = T_d = 325$ sec

2 X-band Start from $f = 10^{-2}$ Hz/sec, $(P/N_0)_{iso} = 6\,03 \times 10^{-4}$ sec^{-1} The analyzer bandwidth is 1000 Hz, so $b = 4$ Hz Equation (13) with $\sigma_y = 3 \times 10^{-11}$, $\tau_1 = 0\,5$ sec gives $G_J = 0\,81$ From Fig 2 we get the r_{min} system $\delta_{opt} = 1\,63$, $r_{min} = 0\,409$, $L = 2608$ looks, $T_d = 652$ sec, $G_a = 2715$, $d = 0\,791$ m, $\theta_a = 2\,83$ deg, and $T_a = 340$ sec

The parameters of the $T_d = T_a$ system are $\delta = 0\,554$, $L = 886$ looks, $G_a = 6387$, $d = 1\,21$ m, $\theta_a = 1\,85$ deg, and $T_a = T_d = 222$ sec

VIII. Conclusions

Provided that certain assumptions about Doppler rate error and spacecraft oscillator phase stability are met, an alternating-tone signal from a spacecraft 4 AU away can be acquired by a ground antenna a few meters in diameter, a receiver with noise temperature of order 200 K, and a commercial 256-channel spectrum analyzer Although our design examples assume parabolic antennas, other types such as fan-beam antennas or electronically steerable arrays should be studied, especially if one wants to avoid mechanical tracking

Our analysis has included an estimate of the effect of oscillator flicker noise on MFSK detection A preliminary theory with a certain amount of heuristic argument has yielded the approximation Eq (13) for the spectral mean loss More work on this theory is needed to improve its accuracy

References

1 Chadwick, H D , "Frequency Acquisition in an MFSK Receiver," *Space Programs Summary 37-52*, Vol III, pp 47-54, Jet Propulsion Laboratory, Pasadena, Calif , 1968

2 Chadwick, H D , and Springett, J C , "Design of a Low Data Rate MFSK Communication System," *IEEE Trans Comm Tech* , Vol COM-18, pp 740-750, 1970

3 Levitt, B K , "Analysis of a Discrete Spectrum Analyzer for the Detection of Radio Frequency Interference," *DSN Progress Report 42-38*, pp 83-98, Jet Propulsion Laboratory, Pasadena, Calif , 1977

4 Hill, P G , and Peterson, C R , *Mechanics and Thermodynamics of Propulsion*, Addison-Wesley, 1965

5 Lindsey, W C , and Simon, M K , *Telecommunication Systems Engineering*, Prentice-Hall, 1973

6 Middleton, D , *Introduction to Statistical Communication Theory*, McGraw-Hill, 1960

7 Edelson, R E , ed , *Telecommunications Systems Design Techniques Handbook*, Jet Propulsion Laboratory, Pasadena, Calif , 1972

8 Yaglom, A M , "Correlation Theory of Processes With Random Stationary *n*th Increments," *American Math Soc Translations*, Series 2, Vol 8, pp 87-141, 1958

9 Abramowitz, M , and Stegun, I A , ed , *Handbook of Mathematical Functions*, National Bureau of Standards, 1964

Table 1 Design parameters for ICE surveillance systems

	S-band, tracking	S-band, nontracking	X-band, tracking	X-band, nontracking
Doppler rate error f (Hz/sec)	0 0028	0 0028	0 010	0 010
Spectrum analyzer bandwidth (Hz)	250	250	1000	1000
Word time T_d (sec)	570	330	650	220
Antenna gain G_a (dBi)	32 4	34 7	34 3	38 1
Antenna diameter d (m)	2 3	3 0	0 79	1 2
Half-power beamwidth θ_a (deg)	3 6	2 7	2 8	1 9

Table 2 Design control table

		S-band	X-band
1	RF power to antenna, dBm		
	Transmitter power, dBm	37 0	40 0
	Circuit losses, dB	-0 7	-0 7 (?)
2	High-gain antenna gain, dBi	28 5	39 7
3	Space loss, dB		
	loss = $\lambda^2/(4\pi R)^2$, R = 5 8 X 10^8 km	-275 0	-286 2
	λ = 0 13 m or 0 356 m		
4	Power received by isotropic antenna, dBm (1 + 2 + 3)	-210 2	-207 2
5	Noise spectral density, dBm/Hz	-177 5	-175 0
	$N_0 = kT$, k = 1 38 X 10^{-20} mW sec/K		
	GaAs FET front end, K	120	220
	Noise from ground, cosmos, atmosphere, K	10	10
6	P/N_0, isotropic antenna, dB sec^{-1} (4 - 5)	-32 7	-32 2

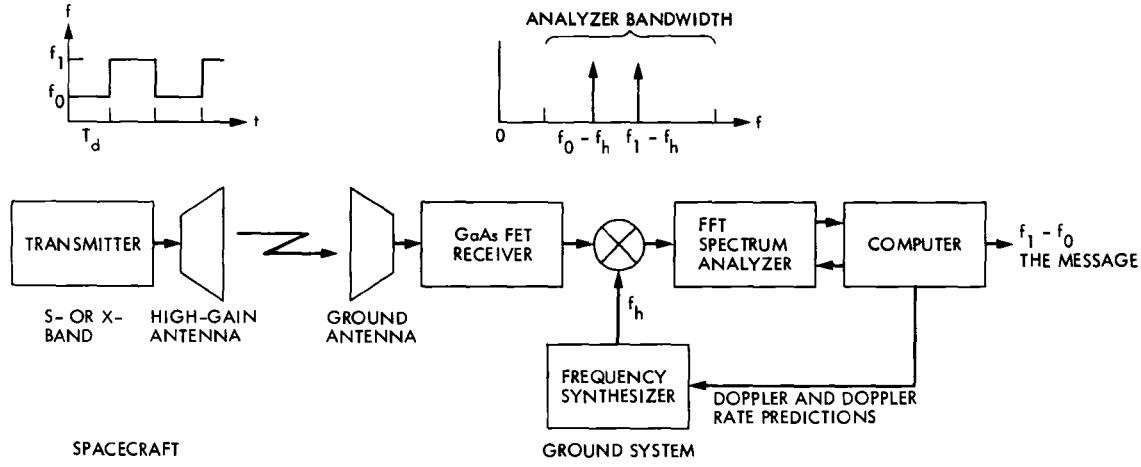

Fig 1. Surveillance system block diagram

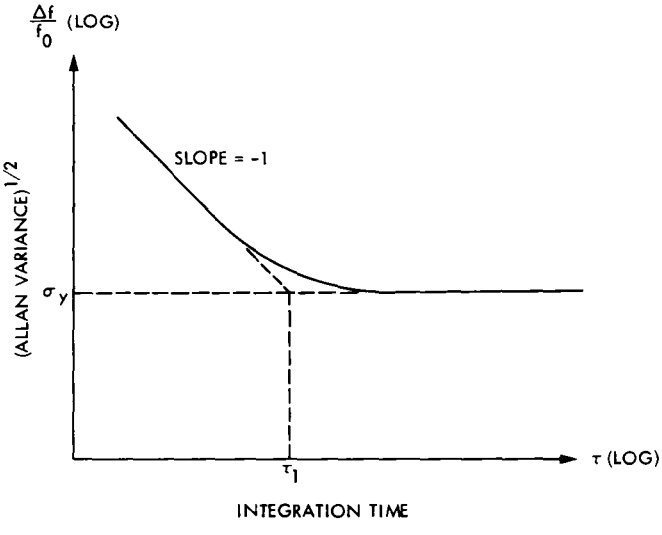

Fig 2 Typical Allan variance plot for a quartz oscillator

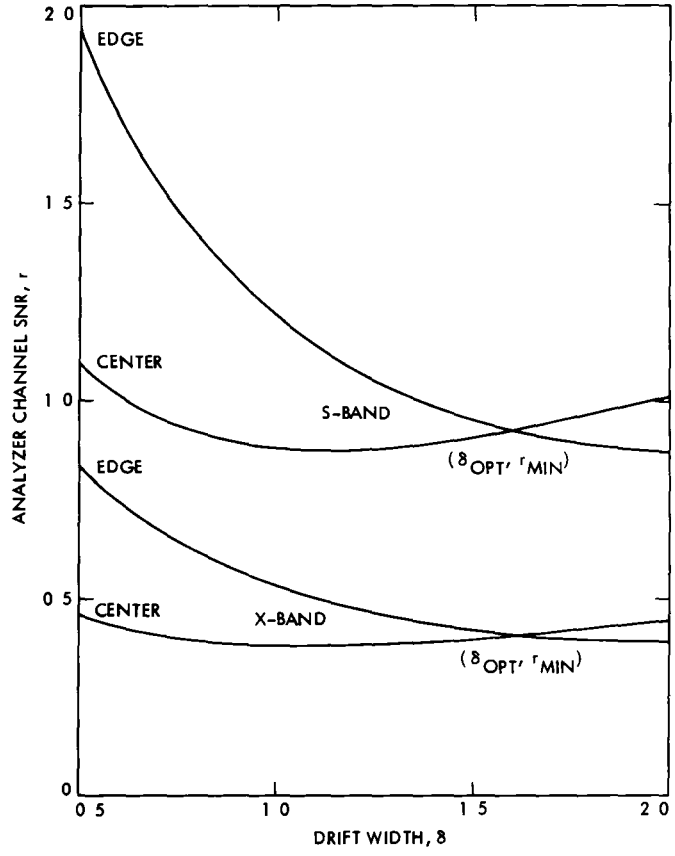

Fig 3 Finding the minimum SNR

Appendix A
Loss From Oscillator Phase Jitter

The foundations of the second-moment theory of processes with stationary nth differences are set out by Yaglom (Ref 8) These processes provide rigorous models for phenomena which appear to have spectral densities behaving like $1/f^{\alpha}$ as $f \to 0$, where $\alpha < 2n + 1$ For our case, $\alpha = 3$, so $n = 2$ suffices while $n = 1$ does not

Let $\theta(t)$ (the phase of an oscillator) be a process with stationary second differences Its spectral representation is

$$\theta(t) = a_0 + a_1 t + \frac{1}{2} ct^2 + \int_{-\infty}^{\infty} [e^{i\omega t} - 1 - F(\omega) i\omega t] \frac{dZ(\omega)}{-\omega^2} \tag{A-1}$$

where c is a constant, a_0 and a_1 are random variables, $F(\omega)$ is a bounded function satisfying

$$F(\omega) = 1 + O(|\omega|), \quad \omega \to 0$$

$$= O(1/|\omega|), \quad \omega \to \pm \infty \tag{A-2}$$

and $Z(\omega)$ is a complex-valued process with orthogonal increments, related to the two-sided spectral density ½ $S_{\theta\theta}$ (ω) by

$$E|Z(\omega') - Z(\omega)|^2 = \frac{1}{2} \int_{\omega}^{\omega'} \omega^4 S_{\theta\theta}(\omega) \frac{d\omega}{2\pi} \tag{A-3}$$

The spectral density must satisfy

$$\int_{-\infty}^{\infty} \frac{\omega^4}{1 + \omega^4} S_{\theta\theta}(\omega)\, d\omega < \infty \tag{A-4}$$

We have assumed that the measure given in Eq (A-3) (the spectrum of the generalized process θ (t)) is absolutely continuous

Changing $F(\omega)$ while retaining Eq (A-2) simply adds a new component to a_1, which is just a constant of integration, a frequency offset If one formally integrates the spectral representation of a stationary process twice, one obtains Eq (A-1) with $F(\omega) = 1$ Such a representation for $\theta(t)$ is valid only if $\theta(t)$ has so little high-frequency power that $\theta(t)$ exists When one attempts to do calculations, one gets results that depend strongly on the high-frequency components of $\theta(t)$, which we know intuitively to be irrelevant to the situation The instantaneous oscillator frequency is perhaps meaningless It is essential to use the correct version Eq (A-1) with a cutoff function $F(\omega)$

We now compute an estimate of the mean loss incurred when measuring the spectrum of an oscillator with phase $\theta(t)$ We can assume that the output has been heterodyned to baseband and that we are measuring the power in a frequency band of width b centered at zero frequency Let $bh(bt)$ be the time window of the measurement, where h satisfies

$$h(x) = h(-x) \geqslant 0$$

$$\int h(x)\, dx = 1, \int x^2 h(x)\, dx < \infty$$

For later use define

$$H(y) = \int e^{ixy} h(x)\, dx$$

The mean spectral loss is given by

$$G_l = \iint E\, e^{i[\theta(s) - \theta(t)]} b^2 h(bs) h(bt)\, ds dt \tag{A-5}$$

Assume that $\theta(t)$ is a Gaussian process Then

$$E\, e^{i[\theta(s) - \theta(t)]} = \exp\left(-\frac{1}{2} D(s,t)\right)$$

where

$$D(s,t) = E[\theta(s) - \theta(t)]^2$$

Since $b^2 h(bs) h(bt)\, ds dt$ is a positive measure with total mass 1, Jensen's Inequality gives

$$\ln \frac{1}{G_l} \leqslant \frac{1}{2} \iint D(s,t)\, b^2 h(bs) h(bt)\, ds dt \tag{A-6}$$

To first order in $D(s,t)$, the two sides of Eq (A-3) are equal

In computing $D(s,t)$ from Eq (A-1) we assume that $c = 0$, $a_1 = 0$ The assumption $c = 0$ means that there is no average frequency drift The assumption $a_1 = 0$ means that we don't want a constant frequency offset to affect the measurement Also, it is convenient to replace $F(\omega)$ by $F(\omega/b)$

Let

$$W(t,\omega) = e^{i\omega t} - 1 - i\omega t F\left(\frac{\omega}{b}\right)$$

Then

$$D(s,t) = \int_0^\infty |W(s,\omega) - W(t,\omega)|^2 S_{\theta\theta}(\omega)\frac{d\omega}{2\pi}$$

and

$$\ln\frac{1}{G_J} \leqslant \int_0^\infty V\left(\frac{\omega}{b}\right) S_{\theta\theta}(\omega)\frac{d\omega}{2\pi} \qquad \text{(A-7)}$$

where

$$V(y) = \int |e^{ixy} - H(y) - ixyF(y)|^2 h(x)\,dx$$

We still consider the function F to be at our disposal Fixing y we find the number $F(y)$ that minimizes $V(y)$ This is done by projecting $e^{ixy} - H(y)$ onto the vector ix in the space $L^2[h(x)]$ The answer is

$$F(y) = \frac{H'(y)}{yH''(0)} \qquad \text{(A-8)}$$

$$V(y) = 1 - H(y)^2 + \frac{H'(y)^2}{H''(0)} \qquad \text{(A-9)}$$

It happens that the function F given by Eq (A-8) satisfies Eq (A-2) The function $V(y)$ given by Eq (A-9) is a high-pass frequency response, and the right side of Eq (A-7) is a "high-pass variance" of $\theta(t)$ with cutoff frequency proportional to b

Concerning the way we have played around with F, we can say only that it seems to be the right thing to do Since changing F only changes the offset frequency a_1 and the effect of frequency offset is covered by the loss G_{pd}, we feel free to minimize the effect of the offset on G_J We want the average frequency during the measurement to be zero in some sense More work on this part of the theory is needed

Now set

$$h(y) = 1, \quad |y| \leqslant 1/2$$

$$= 0, \quad \text{elsewhere}$$

$$S_{\theta\theta}(\omega) = S_{\phi\phi}(\omega) + \frac{A}{\omega^3}$$

where $\phi(t)$ is a stationary process with bandwidth much greater than b, so that $V(\omega/b)$ passes most of the energy in $\phi(t)$ Then Eq (A-7) becomes

$$\ln\frac{1}{G_J} \leqslant \sigma^2(\phi) + \frac{A}{2\pi b^2}\int_0^\infty V(y)\frac{dy}{y^3} \qquad \text{(A-10)}$$

By numerical integration we find that the last integral is 1/36 (approximately) Substituting for $\sigma^2(\phi)$ and A from Eqs (11) and (12) we get Eq (13)

Appendix B

Chi-Squared Tail Estimates

Equation 26 4 31 of Ref 9 is used to express the tails of a noncentral (or central) χ^2 in terms of the tails of a standard Gaussian For our situation there are $\nu = 2L$ degrees of freedom and a noncentrality parameter $\lambda = 2Lr'$ (or zero) The approximation requires $L > 50$ Let X be a scaled version of the noncentral χ^2, define $X^* = [X - E(X)]/\sigma(X)$, and let Z be a standard Gaussian Given a probability p define x and z by

$$P\{X^* > x\} = P\{Z > z\} = p$$

Straightforward manipulation of the approximation in Ref 9 gives the approximation

$$x = z\sqrt{1 - \beta/(4L)} + \frac{1}{2}(z^2 - 1)\sqrt{\beta/(4L)} \qquad \text{(B-1)}$$

where

$$\beta = \frac{1 + 2r'}{(1 + r')^2}$$

To get an approximation for the lefthand tail $P\{X^* < x\}$, replace x by $-x$ and z by $-z$ in Eq (B-1) The righthand tail of X is heavier than the Gaussian tail, the lefthand tail of X is lighter

The Practical Limits of Photon Communication

R J McEliece, E R Rodemich, and A L Rubin
Communications Systems Research Section

We show that for photon communication, the rate $R_0 = 1$ nat per photon is the rate beyond which one encounters an explosive increase in both the required ratio of peak-to-average signal power and in the required bandwidth expansion On the basis of these results we conjecture that no practical photon communication system can be designed to operate above 10 nats per photon

I. Introduction

In a recent report (Ref 1), it was shown that the R_0-parameter associated with noiseless optical communication using photon-counting techniques (hereafter we call this "photon communication") is one nat per photon Now for any channel, R_0 is widely believed to be the rate above which the implementation of a reliable communication system becomes very difficult, but there is no really sound mathematical support for this belief In this paper, however, we will give rigorous mathematical substantiation to this "R_0 conjecture," for the special case of photon communication

Roughly speaking, we shall prove that for photon communication, the rate $R_0 = 1$ is the rate beyond which one encounters an explosive increase in both the required ratio of peak-to-average signal power and in the required bandwidth expansion

Precisely speaking, what we shall prove is this Let ρ denote the rate (in nats per photon) of a given reliable photon communication system, let α denote its required ratio of peak-to-average signal power, and let β denote its required bandwidth expansion factor Then necessarily, as we will show in Sections II and III,

$$\alpha \geq e^{\rho-1} - 1 \tag{1}$$

$$\beta \geq \frac{e^{\rho-1} - 1}{\rho} \tag{2}$$

Thus as ρ increases linearly, both α and β must increase exponentially On the basis of Eqs (1) and (2), we conjecture that no practical photon communication system can be designed with $\rho \geq 10$ On the other hand, in Ref 2 it was shown that one could design a practical system at about $\rho = 3$ using pulse position modulation and Reed-Solomon codes Thus, the gap between what is presently practical and what may someday be practical is reasonably small This is in spite of the fact that channel capacity (i e , the largest ρ that is theoretically possible) is extremely large (Ref 3)

II. The Poisson Channel Model

We assume that any photon communication system works as follows The time interval during which communication

takes place is divided into many subintervals ("slots"), each of duration t_0 seconds The transmitter is a laser which is pulsed during each time slot, it may be pulsed with a different intensity in each slot At the receiver is a photon counter, which accurately counts the number of photons received during each time slot We denote by x_i the expected number of photons received during the ith time slot, x_i will be called the *intensity* of the ith pulse

It may be that "noise photons" are present in such a system, but in many cases of practical interest, noise photons are extremely rare (For example, in a careful analysis of a potentially practical system, Katz estimated the rate of arrival of noise photons to be around 10^{-3} per second) In any event we shall make the assumption that no noise photons exist In this case, because of the Poisson nature of photon arrivals, the probability that exactly k photons will be received during a slot in which the laser was pulsed with intensity x is $e^{-x}x^k/k!$

Thus described, the optical channel is a discrete memoryless channel with input alphabet equal to the set of nonnegative real numbers (the possible values for the intensities x_i), and output alphabet equal to the set of nonnegative integers (the possible outputs of the photon counter) If a real number x is transmitted, the probability that the integer k will be received is given by

$$p(k|x) = e^{-x}\frac{x^k}{k!} \tag{3}$$

We call the channel described by Eq (3) the *Poisson channel*

A code for this channel is a set of vectors $x_i = (x_{i1}, \quad , x_{in})$, $i = 1, \quad , M$, of length n Each component x_{ij} is a nonnegative real number and represents an intensity of the transmitting laser Assuming that each component of a code word requires one time slot for transmission, the rate of such a code is

$$R = \frac{\log M}{n} \text{ nats per slot} \tag{4}$$

On the other hand, each component x_{ij} represents an average number of (received) photons, and so the code's rate in nats per photon is

$$\rho = \frac{R}{\mu} \text{ nats per photon, where} \tag{5}$$

$$\mu = \left(\sum_{i,j} x_{ij}\right) \Big/ nM, \text{ photons per slot (average)} \tag{6}$$

The rate R in Eq (4) is a measure of "bandwidth expansion " If, for example, we are transmitting at a rate of A nats per second, using a code of rate R nats per slot, it follows that we require A/R slots per second Thus the slot rate is equal to the nat rate multiplied by the factor $1/R$ We thus define

$$\beta = \frac{n}{\log M} \text{ slots per nat} \tag{7}$$

and call β the *bandwidth expansion factor*

In Eq (6), μ represents the *average* pulse intensity, i e the average number of photons received per time slot At a given frequency this number is proportional to the *average* received power On the other hand, the quantity

$$L = \max_{i,j} x_{ij} \tag{8}$$

represents the *maximum* required pulse intensity required by this particular code, and it is proportional to the maximum or *peak* received power We denote the ratio of L to μ by α

$$\alpha = \frac{L}{\mu} = \frac{\max_{i,j}(x_{ij})}{\frac{1}{n \cdot M}\sum_{i,j} x_{ij}} \tag{9}$$

We have now precisely defined the quantities α, β, and ρ mentioned in Section I Our proof of inequalities in Eqs (1) and (2) rests on certain information – theoretic results about the Poisson channel, which we now describe

We would like to compute the information – theoretic capacity of the Poisson channel, whose statistics are given in Eq (3), that is, the maximum possible mutual information $I(X,K)$, where X is a nonnegative random variable, and K is a nonnegative integer-valued random variable related to X by the conditional probabilities However, it is very easy to see that this maximum is infinite (take X to be a discrete random variable which assumes a very large number of values which are very far apart) To get a meaningful problem, we must restrict X somehow The most natural restriction (Eq (6)) is to fix the *mean* of X, and so we define

$$C(\mu) = \sup\,[I(X,K) \;\; E(X) = \mu] \tag{10}$$

According to Shannon's noisy-channel coding theorem (see Ref 4, Chapter 7), $C(\mu)$ represents the maximum possible rate (in nats per channel use) of a reliable photon communication system which is restricted to operate at an average of μ photons per slot or less

A second possible restriction is on the *maximum* value that X can assume (Eq (8)) Thus we define

$$C(\mu,L) = \sup [I(X,K)\ E(X) = \mu, X \leqslant L] \tag{11}$$

Again, according to Shannon's theorem, $C(\mu,L)$ represents the maximum possible rate for any photon communication system which is restricted to operate at an average of $\leqslant \mu$ photons per slot, and a maximum of L photons per slot

In Section III, we will prove the following results about $C(\mu)$ and $C(\mu,L)$

$$C(\mu) \leqslant \log (1+\mu) + \mu \log \left(1+\frac{1}{\mu}\right) \tag{12}$$

$$C(\mu,L) \leqslant \mu \log \frac{L}{\mu} \text{ if } L \leqslant 1 \tag{13}$$

In the remainder of this section, we will show how Eqs (12) and (13) can be used to prove our main results, Eqs (1) and (2)

First, note that by the converse to the noisy-channel coding theorem, the rate R of a reliable communication system which operates at an average of μ photons per slot is bounded by

$$R < C(\mu) \tag{14}$$

Now $C(\mu)$ itself is bounded by Eq (12), and since $\log (1+\mu) < \mu$, we have

$$R < \mu \left[1 + \log \left(1+\frac{1}{\mu}\right)\right] \tag{15}$$

The rate of this system measured in nats per photon is, by Eq (5), R/μ, and so

$$\rho < 1 + \log \left(1+\frac{1}{\mu}\right) \tag{16}$$

for $\rho > 1$ a simple algebraic manipulation of Eq (16) yields

$$\mu < (e^{\rho-1} - 1)^{-1} \tag{17}$$

Now since the bound on the right of Eq (15) is easily seen to be an increasing function of μ, it follows from Eqs (15) and (17) that

$$R < \frac{\rho}{e^{\rho-1} - 1} \tag{18}$$

but $R = \beta^{-1}$ This proves Eq (2)

To prove Eq (1) observe that Eq (13) tells us that $\alpha \geqslant e^{\rho}$ for $L \leqslant 1$ This is stronger than Eq (1), thus Eq (1) can only fail for $L > 1$ But if $L > 1$, the ratio $\alpha = L/\mu$ is by Eq (17) greater than $e^{\rho-1} - 1$ This proves Eq (1)

It now remains to prove Eqs (12) and (13) This we do in the next section

III. Proof of Eqs. (12) and (13)

In this section we shall give proofs of the important inequalities of Eqs (12) and (13) We begin with Eq (12)

By definition, $C(\mu)$ is the largest possible value which can be assumed by the mutual information $I(X,K)$ when the test source X is restricted to satisfy $E(X) = \mu$ But by well-known results on mutual information (see Ref 5, Chapter 1),

$$\begin{aligned} I(X,K) &= H(K) - H(K|X) \\ &\leqslant H(K) \end{aligned} \tag{19}$$

where in Eq (19) $H(K)$ denotes the entropy $\Sigma_k p_k \log p_k^{-1}$ of the random variable K Since for the Poisson channel, $E(K|X) = X$, it follows that $E(K) = E[E(K|X)] = E(X)$, and so the random variable K has the same mean as X, viz , μ

The problem of maximizing the entropy of a nonnegative integer-valued random variable with a given mean is easily handled with standard information-theoretic techniques Omitting the details (see Ref 5, Problem 1 8), the result is

$$H(K) \leqslant \log (1+\mu) + \mu \log \left(1+\frac{1}{\mu}\right) \tag{20}$$

(provided $E(K) = \mu$, K assumes only nonnegative integer values) Equations (19) and (20) combine to give Eq (12)

We turn now to Eq (13), which lies somewhat deeper The problem is to maximize $I(X,K)$ given that the distribution of X is restricted to $[0,L]$ and has mean μ

We introduce the notation (see Eq (13))

$$p_k(x) = e^{-x} \frac{x^k}{k!} \tag{21}$$

to denote the probability that k will be received given that x is transmitted We define

$$\overline{p}_k = E[p_k(X)] \tag{22}$$

the expectation being with respect to the distribution of X The quantity $\overline{p}_k$ represents the probability that k will be the channel's output, given that the input is the random variable X

Using standard techniques of convex analysis, it is now possible to show that a particular distribution confined to $[0,L]$ with expection μ maximizes $I(X,K)$ if and only if for some constants C and λ,

$$F(x) = \sum_{k=0}^{\infty} p_k(x) \log \frac{p_k(x)}{\overline{p}_k} + \lambda(x-\mu) - C \leqslant 0, \; 0 \leqslant x \leqslant L \tag{23}$$

where equality holds in Eq (23) at all points of support of the distribution (Eq (23) is essentially the same as Theorem 4 5 1 in Gallager (Ref 4) The only differences are that our channel has a countably infinite alphabet, rather than a finite one, and that we have an extra constraint $E(X) = \mu$, which necessitates the Lagrange multiplier term $\lambda(x - \mu)$ However, the modification of Gallager's analysis needed to arrive at Eq (23) is quite easy, and we omit it)

Equation (23) is a very strong condition that must be satisfied by an extremel distribution For example, we use it to show the following

Lemma For any L,μ, a maximizing distribution can have mass at at most one point on (0,1)

Proof Define

$$g_k = k! \overline{p}_k = E(e^{-X} X^k) \tag{24}$$

Then by Schwarz's inequality $[E(X_1 X_2)]^2 \leqslant E(X_1^2) E(X_2^2)$ applied to $X_1 = e^{-X/2} X^{(k-1)/2}$, $X_2 = e^{-X/2} X^{(k+1)/2}$, we have

$$g_k^2 \leqslant g_{k-1} g_{k+1}, \quad k \geqslant 1 \tag{25}$$

The function $F(x)$ of Eq (23) can be written in the form

$$F(x) = x(\log x - 1) + \sum_{k=0}^{\infty} p_k(x) \log \frac{1}{g_k} + \lambda(x-\mu) - C \tag{26}$$

If we differentiate $F(x)$ twice, using the formula $p_k'(x) = p_{k-1}(x) - p_k(x)$, we get

$$F''(x) = \frac{1}{x} + \sum_k [p_{k-2}(x) - 2p_{k-1}(x) + p_k(x)] \log \frac{1}{g_k}$$

$$= \frac{1}{x} + \sum_k p_k(x) \log \frac{g_{k+1}^2}{g_k g_{k+2}} \tag{27}$$

$$e^x F''(x) = \frac{e^x}{x} - \sum_{k=0}^{\infty} \frac{x^k}{k!} \log \frac{g_k g_{k+2}}{g_{k+1}^2} \tag{28}$$

Each coefficient in the series Eq (28) is by Eq (25) non-negative Since e^x/x is a decreasing function for $0 < x < 1$, it follows that $e^x F''(x)$ is decreasing in this range also Since $e^x F''(x)$ is positive at $x = 0+$, $e^x F''(x)$, and so $F''(x)$ also, can be zero for at most one value of $0 < x < 1$

An extremel distribution by Eq (23) must have $F(x) \leqslant 0$ for all $0 < x < L$ Since $F(x)$ is differentiable, it follows that $F'(x) = 0$ whenever $F(x) = 0$ Now if say $F(x_1) = F(x_2) = 0$ with $0 < x_1 < x_2 < 1$, then there exists $x_1 < x_3 < x_2$ with $F'(x_3) = 0$ By the above remarks $F'(x_1) = F'(x_2) = 0$ as well This in turn implies the existence of x_4, x_5 $x_1 < x_4 < x_3 < x_5 < x_2$ with $F''(x_4) = F''(x_5) = 0$ But we argued above that $F''(x)$ could vanish at most once on (0,1) Thus, $F(x)$ can vanish at most once on (0,1), i e , the optimizing distribution can have mass, at most, at one point in (0,1) This completes the proof of the lemma

We now use the lemma to prove Eq (13) Since $L \leqslant 1$, the lemma tells us that a distribution on $[0,L]$ with $E(x) = \mu$ can have mass only at $x = 0$ and one other point $x = \ell \leqslant L$ We shall complete the proof of Eq (13) by showing that for any distribution concentrated at $x = 0$ and $x = L$ the resulting mutual information $I(X,K)$ satisfies

$$I(X,K) \leqslant \mu \log \frac{L}{\mu} \tag{29}$$

(It is sufficient to take $\ell = L$ because the right side of Eq (29) is an increasing function of L)

Thus, let X have distribution

$$P(X = 0) = p$$
$$P(X = L) = q, \quad p + q = 1 \tag{30}$$

Then a straightforward calculation yields

$$I(X,K) = (1 - Q) \log \frac{1}{1 - Q} + Q \log \frac{1}{q} - L(q - Q)$$

$$Q = q(1 - e^{-L}) \tag{31}$$

Our goal is to show that this quantity is $\leqslant \mu \log (L/\mu)$, but $\mu = E(X) = qL$ So we must show that the right side of Eq (31) is $\leqslant qL \log 1/q$ Subtracting this quantity from Eq (31), we define for a fixed $L > 0$

$$F(q) = (1 - Q) \log \frac{1}{1 - Q} + (Q - qL) \log \frac{1}{q} - L(q - Q)$$

and wish to show that $f(q) \leqslant 0$ for $0 \leqslant q \leqslant 1$ This is easily seen, given the following (whose straightforward verifications are omitted)

$$f(0) = f(1) = 0 \tag{32}$$

$$f'(0) = -\infty, f'(1) = 0 \tag{33}$$

$$f''(q_0) = 0 \text{ only for } q_0 = \frac{1}{1 - e^{-L}} - \frac{1}{L} \tag{34}$$

Because $f(0) = 0$, $f'(0) = -\infty$, $f(q)$ is negative for all sufficiently small q If now $f(q) = 0$ for $0 < q < 1$, it would necessarily follow that f' would vanish at two interior points of (0,1) Since also $f'(1) = 0$, f'' would vanish at two points of (0,1), contradicting Eq (34) Thus $f(q) \leqslant 0$ for all $0 \leqslant q \leqslant 1$, and this completes the proof of Eq (13)

References

1 McEliece, R J , "The R_0-Parameter for Optical Communication Using Photon Counting," *DSN Progress Report 42-53*, Jet Propulsion Laboratory, Pasadena, Calif , Oct 15, 1979, pp 62-65

2 McEliece, R J and L R Welch, "Coding for Optical Channels With Photon Counting," *DSN Progress Report 42-52*, Jet Propulsion Laboratory, Pasadena, Calif , Aug 15, 1979, pp 61-66

3 Pierce, J R , "Optical Channels Practical Limits With Photon Counting," *IEEE Trans Commun* , COM-26 (1978), pp 1819-1821

4 Gallager, R G , *Information Theory and Reliable Communication* Wiley and Sons, New York, 1968

5 McEliece, R J , *The Theory of Information and Coding*, Addison-Wesley, Reading, Mass , 1977

An Evaluation Criteria Model for the Navigation Network System Design

E Hird
Mission Support Operations Division

The classic framework for analysis ultimately follows a series of rules whether or not those rules are consciously applied The rules usually take the form of define the problem (system), define a measure of effectiveness, generate alternatives based on analysis, and, weigh and decide Many methods have been developed and many analytical and quantitative techniques and tools designed for general applications to different models This paper describes the approaches used in developing the basis for a system design evaluation model Two well known evaluation cases are modeled, leading to a general model that is then detailed for application specifically to the Navigation Network conceptual designs Identification of the system attributes and their associated perspectives and the method of scoring and ranking a candidate design are discussed

I. Introduction

In the conceptual phase of development of any new system, several approaches are taken to ensure the best possible solution of the design problem, several because there is simply no a priori way of knowing which approach will best meet the user's need within a defined set of constraints Since it is not cost effective to expend resources in constructing different prototypes to physically (actually) test each of the approaches, evaluations need to be performed during the paper stage of design

There are two factors that make evaluation difficult First, although attributes such as growth potential and operability tend to be common to all purpose-designed systems, all such systems are not alike Therefore, the capacity to view each of the attributes in their true relations or relative importance assumes a system uniqueness that makes their definition elusive and time-consuming, especially since both the attributes and their perspectives must have the support of a consensus of those persons representing the organizations that ultimately have a stake in the new system These are among the matters that must be dealt with at the engineering level of the design organization

The second factor is that decisions regarding the choice of approach to be used in building the system have to be lived with for many years after implementation Modifications are expensive and the downtime, for example, may be unacceptable to the system user In this context, the choice, or decision, is made at the management level but the quality of the choice is heavily dependent upon the degree of professionalism applied in the development and application of the system evaluation criteria at the engineering level

II. Considerations and Requirements

One of the tasks defined in the pre-Project phase of the Navigation Network Study was the determination of a set of

evaluation criteria for the candidate designs, which were to be developed under yet another task

The principle purpose of the evaluation criteria was to provide Project Management with an acceptable means of judging the merit of each candidate design and an acceptable, uniform method of scoring and ranking each Subsidiary purposes were to

(1) Assist the Design Study Team by suggesting topics to consider in their efforts to produce acceptable candidate designs

(2) Assist in identifying the level of work necessary and the amount to be done in completing a candidate design through the research/reference stage to provide the data needed to respond to relevant evaluation criteria

(3) Give DSN Management, in association with the Project Report on how designs are ranked, another input to use in reaching a decision whether or not to proceed with the Navigation Network implementation

The requirement that the evaluation criteria had to be developed separately and independently from the candidate designs themselves posed an initial difficulty in getting a useful word picture, or model, of just *what* would constitute a candidate design No written, formal definition was available, so a definition was developed and given for practical purposes as a "functional design " To expand this a bit further, the planning configuration design used to develop future budget line items for the Navigation Network served as a useful example The planning configuration is described here simply as a set of configured generic hardware, and for the sake of completeness as receiving instruments consisting of a 10- or 20-meter antenna, a cryogenic front-end amplifier, the VLBI receiver and sampler, a frequency and time standard (H-maser), a control computer, and the communications equipment (DOMSAT)

III. Model Development Approaches

Three different approaches were investigated, initially, in an attempt to find an acceptable model of the evaluation process an engineering approach, a library research approach, and a strawman approach

A. Engineering Approach

In the engineering approach, a survey was made of the work other persons in the DSN had done in the area of evaluation criteria The results of the survey were so meager they could not be used

B. Library Approach

Concurrent with the engineering approach, a library research effort was initiated to determine the availability of useful literature on evaluation criteria that could be obtained and used within a reasonable time period This research also proved fruitless in revealing how an evaluation criteria process might be developed

C. Strawman Approach

The criteria for the strawman approach were developed from suggestions made by various DSN personnel The criteria were partitioned under topic headings, for example, Design and Operation, using very flexible rules to afford the semblance of order that was needed because the randomness of criterion input was not conducive to their falling into cognitive relationships In retrospect, the strawman criteria can be viewed as a set of unstructured attributes mixed-in with system requirements

The strawman criteria were sent to a number of managers who had fiscal, technical, or user interests in the proposed Navigation Network, their comments were solicited, and responses received were carefully reviewed and were interpreted to mean that

(1) A series of filters or gates were needed to weed out candidate designs that were unresponsive to the desired attributes

(2) Cost and risk were elements of the evaluation process that should be treated as parameters and not as attributes

An analysis of the comments received pointed to the inadequacy of the strawman approach to develop evaluation criteria, however, the comments nourished the thought that a generalized case model would be feasible

IV. Definition of a Case Model

The basic ground rules for a generalized case model were established as simply as possible The case model

(1) Should not be associated with the DSN

(2) Had to be sufficiently complex to require more than a superficial effort to develop

(3) Had to be one that most people could readily identify with and understand in order to sustain their interest

The methodology was to distil the underlying philosophy of evaluation from the case model and to adapt it to the current need With the ground rules in mind, two cases were

identified where individuals make large expenditures in relation to their personal income that require prudent consideration at each stage of their involvement the purchase of an automobile and the purchase of a home

It was decided to look at both cases to determine what concepts were involved in the respective evaluation processes Since the Navigation Network could conceivably involve the use of new equipment at new locations, it was further decided that the cases to be defined should be the purchase of a new automobile and a new custom home In citing the need for new and custom items, it was felt that a greater effort would be required and thus result in a more definite process than cases involving the upgrading of an existing automobile or home

Although both case study results are available to the interested reader, only one – the purchase of a new automobile – is described further for the purposes of illustration

A. Purchase of a New Custom Home

Not described further due to time and space limitations

B. Purchase of a New Automobile

1 Requirement. The requirement for a new car has to be formulated in general terms as a first step in satisfying the need As an example, the requirement could be for a sedan in which a family may be transported on short urban journeys with economy of operation, after incurring a certain initial cost

The first logical step is to obtain automobile marketing data, which may be accomplished by obtaining brochures of various models handled by local dealers representing several different manufacturers At this point the prospective purchaser goes through a preliminary elimination or weeding-out process of candidates by reviewing the contents of the brochures This will eliminate automobiles that

(1) Are not sized for that particular family

(2) Have a fuel consumption that delivers fewer miles per gallon than required

(3) Exceed the upper cost limit

2 Technical constraints Models that meet the initial requirements are then subjected to further scrutiny based upon technical constraints Here the criteria will reflect personal experience and may perhaps include

(1) Number of years the model has been available to the public without significant modification or manufacturer's recall to rectify design defects

(2) Resale value of earlier version of the model

(3) Opinions of other users of a particular model who are qualified in the eyes of the prospective purchaser

Additional models may be eliminated at this point through their subjective failure to meet all, or most, of the technical attributes considered relevant by the prospective purchaser Those candidates that survive are given some preliminary order of preference, based on how well they subjectively meet the technical attributes overall

3 Optimization evaluation Each of the remaining candidates then goes through an optimization evaluation to determine how closely certain needs are satisfied These needs might include

(1) Driveability

(2) Passenger comfort and convenience

(3) Performance improvement

(4) Appearance

(5) Safety

The candidates are then ranked accordingly to how well all the criteria have been satisfied by different manufacturer's models and option combinations

4 Cost In parallel with the optimization process, the cost of ownership is being developed Costs include

(1) Cost of basic vehicle and selected options

(2) License fees and taxes, annual

(3) Insurance, annual

(4) Estimate of annual fuel costs, based on some arbitrary distance

(5) Maintenance costs, annual

5. Additional considerations The final choice of vehicle, or even a decision to buy one at all, may depend upon additional considerations such as

(1) Availability of the model in the desired configuration at the needed date

(2) Dealer concessions on the total price

(3) Availability and cost of financing under different purchasing plans

(4) Ability of the prospective buyer to dispose of his existing vehicle at what he considers to be a fair price

(5) A willingness to relinquish or defer one or more options to meet cost constraints

(6) Opportunity costs

C. Workability of the Case Model

The workability of the two case models must be demonstrated, the best way would be to use them in the respective process of new car and custom-home purchasing Since neither activity is feasible, the next best thing is to obtain the opinion of experts as to the usefulness of the case models

1 Expert opinion, model 1, new custom-home This case model was first reviewed separately by two practicing civil engineers They both agreed that the process was acceptable but recommended changes and additions to the evaluation criteria, which were included in the model

The revised model was then reviewed by a mechanical engineer who is in the process, personally, of constructing his own home He agreed that the process was essentially correct and that although he thought that some more evaluation criteria might be included, the model was adequate for the present purposes

2 Expert opinion, model 2, new automobile This case model was reviewed separately by two managers who had recently purchased new vehicles for themselves Each one agreed that the process was essentially the one they had gone through, although neither one had written it down on paper Both remarked that they would use some additional criteria and these were added to the model used in this report

Based upon the interview statements, it was concluded that the evaluation processes of the two case models were workable and useful

D. Word Representation

A word representation of the evaluation process was developed for each of the two case models A comparison revealed a close degree of correspondence in their respective structures The result of that comparison may be characterized as follows

(1) Requirements have to be expressed in terms of

  (a) What has to be done

  (b) How well the purpose has to be done

  (c) A ball-park cost limit expressed in terms broad enough to invite effective competition

(2) A wide range of candidate designs, products, properties, and services already exist to satisfy the most discriminating of needs The market has to be researched for those that might qualify for candidacy

(3) An initial evaluation is necessary to eliminate those candidates

  (a) That do not meet the functional and performance requirements

  (b) That exceed the upper cost bound

(4) Survivors of the preliminary requirements evaluation then have their capabilities subjected to a technical attributes evaluation where some feelings as to order of choice are expressed and some final candidate rejections may be made because the risks and inconveniences outweigh the benefits and conveniences of ownership

(5) The initially ranked candidates are studied in detail and the optimization of the attributes within the physical constraints imposed by a particular design are evaluated Then for each feature of design, the evaluation results of the candidates are compared and a final order of technical preference is established

(6) In parallel with the optimization evaluation process, the fixed, one-time costs and the continuing costs are estimated to an accuracy that is consistent with the available data

(7) The decision to procure any of the final candidates is developed from weighing different financing plans, for example, outright purchase, deferred payments, leasing or rental, and constraints (a set of evaluation criteria reflecting the state of family affairs) imposed by the business climate against the technical capabilities to be offered in each case The choice may also be influenced by the ability of any of the final candidates to tolerate changes of certain feature optimizations in order to meet cost limitations while still being able to perform the essential task

Alternative representations are often useful in developing additional perspective on a problem Figure 1 shows a top-level block diagram of the generalized evaluation criteria process, derived from the word representation of the case models

In practice, the expansion of each of the block diagram boxes to give increasing detail of the internal processes will be dependent upon the point in the diagram that the action has reached Initially, it is desirable to minimize the work to be done because the number of candidates will be greatest Therefore, it would be expected that the processes at the top

of the block diagram would be simplest, i e , the go/no go kind

At the next level, more judgement and consideration would be needed in evaluating each attribute of the candidate, with rejection still being a more or less probable result At the technical optimization evaluation and life cycle costing stage, however, more detailed processes would be expected since more precise data need to be generated to satisfy the desire to "get the best for the least " It is also conceivable that the block diagram process as a whole may be repeated more than once if some of the criteria applications reveal marginal technical capabilities that can be relieved only by changing the functional, performance, or initial cost requirement

V. Definition of the Evaluation Criteria Process

Figure 2 shows the top level flow chart that evolved from the task of developing the Navigation Network evaluation criteria process from the general model It has the same essential flow of data as shown in Fig 1 The major change has been to differentiate between the processes and decisions to emphasize the progressiveness of the acceptance or rejection of candidate designs

The flow chart (Fig 2) may be regarded as being divided into four stages in series The first stage consists of the functional requirements, performance requirements, and upper cost limit gates Simple decisions are made here on whether a candidate design will be able to do all things it is supposed to do and do all of those things as well as it should at an affordable cost

In the next stage, the remaining candidates are evaluated and scored for their compliance with Technical Attributes and given a preliminary ranking If there is an obvious dichotomy in that ranking, those candidates in the lower subset will be eliminated at the Technical Ranking gate Candidate design rejections occurring at this point will further reduce the amount of detail work that has to be done in the third stage Here the surviving candidate designs go through two parallel processes

In the one, they are evaluated and scored on how well the competing needs of Implementation and Operations are satisfied, and the Intermediate Ranking that follows is critically reviewed to determine if there are any obvious inconsistencies in that ranking, caused by scoring subjectivity, that need to be corrected Any subsequent ranking changes are justified and documented In the second parallel process, the life cycle cost of each candidate is estimated to a level of accuracy consistent with the available data

These two data components constitute the output requirements of the Navigation Network study and are two of the inputs to the Management Review process Other inputs include the alternative funding plans that are created to meet the different costs of each of the candidate designs and business constraints, such as the choice of performing the detail design of the selected system in-house, or to let a system mode contract

To define the system attributes needed at the Technical Evaluation stage, the various constraints to be placed upon each candidate design were considered They were loosely identified as Implementation, Operation, Management, and User, a general question was formulated in each case to relate them to the Navigation Network Typically, for the Operation constraint the question was, "How will this design affect existing operational activities and procedures?" Answering this question made it easier to see the relationship between the constraints and the system attributes, as well as between the constraints and the general model, so as to be able to place them in the model accordingly

Each attribute needs one or more perspectives in the shape of a question that will act as an evaluation criterion or discriminant This part of the task is difficult to do because a thorough knowledge of each of the constraints is needed So both the attributes and the perspectives have to be developed and refined through iterative discussions with the numerous persons possessing the appropriate knowledge and an interest in the quality of the final design

To define the system attributes and perspectives for the third or Technical Optimization stage (see Fig 2) the constraints considered were Implementation, Operation, and Cost The question used, for example, to relate the Implementation constraint to the general model was "Is this candidate system easy to design?"

An essential part of the evaluation process is the recording of how effectively a candidate satisfies a particular criterion The purpose of setting score values for the evaluation criteria is to provide the evaluators with a first indication of how the various designs rank against each other To decide on the score values, the set of evaluation criteria has to be complete, that is, the system attributes to be evaluated and the wording of the associated perspective statements must have had consensus approval before development of the scoring can begin The set of evaluation criteria have to be searched for a theme that can be used to partition them into subsets If more than six subsets result from this process it is probably too many and another theme should be considered In the Navigation Network evaluation task, four different levels of risk were conceived and used to score the evaluation criteria as follows

(1) Criteria that must have a positive response since failure to satisfy them could mean failure of the design to meet the user need

(2) Criteria related to those areas of relative inflexibility, and therefore high risk, that could impact costs severely if it turns out later that the wrong decision had been made For example,

   (a) Key equipment characteristics that, once fixed, cannot be changed without impacting operational requirements, commitments, and costs

   (b) User costs

(3) Criteria related to Operations where the risks may be considered as next lower, because of the potential for flexibility and work-around

(4) Criteria that are considered to be related to the lowest, most controllable risks

Clearly, four scoring values are needed There is, however, a second condition to be satisfied Some of the perspectives are worded to determine whether the candidate design will be advantageous, neutral, or disadvantageous in terms of the attribute being assessed In such instances the scoring value is given a plus and minus range

Those criteria concerned with the highest risk were given a yes/no response The next level was given a score of 10 No attempt has been made to differentiate between the criteria in this subset in order to establish the range of severity of risk It is felt that if any such differentiation becomes necessary it will occur naturally during the ranking review when each case will be argued on its own specific merits The subset of criteria whose level of risk is associated with "flexibility" and "workaround" is given a scoring value of 6 while those criteria associated with the lowest level of risk are given a scoring value of 3

The ranking of the Navigation Network design evaluations is to be carried out in three phases Candidates that reach the Technical Attributes Evaluation stage are evaluated and scored Their scores are then individually totaled and the preliminary rank is decided on the relative total score so that the highest scoring candidate will be ranked first A similar activity takes place at the Technical Optimization Evaluation stage Here the scores for a candidate design are added to those it obtained at the previous level of evaluation to produce a total score on which to base the intermediate ranking This ranking is not the final arbiter A review of how each score is obtained and how it influences the ranking may uncover doubtful or unacceptable conditions existing among the rank leaders and underrated or highly attractive conditions lurking among the rank trailers This situation can only be resolved by a round of evaluation that concentrates on the perceived inequities created by the first round This review will be conducted by the Navigation Network Project team Their determination of the ranking with the reasons for any changes that they make will be presented to the Technical Steering Committee with an open forum for comment Further reasons for ranking changes made at this meeting will be considered by the Project Manager before he makes his ranking recommendation to the DSN management

Some dissimilarities have been noted between the general model evaluation process and the Navigation Network evaluation process, these are

(1) Detailed designs for new homes and production models of new automobiles are readily available from which the individual may make a choice, whereas the Navigation Network functional designs have yet to be developed This dissimilarity may be disregarded, however, because if no candidate designs are developed the Evaluation Criteria will serve no useful purpose

(2) The intent to procure a new home or automobile has to be of a high order or the individual will not undertake such a time consuming task, whereas the decision to build a Navigation Network is an institutional, rather than an individual, decision Since the decision is outside the scope of the Evaluation Criteria this dissimilarity may be disregarded

(3) There is an opportunity in the Navigation Network evaluation process to modify candidate rankings by a review procedure that was not observed in the general mode There are two possible reasons for this First is that an individual who is evaluating automobiles or home designs is most likely doing that job with little formality, the "scoring" being done mentally So the need for the ranking review would not arise Second, one or two persons with fairly identical interests will be concerned in an automobile or new home purchase whereas a number of users having considerable diversity of interests are concerned in getting the greatest group use out of a unique facility such as the Navigation Network

(4) The costing of a new home or automobile at the detail level is a very much simpler task than costing a new design for a Navigation Network at the conceptual level Also, the differences in cost are of several orders of magnitude greater for the Navigation Network compared with the car or home

Table 1 lists the complete set of Evaluation criteria that will be used in the evaluation process of the Navigation Network as

illustrated in Fig 2 Considerable care was exercised in writing the various perspective statements As a result they are concise, and to stimulate discussion during their development a short note was written about each one to explain the background and to suggest how a candidate design under consideration might be scored A subset of these notes that refer to the Implementation constraint are appended below

A. Maturity

The purpose of the question is to find out (a) if the theory of the basic principles of the design has been developed to the satisfaction of the scientific community concerned with such matters, and (b) if these principles have been adequately demonstrated in practice through the use of purposefully designed hardware/software A "Yes" answer to the question should get the maximum score There is also a case for considering the question to rate "Yes" or "No" only, with acceptance of the design for a "Yes" response and rejection for a "No " This approach, however, has not been selected for these Evaluation Criteria

B. Buildability

If the design under consideration is considered to be so specialized that a qualified electronic equipment manufacturer would need special facilities, tools, or skills to do the job, then the design should be given a zero score If, on the other hand, it is considered that the design can be built commercially with a very low probability of a cost overrun or late delivery, or both, then the questions should receive the highest possible score

C. Practicability

If the baseline geometry permits view periods of sufficient duration to enable the ground station equipment to acquire necessary and sufficient data to satisfy the needs of all the expected concurrent users, then the question should receive the highest score Otherwise, the specific design under consideration should receive a lower score

D. Testability

The purpose of the first question is to ensure that the design, if built, can be tested simply and easily whenever necessary to ensure that the capabilities are within specification In addition, the testing has to be accomplished with ordinary test equipment used by trained maintenance technicians in a short time span at low cost There is a strong desire to be able to test the design performance by independent means This could be accomplished by using other DSN equipment or the facilities of other organizations These independent verifications, therefore, will have to be done infrequently because of the coordination effort required and the extra cost involved If the answer to either question is "Yes," then the design should be awarded the highest score For a "No" answer the score should be zero

E. Compatibility

Integration of the Navigation Network with the DSN could disturb the planned or implemented compatibility of the major interfaces These interfaces involve equipment, software, RF links, technical information, data and operations Some of these interfaces will be of interest only if a Project is in a flight phase, if a Project is in any pre-flight phase then all of the interfaces would be of interest If any interface

(1) Will remain unchanged, then a zero score should be awarded

(2) Is changed in a beneficial way, then it should be given a positive score

(3) Is changed in a way that creates any new burden or imposition, then it should be given a negative score

F. Growth Potential

Past experience had shown that DSN equipment has been used in a capacity or has served a purpose that was not perceived at the time of its original design On other occasions, equipment has been modified to do additional tasks without detriment to the original task But here we are concerned with equipment in the conceptual stage and yet to be built If we know that the capability has been deliberately limited for reasons of time or cost, we know that there is growth potential If we can observe a recognizable innovation rate in the technical field of interest, we can expect growth potential Those designs that have an identifiable growth potential should receive a positive score, whereas those with obvious growth limitations should receive a negative score Designs with no identifiable growth potential and no obvious limitations should be given a zero score

G. Schedule

At the conceptual level, the only schedule data available is the PERT/CPM chart maintained by the Project Office If that chart shows completion on schedule for a particular design then a maximum score should be given

H. Safety

The question here is not whether the equipment can be designed to meet federal or state safety standards, since that is mandatory The question is how fault tolerant can the equipment be designed to localize failure damage, and will the risk to life be no worse than already experienced within the DSN, keeping in mind the need to implement a highly automated system A design meeting such requirements should be given the maximum score

Table 1 Navigation Network evaluation criteria

Navigation Network evaluation criteria requirements		
Attribute	Perspective	Response
Functional	Can the measurement types required to navigate all missions in the mission set be obtained?	Yes/No
Performance	Can the most stringent accuracy requirements of the ground based system be attained?	Yes/No
Cost	Is the preliminary cost estimate within the limitation set by management?	Yes/No
Technical attributes evaluation process Implementation		
Attribute	Perspective	Score range
Maturity	Is the technology of the design well understood?	0 - +10
Buildability	Can the design be built in a production environment to meet the requirements?	0 - +10
Practicability	Can the design acquire data often enough and long enough to meet user requirements?	0 - +10
Testability	Can the design performance be validated	
	Simply and repeatably?	0 - +10
	By an independent technique?	0 - +10
Compatibility	Will implementation be favorable to ground/flight interface compatibility at the following points for any approved mission?	
	Tracking and data system (TDS)/mission design?	-10 - +10
	TDS/spacecraft?	-10 - +10
	TDS/launch vehicle?	-10 - +10
	TDS/mission operations system?	-10 - +10
	TDS/integrated systems?	-10 - +10
	Will the implementation have a favorable interface compatibility with other TDS data types?	-10 - +10
Growth potential	Can the design	
	Serve additional purposes without modification?	-10 - +10
	Be modified to serve additional purposes without affecting the original purpose?	-6 - +6
	Can the system capabilities improve with anticipated advances in technology?	-10 - +10
Schedule	Can the design be implemented in time to meet the need date?	0 - +3
Safety	Under fault conditions can the design be made to fail without damaging equipment or injuring personnel?	0 - +3
Technical attributes evaluation process Operation		
Operability	Is the approach consistent with unattended operation?	0 - +6
Availability	Can the system operate for an extended time period without the need for maintenance?	0 - +3
Restorability	Can the system operation be restored after failure by using DSN resources alone?	0 - +3
Repairability	Can all equipment be repaired by using DSN resources alone?	0 - +3
Capability	Will implementation increase DSN capacity to meet operational commitments?	-10 - +10
System validation	Can the system performance be validated within the TDS?	-10 - +10
	Can the user product be validated within the TDS?	-10 - +10
Technical attributes evaluation process Management		
Communications	Will implementation be favorable to existing and planned DSN communications arrangements?	-6 - +6
Data Processing	Will implementation be favorable to existing and planned DSN computing capabilities?	-6 - +6
Energy	Will implementation be favorable to DSN mean energy consumption?	-6 - +6
Manageability	Will implementation be favorable to existing management arrangements?	-10 - +10

Table 1 (contd)

Attribute	Perspective	Score range
	Technical attributes evaluation process User	
Spacecraft	Will implementation be favorable to existing spacecraft operations and the spacecraft design of all approved but unflown projects?	-10 - +10
Mission operations system	Will implementation be favorable to MOS arrangements for all existing spacecraft and all approved but unflown projects?	-10 - +10
Data processing	Will implementation be favorable to existing and planned computing arrangements?	-10 - +10
Costs	Will implementation be favorable to user costs?	-10 - +10
	Technical optimization evaluation process Implementation	
Ease of design	Is the task within design organization experience?	0 - +10
	Are all the functions easy to understand?	0 - +6
Ease of installation	Can installation be done without any	
	Site preparation?	0 - +6
	Special equipment?	0 - +6
	Specially trained personnel?	0 - +6
Ease of modification	Are all the functions mechanized simply?	0 - +6
	Are the functions nearly independent?	0 - +6
	Are the function interfaces simple?	0 - +6
	Technical optimization evaluation process Operation	
Ease of operation	Are the periods of operator activity short?	0 - +6
	Are there few periods of operator activity in a duty cycle?	0 - +6
Ease of maintenance	Is there sufficient time in the duty cycle to perform necessary maintenance?	0 - +10
Ease of repair	Will failed equipment be repairable in a reasonable time period without the need for high skills, long experience, or special equipment?	0 - +6
	Life cycle cost	
	Perspective	Response
	What are the life cycle costs for each design?	Dollar value
	What is the DSN differential life cycle cost for each design?	Dollar value
	What is the annual differential cost to each user for each design?	Dollar value
	Are there any costs that are soft or fuzzy?	Yes/No
	Is the implementation favorable to DSN cost-effectiveness in terms of user hours per dollar of DSN funding?	Yes/No

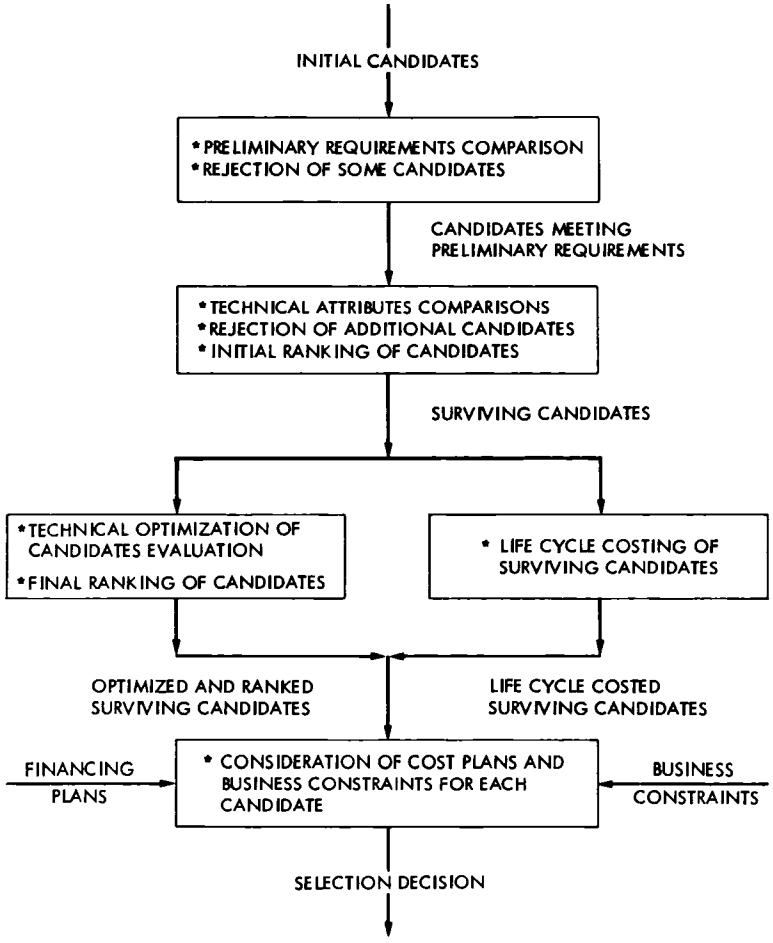

Fig. 1 Top level block diagram of the generalized evaluation criteria process for selecting a design candidate

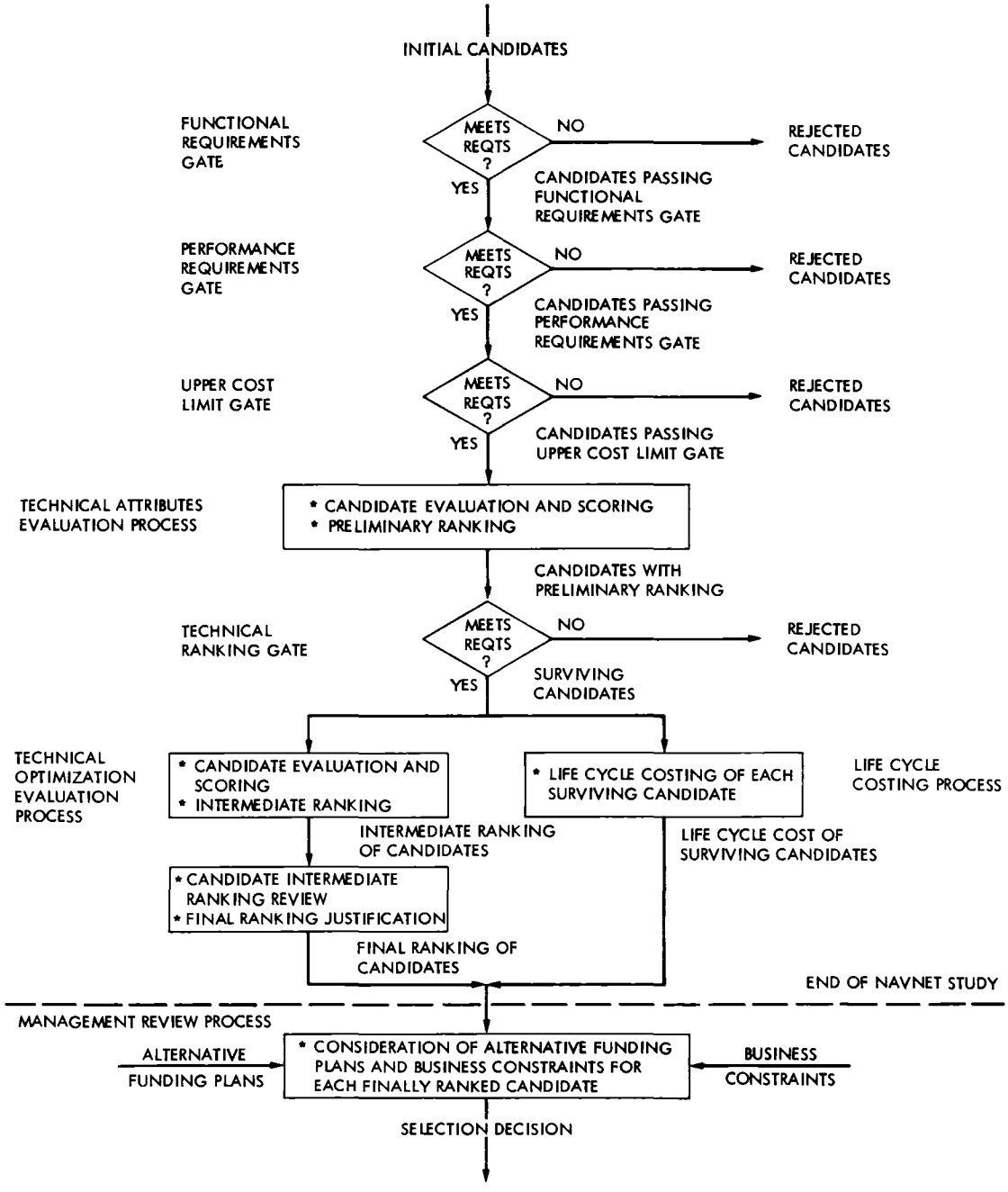

Fig 2 Top level flow chart, NAVNET project evaluation criteria process

Tropospheric Path Length Fluctuation in Temperate Semiarid Locales: Application to the Gravitational Wave Detection Experiment

A L Berman
TDA Mission Support Office

S D Slobin
Radio Frequency and Microwave Subsystems Section

Wet tropospheric path length fluctuation will, at some level of system sensitivity, begin to interfere with the search for gravitational waves using the spacecraft doppler method This article investigates radiosonde data from Edwards Air Force Base and radio metric scintillation data collected over a long, nearly horizontal path in Hawaii Utilizing a previous hypothesis that wet tropospheric path length fluctuation is proportional to total wet tropospheric signal delay, the two types of data are shown to be in reasonable agreement for averagings times (τ_a) of approximately 3000 seconds The two-way modeled tropospheric fractional frequency fluctuation at τ_a = 1000 seconds is 1 6 × 10^{-14}

I. Introduction

Proposals have recently been advanced to search for gravitational waves in ultraprecise two-way doppler data Preliminary estimates of gravitational wave characteristics indicate that a total measurement system fractional frequency fluctuation ($\sigma(\Delta F/F)$, where F is an S- or X-band frequency) of 1 × 10^{-15} over the time scales of interest (50 to 5000 seconds) will be required (Ref 1) At this level, fluctuations in the wet (water vapor) component of the tropospheric signal delay (R_w) will surely constitute a major error source

In a previous article (Ref 2), Berman modeled wet tropospheric fluctuation under the *assumption* that wet tropospheric path length fluctuation is proportional to the total wet tropospheric signal delay In this article, a very low frequency wet tropospheric path length fluctuation spectrum is constructed from radiosonde data measured at Edwards Air Force Base, and a high frequency fluctuation spectrum is constructed from tropospheric radio metric scintillation data taken by Thompson (Ref 3) in Hawaii It is shown that the two mean spectra are reasonably consistent for fluctuation frequencies (ν) ~ 3 × 10^{-4} Hz under the assumption that the wet tropospheric path length fluctuation is proportional to the total wet tropospheric delay

II. Radiosonde Data

Wet zenith tropospheric signal delay values (R_{wz}, cm)were computed from radiosonde measurements made at Edwards AFB during June through November 1977 and April 1978 through March 1979 Edwards AFB is located in the Mojave Desert about fifty miles north of Los Angeles and has a climate similar to that of the Deep Space Network (DSN) Goldstone tracking complex The radiosonde measurements

were made at irregular intervals ranging from periods of several hours to approximately one day Changes in zenith delay (ΔR_{wz}) as a function of separation time (τ_a) were computed for all measurements within 3 days of each other These were then sorted into "bins" of 1/10-day each and the mean value of each bin calculated Figures 1 and 2 display these mean bin averages (in cm)

As previously noted, Berman (Ref 2) has hypothesized that *fluctuation* in wet tropospheric delay is proportional to the *total* wet tropospheric delay To test this hypothesis, the changes in wet zenith delay (ΔR_{wz}) were correlated with mean zenith delay (R_{wz}) for each of the bins in both data sets Computed correlation was significant in almost every case, with the average computed correlation coefficient (r) being

1977 data (6 months)	$r = 0\ 59$
1978-1979 data (12 months)	$r = 0\ 26$

Based on this observed correlation, it is considered that the heuristic assumption of proportionality between wet tropospheric fluctuation and mean wet tropospheric delay continues valid

To utilize this relationship, each of the changes in wet tropospheric delay was normalized ($\Delta R_{wz}/R_{wz}$) by the average value of the delay Again, these were sorted into 1/10-day (2 4-hour) bins Figures 3 and 4 present the mean bin values for the normalized (fractional) fluctuations The lines in Figs 3 and 4 represent least squares linear curve fits to these data The equivalent parametric forms for these data fits are (τ_a in seconds)

1977 data (6 months)

$$\sigma_{R_{wz}}(\tau_a) = 0\ 079 R_{wz} \left(\frac{\tau_a}{1000}\right)^{0\ 24}$$

1978-1979 data (12 months)

$$\sigma_{R_{wz}}(\tau_a) = 0\ 069 R_{wz} \left(\frac{\tau_a}{1000}\right)^{0\ 33}$$

These can be compared to the estimate Ref 2 made based on a very preliminary examination of tropospheric fluctuation obtained from water vapor radiometer data

$$\sigma_{R_{wz}}(\tau_a) = 0\ 02 R_{wz} \left(\frac{\tau_a}{1000}\right)^{0\ 6}$$

Whereas the radiosonde data show greater $\tau_a = 1000$ second (17 minute) fluctuation that the water vapor radiometer data (7% versus 2%), the one-day modeled fluctuations are comparable at 27% and 29%, respectively

In the remainder of the article, the 1977 and 1978–1979 data fits will be combined into a single model as follows

$$\sigma_{R_{wz}}(\tau_a) = 0\ 074 R_{wz} \left(\frac{\tau_a}{1000}\right)^{0\ 29}$$

A fractional frequency fluctuation may be defined for this data

$$\sigma(\Delta F/F) = \sigma_{R_{wz}}(\tau_a)/c\tau_a$$

where

c = velocity of light, cm/second

τ_a = doppler averaging time, seconds[1]

The fractional frequency fluctuation for the Edwards AFB radiosonde data thus becomes

$$\sigma(\Delta F/F) = 2\ 0 \times 10^{-14} \left(\frac{\tau_a}{1000}\right)^{-0\ 71}$$

when a (yearly average) value of 8 cm is assumed for R_{wz}

III. Tropospheric Radio Metric Scintillation Data

In Ref 3, Thompson, et al , describes the phase spectral density of wet tropospheric signal delays over a 64-km Hawaiian (nearly horizontal) range The fluctuation frequency (ν) range of validity for this data is

$$3 \times 10^{-3}\ \text{Hz} < \nu < 3 \times 10^{-1}\ \text{Hz}$$

To compare these data to the Edwards AFB data, one must scale the results by the appropriate total wet delays The exact tropospheric water vapor distribution at the time of the Thompson experiment over the 64-km Hawaii radiometer

[1] For the remainder of this article, "measurement separation time" will be equated with "doppler averaging time "

range is unknown Using the U S Standard Tropical Atmosphere, 15° N (Ref 4), it is estimated that there were a total of 87 gm/cm^2 precipitable water along the 64-km path A standard year-average zenith atmosphere at Edwards AFB has 1 3 gm/cm^2 of precipitable water This ratio of nominal delays (proportional to integrated water vapor) is 66 9 and therefore the phase spectral density of the Thompson data must be scaled downward by (66 9)^2 Thus, the Edwards AFB equivalent zenith troposphere X-band phase spectral density (based on Hawaii measurements) is

$$P_\phi(\nu) = 1\ 09 \times 10^{-7}\ \nu^{-2\ 57}\ \text{rad}^2\ \text{Hz}^{-1}$$

$$3 \times 10^{-3}\ \text{Hz} < \nu < 3 \times 10^{-1}\ \text{Hz}$$

Reference 5 provides the following expression (with the Ref 6 correction) for Allan variance (σ_y^2) derived from phase spectral density (ν_0 is transmission frequency)

$$\sigma_y^2(\tau_a) = 4\pi^{-2}\nu_0^{-2} A \tau_a^{a-3} \left[\int_0^\infty Z^{-a} \sin^4(\pi Z)\, dZ\right]$$

where A and a are defined from the expression for phase spectral density $P_\phi(\nu) = A\nu^{-a}$ (as previously given)

Hence from the above one obtains from the Thompson data as corrected to Edwards AFB, for X-band frequency (ν_0 = 8 4 GHz) and a nominal 8-cm delay

$$\sigma_y(\tau_a) = 1\ 15 \times 10^{-14} \left(\frac{\tau_a}{1000}\right)^{-0\ 22}$$

The radiosonde fractional frequency fluctuation and radio metric scintillation Allan variance data[2] are plotted in Fig 5 As can be seen, they are reasonably consistent In fact, the steeper slope of the very low frequency (Edwards AFB) data is reasonable, since one would expect the tropospheric fluctuation spectrum to begin to flatten at about 3 days (4 X 10^{-6} Hz) due to movement of large-scale air masses

[2]For the purpose of this article, the radiosonde fractional frequency fluctuation is considered to be equal to the square root of the Allan variance

IV. Comparison of Radiosonde and Radio Metric Scintillation Phase Spectral Density

By equating the radiosonde fractional frequency fluctuation (squared) with the previous expression for Allan variance, a value of A may be deduced Using this procedure, a phase spectral density for Edwards AFB radiosonde data is obtained

$$P_\phi(\nu) = 6\ 76 \times 10^{-14}\nu^{-1\ 58}\ \text{rad}^2\ \text{Hz}^{-1}$$

over the range of validity $3 \times 10^{-6} < \nu < 10^{-4}$

Figure 6 shows the phase power spectra for both the Hawaii microwave data and the radiosonde data taken at Edwards AFB The microwave data have been normalized to year-average zenith values for Edwards AFB, thus, both curves represent phase spectra for the troposphere in temperate semiarid regions As stated in Section III, the spectrum at very low frequencies flattens out due to the decrease in long-term troposphere variation for periods greater than a few days Therefore, the "combination" of the model segments as in Figs 5 and 6 is intuitively agreeable

V. Tropospheric Model

Following Ref 2, a factor of $(\sin\theta)^{-1}$ is added to account for non-zenith delays, where θ = elevation angle One then has a "combined" radiosonde/radio metric scintillation model for tropospheric fluctuation (cm)

$$\sigma_{R_w}(\theta, R_{wz}, \tau_a) = 0\ 074\ (\sin\theta)^{-1} R_{wz} \left(\frac{\tau_a}{1000}\right)^{0\ 29},$$

$$\tau_a > 3000\ \text{s}$$

$$\sigma_{R_w}(\theta, R_{wz}, \tau_a) = 0\ 043\ (\sin\theta)^{-1} R_{wz} \left(\frac{\tau_a}{1000}\right)^{0\ 79},$$

$$\tau_a < 3000\ \text{s}$$

Edwards AFB is a reasonable representative of a temperate, semiarid climate, as are the Deep Space Network stations Table 1 gives the seasonal variation of the mean wet zenith tropospheric signal delay during 1977 through 1979 From this data, a mean yearly value of 8 cm was computed, with a mean summer extreme of 16 cm and a mean winter extreme of

4 cm The combined radiosonde/radio metric scintillation model for these conditions is presented in Fig 7

VI. Discussion

Previous work (Ref 2) modeled wet tropospheric path length fluctuation under the heuristic hypothesis of proportionality between wet tropospheric path length fluctuation and total wet tropospheric signal delay In this article, radiosonde measurements collected over 1 5 years at Edwards AFB are used to demonstrate the soundness of this hypothesis Utilizing the hypothesis, wet zenith tropospheric fractional frequency fluctuation computed from the Edwards AFB radiosonde data and the Hawaiian radio metric scintillation Allan variance data are shown to be reasonably consistent in the region of $\tau_a \sim 3000$ seconds The fractional frequency fluctuation at $\tau_a = 1000$ seconds is approximately $1\,1 \times 10^{-14}$, or about a factor of two higher than the value estimated in Ref 2 from water vapor radiometer data Since this is a "one-way" measurement, a factor of $\sqrt{2}$ is applied to obtain the equivalent "two-way" value of $1\,6 \times 10^{-14}$ Since a value this large will certainly impact any attempts to search for gravitational waves using the spacecraft doppler method, there exists a clear need to measure wet tropospheric path length fluctuation at $\tau_a = 1000$ seconds, instead of relying on extrapolations into this critical fluctuation region The water vapor radiometer is suggested as a possible instrument for measuring tropospheric path fluctuation at $\tau_a = 1000$ seconds, and perhaps ultimately, providing wet tropospheric calibration as well

References

1 Berman, A L , "The Gravitational Wave Detection Experiment Description and Anticipated Requirements," in *The Deep Space Network Progress Report 42-46*, pp 100-108, Jet Propulsion Laboratory, Pasadena, Calif , Aug 15, 1978

2 Berman, A L , "Parametric Modeling of Low-Frequency Water-Vapor-Induced Tropospheric Path Length Fluctuations" in *The Deep Space Network Progress Report 42-47*, pp 72-76, Jet Propulsion Laboratory, Pasadena, Calif , Oct 15, 1978

3 Thompson, M C , et al , "Phase and Amplitude Scintillations in the 10 to 40 GHz Band," *IEEE Transactions on Antennas and Propagation, Vol AP-23, No 6,* Nov 1975

4 Valley, S L , Editor, *Handbook of Geophysics and Space Environments*, 1965 Edition, p 2-10, McGraw Hill Book Company, Inc , New York, 1965

5 Armstrong, J W , Woo, R , and Estabrook, F B , "Interplanetary Phase Scintillation and the Search for Very Low Frequency Gravitational Radiation," in *The Astrophysical Journal, Volume 230*, June 1, 1979

6 Armstrong, J W , Estabrook, F B , and Woo, R "Corrections to Allan Variances ," *Astrophysical Journal* (submitted)

Table 1 Mean zenith wet tropospheric signal delay (R_{wz}) as a function of season during 1977–1979

Period	Delay, cm
January–March	6
April–June	8
July–September	11
October–December	7
Yearly Average	8
Mean Summer Extreme	16
Mean Winter Extreme	4

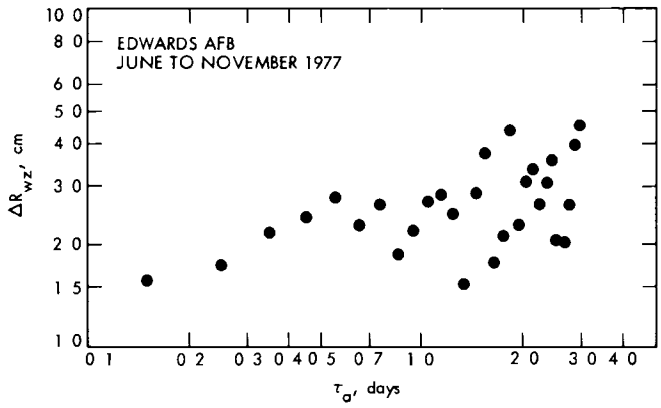

Fig 1 Zenith wet tropospheric path length change versus averaging time, 1977

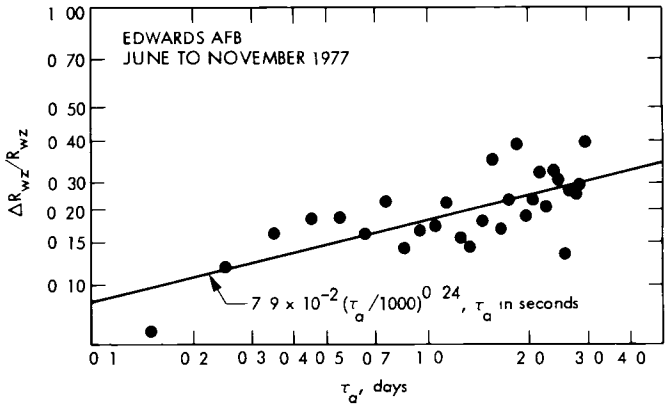

Fig 3 Zenith wet tropospheric fractional path length change versus averaging time, 1977

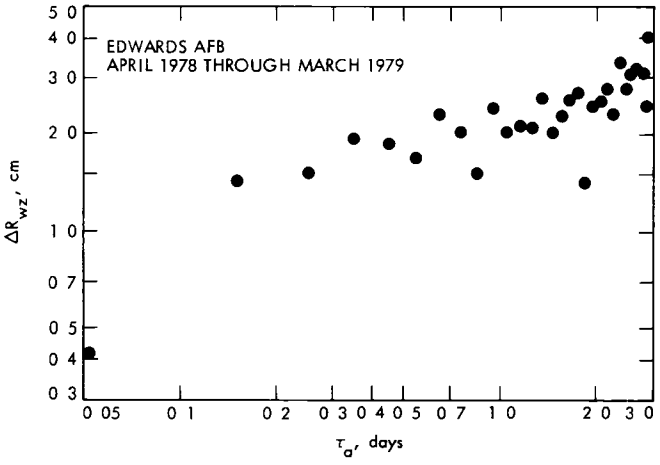

Fig 2 Zenith wet tropospheric path length change versus averaging time, 1978–1979

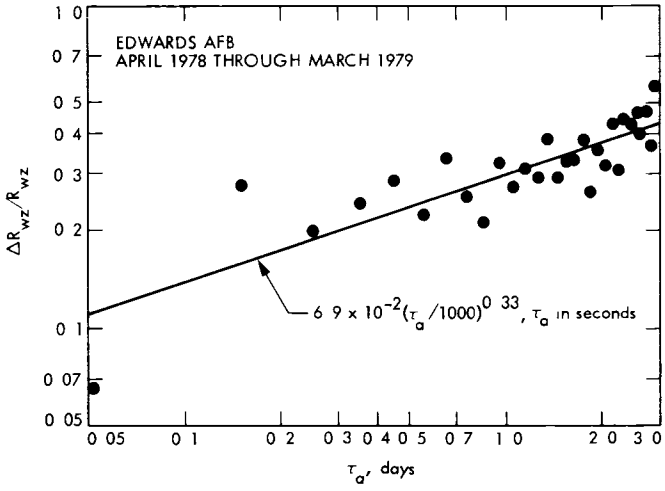

Fig 4 Zenith wet tropospheric fractional path length change versus averaging time, 1978–1979

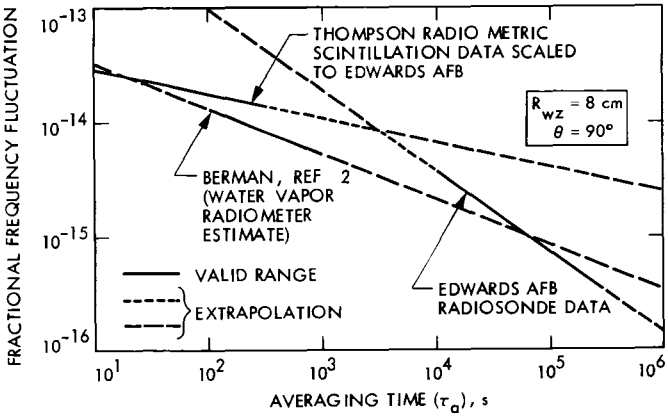

Fig 5 Zenith wet tropospheric fractional frequency fluctuation versus averaging time

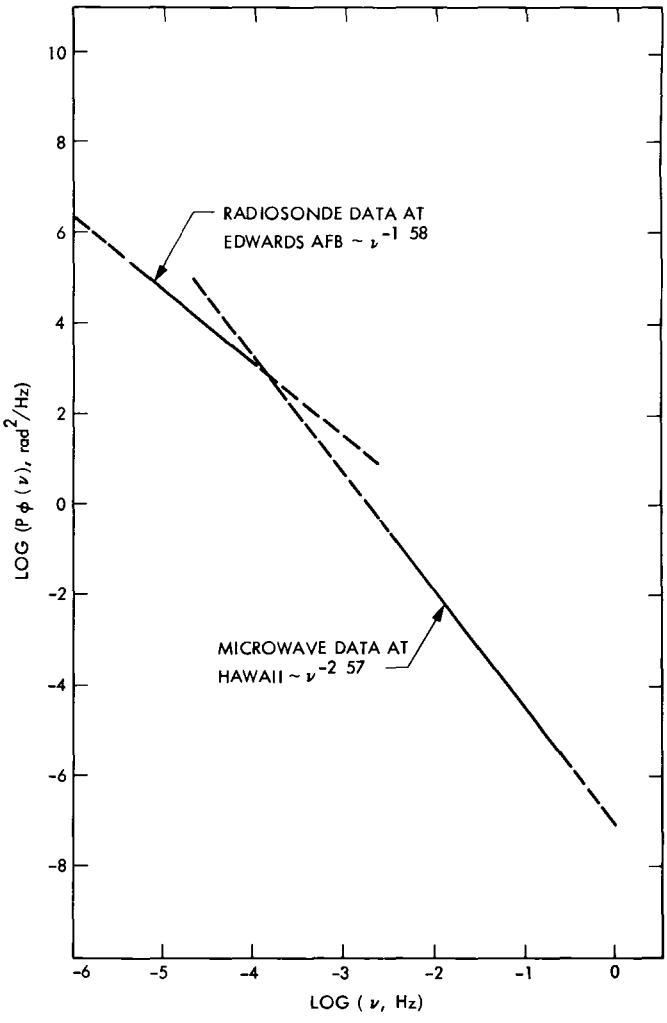

Fig 6 Phase spectral density computed from radiosonde and radio metric data

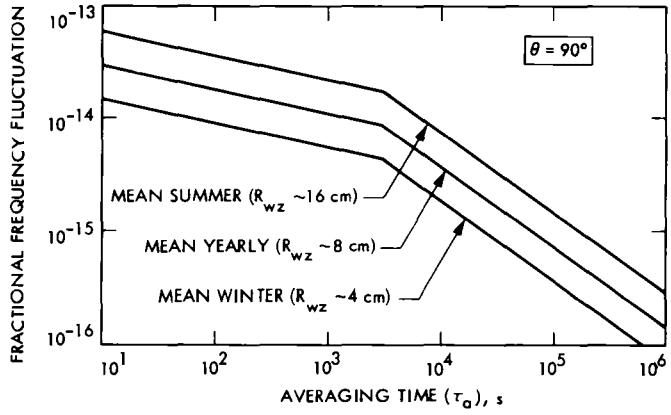

Fig. 7 Seasonal variations in combined radiosonde/radio metric scintillation model

GCF-NOCC Reconfiguration

J P McClure
DSN Data Systems Section

The equipment and computer programs in the Network Operations Control Center (NOCC) and the Ground Communications Facility's (GCF's) Central Communications Terminal at JPL are being rearranged and supplemented to provide an improved operational capability

The computer portion of the GCF's Central Communications Terminal (CCT) in the basement of the Space Flight Operations Facility was designed and implemented separate from the Network Data Processing (NDP) portion of the NOCC These independent designs, implemented at different times, used more computers and programs than an integrated design would have required The desire to reduce the computer count and to provide an improved operational capability led to the GCF-NOCC reconfiguration effort

This effort, when completed in 1981, will

(1) Require fewer minicomputers (16 versus 20)

(2) Require fewer computer programs (6 versus 8)

(3) Significantly reduce magnetic tape handling

(4) Provide a much-improved monitor and control capability

(5) Reduce operator requirements and provide the base for a two-operator CCT

The present configuration of the CCT and elements of the NDP are shown in Fig 1 High-speed data (HSD) are accepted by the Error Detection and Correction (EDC) processors, which operate interactively with the DSSs to correct HSD transmission errors The corrected HSD are fed to the High-Speed Switch computer, which routes the data, as appropriate, to the Mission Operations Centers (MOCs), the Network Log Processor (NLP) and (not shown) the Remote Mission Operations Centers (Ames and Germany) The NLP records both high-speed and wideband data (WBD) on magnetic tape to form a Network Data Log (NDL) The data are also forwarded to the Network Communications Equipment computers in Building 202, which routes the information to the proper NDP computer for analysis

The Data Record Processors (DRPs) recall missing data from the DSSs (in response to data gaps sensed by the NDP machines) and record them on magnetic tape to generate a "fill" tape An off-line DRP merges the NDL and fill tapes to produce an intermediate data record (IDR) The IDR is the prime deliverable product of the DSN

The Central Communications Monitor (CCM) senses and displays the performance of the entire GCF, receiving reports from DSS and CCT equipments

Display information generated by the NDP's Real-Time Monitor (RTM) computers is forwarded via the NLP to the Digital Display Processor (DDP), thence to the Video Assembly

Processor (VAP) for display in the Network Operations Control Center in Building 230

The reconfigured GCF-NOCC, shown in Fig 2, considerably simplifies the data paths and processing Both high-speed and wideband data are routed through automated circuit switches and then accepted by the Error Correction and Switching (ECS) computers The ECSs error correct the HSD, optionally record it on a Front End Record (FER) magnetic tape, and route it, as appropriate, to

(1) The MCCC

(2) Remote Mission Operations Centers

(3) The Data Records Generation (DRG) computers

The DRG records HSD on disc, senses gaps, recalls the missing data from the DSS, and then merges the real-time and recalled data as it writes the IDR on magnetic tape Wideband data are recorded in IDR format directly on magnetic tape If recalls are needed, the DRG also merges the real-time and recalled data to form a complete WB IDR

The CCM, NCE, DDP, and VAP functions are largely unchanged, though the NCE and the DDP communicate directly over their own interconnecting circuits, as do the ECSs and NCEs

The reconfigured GCF-NOCC capability is scheduled to be completed in March 1981 Subsystem-level testing begins in May 1980, accompanied by a phased rearrangement of the hardware Training and operational testing start in November 1980 and continue until the full capability is placed on-line in March 1981

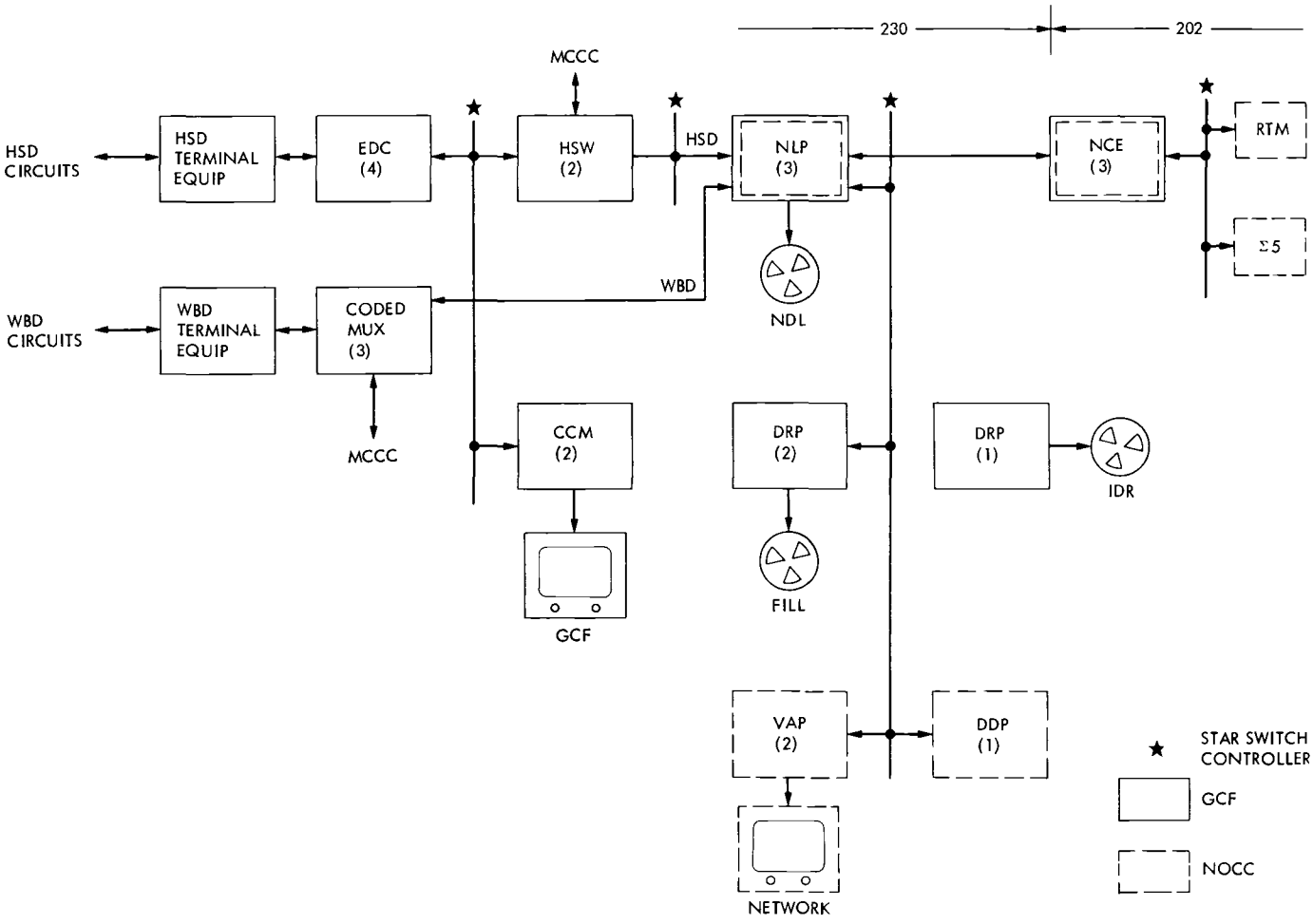

Fig 1 Present configuration

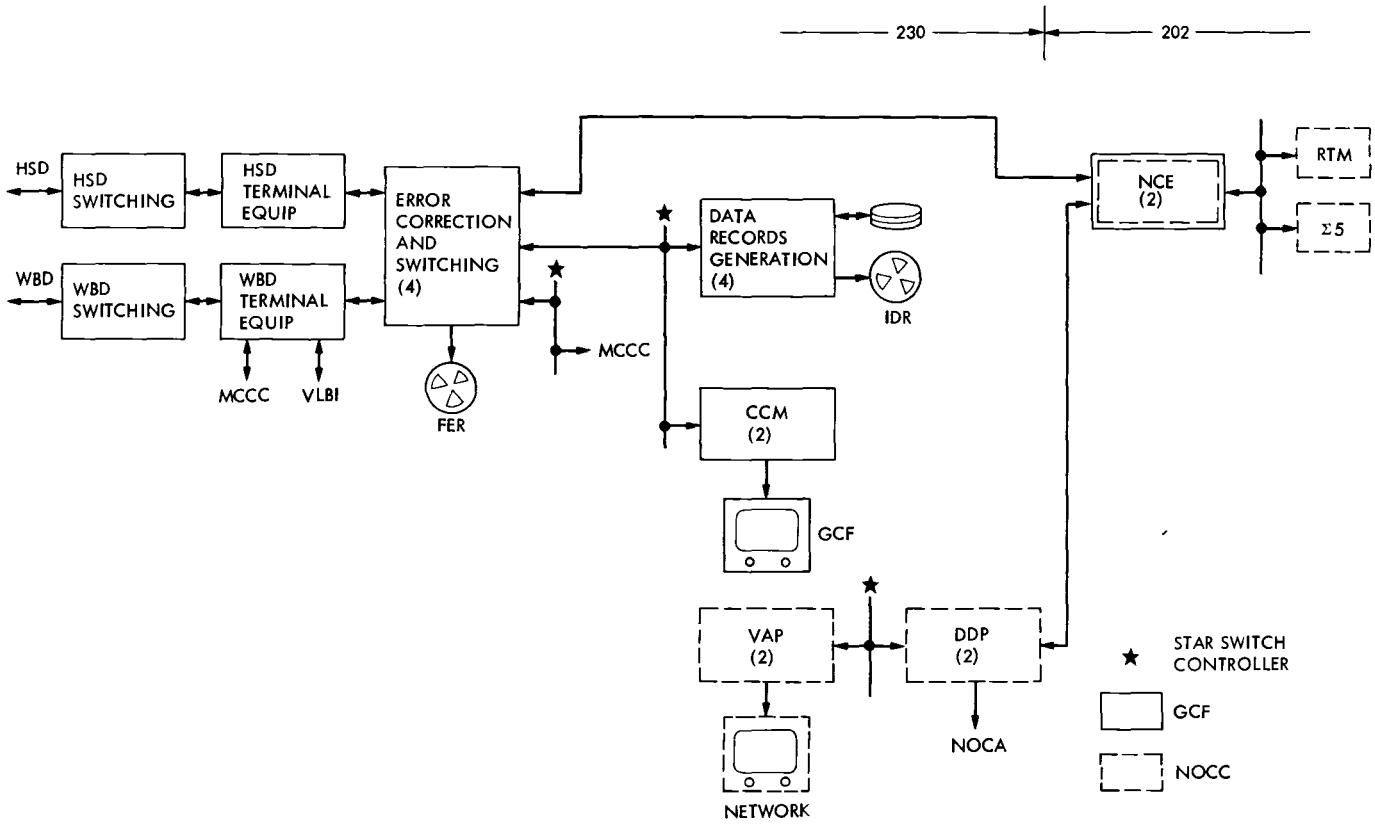

Fig 2 Reconfiguration

Preliminary Telemetry Operations Experience With the Real-Time Combiner: 1 November 1978 to 1 November 1979

N K Simon and C Hoynes
Deep Space Network Support Section

A prototype version of a two station, real-time signal combiner was installed at Goldstone DSS 14/(12) and used to support the Voyager Mission at Jupiter and the Pioneer 11 Mission at Saturn This article reports on early combined station operating experience with a Real-Time Combiner (RTC) in the loop

I. Introduction

On September 21, 1974, the two 26-m antennas at DSSs 12 and 13 were arrayed with the 64-m antenna at DSS 14 to improve the telemetry data received during the Mariner 73 Mercury encounter (Ref 1) The experimenters claimed an improvement in SNR of 0 7 dB over the operation of DSS 14 alone The arraying was accomplished with a signal combiner that took baseband signals and phase correlated them to produce a single additive signal The combined output signal was then input to a DSS 14 receiver and demodulator "for further processing" The experiment was a laboratory research effort meant for one time use during the MVM 73 encounter It also demonstrated the value of arraying the antennas at a DSS complex A reproduced graph of BER vs time from the September 21 encounter is shown in Fig 1

The current effort began in FY78 The objective was to develop a permanent Real-Time Combiner (RTC) installation for the 64-m/34-m net A prototype unit became available in November 1978 and was successfully used for the Voyager 1 and 2 Jupiter encounters and for the Pioneer 11 Saturn encounter It is the operation with the prototype unit that is the subject of this report

The basic system block diagram for RTC operation is illustrated in Fig 2 Baseband signals from a 64-m and 34-m station are fed into the combiner, phase locked, and sent through a standard telemetry string for normal processing The SNR gain from combining over a 64-m station alone is dependent on the actual SNR spread between the two stations For a nominal spread of 5-dB between the 64-m and 34-m antenna the RTC theoretical gain is 1 2 dB This compares with 0 8 dB available from adding two 26-m stations to the 64-m signal

II. Test Program

A. CTA 21

The prototype RTC unit was set up in CTA 21 and initial testing was conducted in November/December 1978

Two methods of simulating a 2-station configuration at CTA 21 for testing RTC performance in an operational system environment were considered Method 1 Receiver input terminations were isolated with a common modulated RF test signal fed to both receivers Levels were adjusted by means of S-band attenuators in each line Method 2 Separate RF signals modulated by a common data-modulated subcarrier from the Simulation Conversion Assembly (SCA) were fed to each Receiver

In both cases the baseband outputs of each receiver were fed into separate RTC channels Results indicated both methods to be acceptable Method 2 was preferred for ease of configuration The actual configuration used for CTA 21 is shown in Fig 3

With 10 dB difference between input signals the combiner provided a 0 4–0 5 dB SNR gain over that of the strong signal alone This is in the correct range for what would be predicted by theory

Although the initial test configuration tried was valid, several tests over a period of weeks were required to obtain the above result This was because the following difficulties thwarted the experimenters during early tests

(1) Laboratory power variations and noise interfered with the signal levels during the tests at CTA 21 It was found that the system appeared to be more stable after 5 p.m Therefore, most testing was shifted from daytime to evenings and weekends

(2) SNR values computed by the Telemetry Processor Assembly (TPA) fluctuated ±1 5 dB In trying to measure a 0 5 dB gain, an SNR value good to ±0 1 dB is needed It took some time before a technique was evolved to do this with any confidence in the results The problem was exacerbated by the power variations noted above

A Block IV receiver degradation problem also existed, and was eventually determined to be in the telemetry phase detector module Several attempts were made to improve its performance, with none of them successful So that testing could proceed, it was decided to use the Block III Receivers, and all successful testing at CTA 21 was performed with these receivers at S-band frequency

Because of the variance in the telemetry processor estimated SNR outputs, a symbol error count was the more desirable criterion for measuring system performance However, because of the delay through the combiner, a symbol error count at the higher data rates could not be made using the more desirable psuedo noise pattern (The system has no provision for varying the delay in the symbol error line from the SCA to the Symbol Synchronizer Assembly (SSA)) Two alternatives remained 1) use a less desirable square wave bit pattern or 2) lengthen test time and use the estimated SNR mean for performance measurements Since combiner performance was measured by serially testing and comparing combined and uncombined performance, and with system stability uncertain, most of the testing at CTA 21 was performed with square-wave data using the symbol error count as the prime measurement data

Note that the purpose of testing at CTA 21 was to measure performance of the RTC only, therefore, all measurements were relative (combined to uncombined), masking degradation of the remaining system components

Of primary concern during this period was the source of the SNR fluctuations

(1) Were the SNR fluctuations real?

  (a) How accurate was the estimator?

  (b) Was it averaged over sufficient time?

(2) Were there system problems causing the fluctuations?

  (a) If so which component in the telemetry string varied?

(3) Was the signal varying?

Solutions included,

(1) Running tests on swing or midshift

(2) Switching hardware to improve the telemetry string

(3) Running extensive BER (bit error rate) tests on the data to determine the appropriate data collection time and isolate causes of SNR variation

It was found that approximately 10 minutes of data at or above 2 kb/s[1] was needed to obtain stable SNR results BER

[1] More specifically @1 dB ± 0 1 dB = SNR

$$\text{SER} = 0\,056 \pm 0\,0025$$

$$n = \frac{\text{SER}(1 - \text{SER})}{\sigma^2}$$

$$= \frac{(0\,056)\,(0\,944)}{(0\,00125)^2}$$

$$n = 350{,}000 \text{ bits}$$

$$t = \frac{3500 \text{ bits}}{2000 \text{ bps}} = 17\,5 \text{ s (@2 kb/s)}$$

Therefore at 2 kb/s it should only take approximately 18 s to establish the SNR to within 0 1 dB But with all the uncertainties of telemetry string operation, a 10 minute test is recommended to assure system stability and to validate proper operation of the string

tests using controlled data verified that SNR data from the TPA was accurate and stable over this time period It is essential that all equipment in the telemetry string be calibrated and in specification, to obtain reliable data

B. Goldstone

The RTC was then moved to Goldstone and installed for a first test with live spacecraft data on December 19, 1978 The first two tests were inconclusive A test was run on February 21, 1979 that showed a combined signal gain of from 0 4 to 1 0 dB This was still inconclusive proof of combiner performance since the expected value was a steady 1 2 dB gain However, there were several hours of combiner operation with positive gain registered This was a step in the right direction Because station availability was extremely limited it was necessary to perform almost all testing at Goldstone during regularly scheduled Voyager passes on a noninterference basis This was highly undesirable in that there was no control over data rates or signal level and available configurations were limited This, coupled with several unknowns (such as proper telemetry receiver phasing requirements, antenna gain at DSS 12, CONSCAN stability, etc) and uncertainties (such as best procedures for configuring an array system, total delay between stations, Block IV receiver performance, etc) was probably the greatest contributing factor to the long time period required to uncover many of the arraying problems, the most significant of which are discussed below

(1) If DSS 12 dropped lock, the only evidence at DSS 14 was that the RTC went from 1 dB gain to 1 dB net loss This relates to how visible the performance of the RTC "system" is to station operators during arraying operations The subject is being studied by a working group

(2) The micro-wave system could invert the signal from DSS 12 This simply required a procedural change

(3) The baseband module in the Block IV receiver cost 1 dB in SNR over that observed in the Block III receiver The baseband module problem is the subject of an approved design change which will be completed in the 64 Meter Network on 1 June 1980 As an interim solution the Block IV 1F was cabled through the Block III baseband modules as shown in Fig 4

(4) The antenna spread between DSS 12 and 14 was 5 to 6 dB at X-band instead of the 4 2 dB expected, due to lower than expected antenna gain at DSS 12 DSS 12 gain was out of specification when the antenna was measured and post encounter adjustments have not improved it

(5) The receiver signal level at DSS 12 would vary ±1 5 dB in a gusty wind (20 knots gusting to 35 knots) The Automatic Gain Control (AGC) variation during gusty winds probably was resolved by antenna servo modifications made to reduce jitter Certainly AGC from both antennas needs to be monitored to track arrayed system performance CONSCAN at DSS 12 was first suspected when this condition occurred Investigation proved otherwise However, CONSCAN does have some glitches with the current software and this is planned to be corrected

(6) No means existed to stop and restart the combiner without complete re-initialization Initialization of the combiner required a minimum of eight operator inputs and is time consuming The production version of the combiner will allow restart with one input and configuration change without restart Configuration and prepass calibration procedures required two hours which was seldom available with the prototype system The Saturn configuration should require no more than 30 minutes if string selection can be eliminated (See discussion, Section VI)

III. Voyager/Jupiter Encounters

The final array configuration at Goldstone used for all encounters thus far is shown in Fig 4 The prototype RTC was used for 10 days around 5 March 1979, for the Voyager I Jupiter encounter, and for 14 days around 2 July 1979, for the Voyager II Jupiter encounter RTC gain was determined to be 0 8 to 1 0 dB and the combined telemetry data stream was used by the project for most of each track Combiner up-time was >95 percent The received carrier frequency was X-band and the SNR difference between DSS 14 and DSS 12 was approximately 5 dB

IV. Pioneer 11/Saturn Encounter

A real bonus was achieved when the array system was used at Goldstone for 10 days around the Pioneer 11 encounter of Saturn on 1 September 1979 Signal levels (at S-band) were too low to use the RTC phase lock loop mode to combine the signals from DSS 12 and 14 DSS 14 is able to improve its gain by 3 dB at S-band by going into a "listen only" mode DSS 12 does not have the listen only option so that its system noise temperature, SNT, remains relatively high[2] For this reason and due to other equipment differences the station SNR difference goes from 5 dB at X-band to 9 dB at S-band With this spread the theoretical combiner gain is only 0 5 dB

[2] at DSS 14, $SNT_{nom} = 16$ K
at DSS 12, $SNT_{nom} = 26$ K

The RTC was operated in the "dead-reckoning" mode whereby the signals are phased by calculating the delay time between the two stations using the combiner minicomputer Normally this calculation is made to bring the signals in range of the phase lock loop (PLL) In the dead-reckoning mode the PLL is bypassed

RTC gain during the Pioneer-Saturn Encounter was 0 3–0 4 dB This was sufficient to permit the project many more hours of 1024b/s data at Goldstone and substantially enhanced the imaging mission With low RTC gain, system performance was difficult to measure in real time The best potential measure of system performance with Pioneer telemetry is frame deletion rate of the sequential decoder Unfortunately, this parameter was calculated based on a running average It proved almost valueless in establishing short term performance of the telemetry string The real measure of performance was Goldstone's ability to receive 1024 b/s data while the rest of the network functioned at 512 b/s

V. Future Use of Arrayed Systems

Permanent RTC installations are to be made at the 64-m net in the first and second quarter of 1980 This will provide the capability to array 64-m/34-m stations at Goldstone, Madrid, and Canberra in time for the Saturn encounters by Voyager in November 1980 and August 1981 Some improvements in display capability will be implemented by that time to permit combined performance evaluation from a central location, either at the 64-m station or at JPL Ninety days of continued RTC operation is currently being planned for the first encounter and 30 days for the second encounter

The most striking operational system problem facing the test investigators at the start of Goldstone array operations was lack of visibility into the arrayed system performance Voice communication provided the most useful means of station status monitoring and very often an investigator had to make trips from DSS 14 to DSS 12 and back to solve problems No information on the microwave system or DSS 12 status was available at DSS 14 where the combiner was installed (see Fig 4) This lack of visibility led to the formation of a combiner working group at JPL This group is concentrating on improving combiner operational visibility for the Voyager/Saturn encounters

The RTC produces a gain of approximately 1 dB when a 34-m signal is added to a 64-m signal in standard X-band configuration In order to measure performance it is necessary to know the gain to, say, 0 1 dB This says that the entire telemetry string must be known to ±0 1 dB Furthermore, each component in that string must be calibrated and within spec to 0 1 dB in order to make combiner gain meaningful During testing, investigators found several instances of 1 dB variations in other components of the telemetry string (refer to earlier discussion of high winds, the Blk IV baseband module, and DSS 12 antenna gain) The message is that a carefully calibrated, tuned, and stable DSS is a prerequisite to successful combiner operations During the encounters, parallel telemetry strings were performance checked daily to determine optimum DSS configuration This was time-consuming and would be unnecessary with proper calibration SPTs run on telemetry strings bi-weekly should ensure good station calibration

VI. Future System Design

The success of increasingly complex arraying operations envisioned in Network Consolidation will depend on sufficient automation in areas of system calibration, array configuration, string selection, and display formatting In particular it would be desirable to have the combiner analyze and disconnect antenna receiver systems that did not meet performance specs As was shown earlier, an out of lock receiver can provide a significant negative gain to combiner system performance These future array systems will be sufficiently complex that operators will not be able to react in real time to system changes

Acknowledgment

The combiner was developed by Larry D Howard under the direction of R Bruce Crow of Section 333 The authors were privileged, as members of DSN Operations Section 377, to become involved in combiner operations during development and early systems testing

Reference

1 R A Winkelstein, "Analysis of the Signal Combiner for Multiple Antenna Arraying", *DSN Progress Report 42-26, January and February 1975*, pp 102-118, 15 April 1975

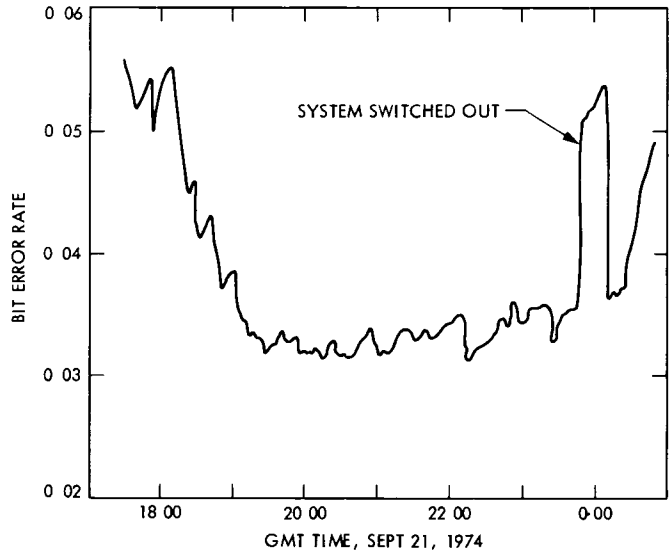

Fig 1 Reproduction of the BER results of the MVM encounter

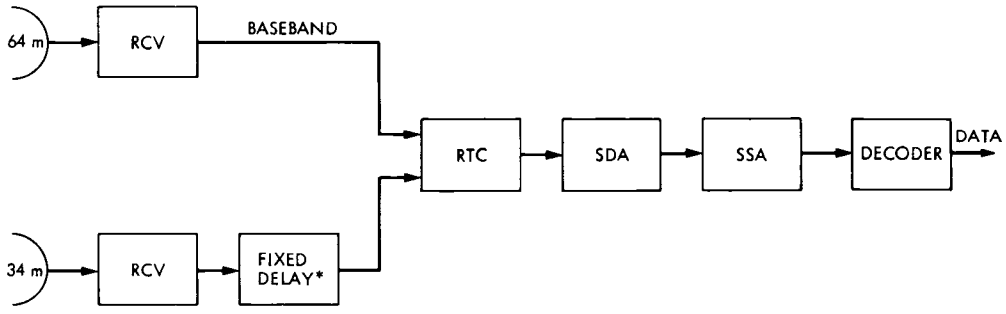

*INTERSITE MICROWAVE LINK DSS 12/14
[CABLES AT CONJOINT STATIONS]

Fig 2 Real-time array system block diagram

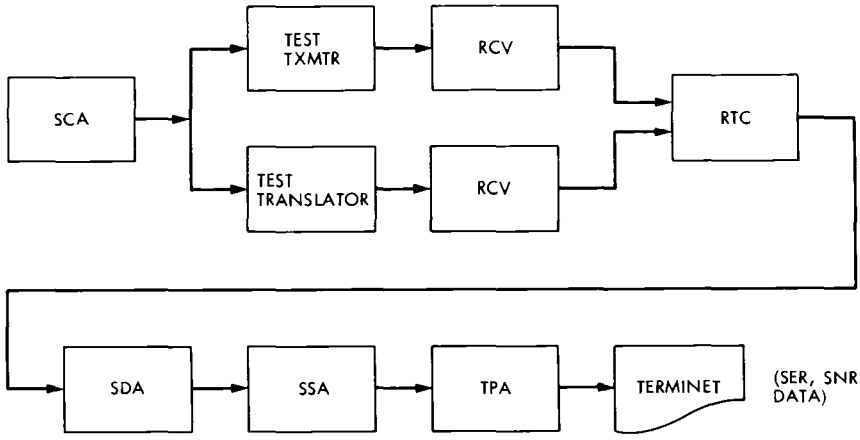

Fig 3 CTA 21 test configuration

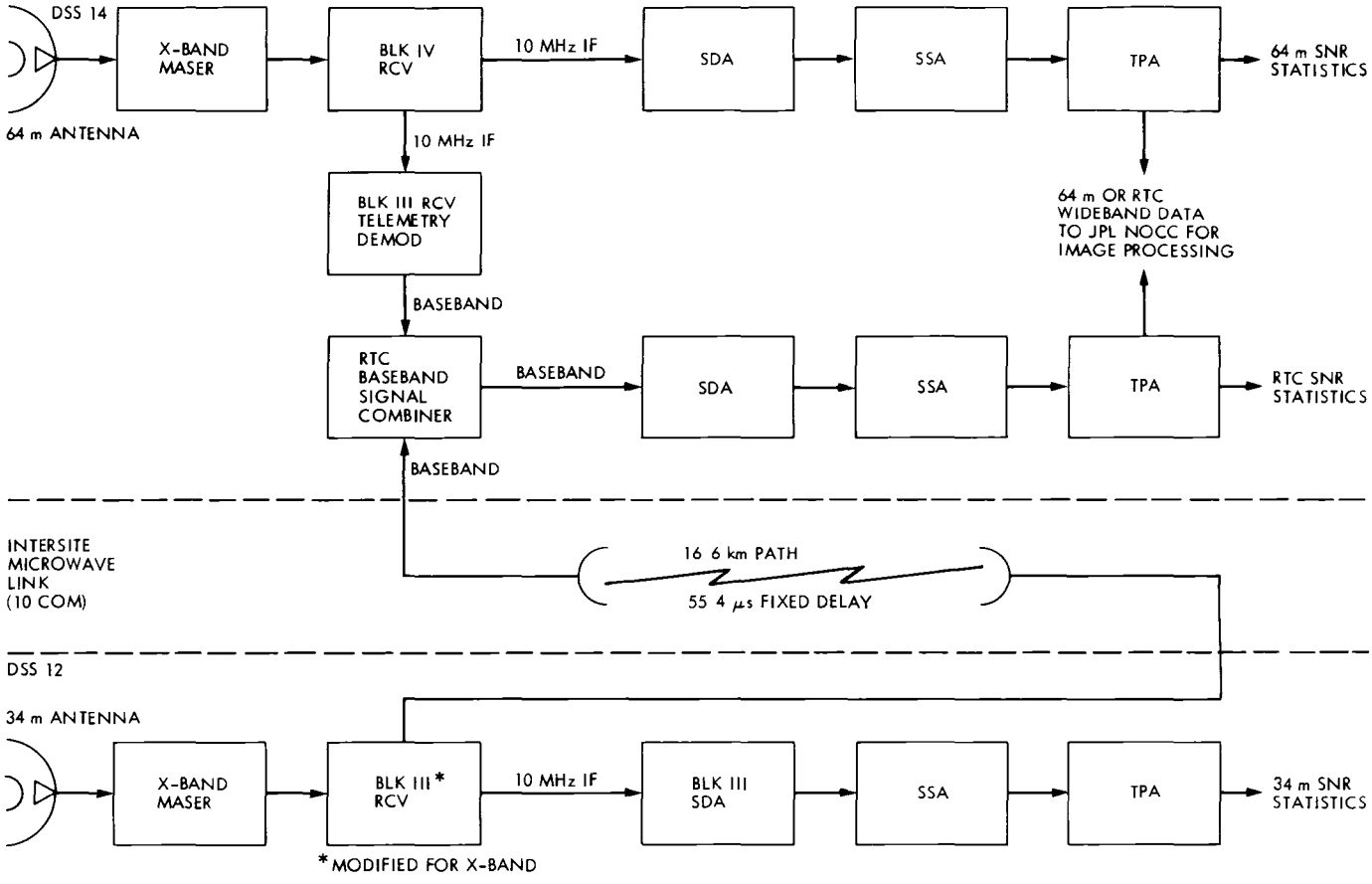

Fig 4 Encounter configuration, real-time combining system block diagram

Viterbi Decoding Modified for Sources With Memory

V Korwar
TDA Planning

This article investigates the gain in signal-to-noise ratio that may be realized by using redundancies inherent in TV data to modify the decoding metric of the DSN Viterbi decoders This modification would take into account the memory in a TV scan line to change the transition probabilities as originally computed using independent data The resulting data rate gain or error probability decrease is achieved without requiring any spacecraft modifications or additions A preliminary examination of this concept on a binary symmetric channel rather than a Gaussian channel and using a simplified Markov source model involving two-level or hard-clipped TV shows that very substantial decreases in error probability may be achieved

I. Introduction

Viterbi decoding for the case where binary messages from a memoryless source are transmitted over a memoryless channel implements maximum likelihood (ML) decoding In this case, this is equivalent to maximum *a posteriori* probability (MAP) decoding since all messages are equally likely However, when the source has memory, such as for video, ML decoding, and hence the Viterbi decoding algorithm, as it is usually implemented, is not optimal For such cases work has been done (see, e g , Ref 1) on encoding the source before transmission and then using a source decoder at the receiver This method utilizes the channel more efficiently However, in cases where the transmitter complexity needs to be minimized, such as when it is on a spacecraft, it is sometimes undesirable to have a source encoder, which may be a complex piece of equipment In such a case, it could be worthwhile modifying the Viterbi decoder at the receiving end so as to increase the transmission rate, while leaving the transmitter untouched

In the present work, we consider the simple case of a Markov source of arbitrary order S, and a memoryless channel, and show how to modify the metric in the Viterbi decoder to implement MAP decoding Calculations of bit error probability (BEP) for a decoder using this new metric become message-dependent An upper bound on the BEP can be obtained for any given message by a method to be described, but elegant bounds similar to those in conventional Viterbi decoding (see, e g , Refs 2 and 3) are only possible for a few messages, and these are derived An upper bound on overall BEP has also been similarly derived for low-entropy sources For a specific $K = 3$ constraint length code, computer simulations of the decoder for a first-order Markov source and a binary symmetric channel (BSC) indicate that the BEP with the new metric are lower than the BEP with the conventional metric, as predicted, with the improvement being more noticeable at rates well below channel capacity However, many more runs of these simulation programs are needed to determine more exactly the extent of the improvement for various parameters

Also, we are interested in the Gaussian channel and not the binary symmetric channel for which the simulations in this work have been done

It has been observed that the Viterbi algorithm (VA), in its most general form, is "a solution to the problem of MAP estimation of the state sequence of a finite-state discrete-time Markov process observed in memoryless noise" (Ref 4) But the Viterbi Algorithm does not seem to have been used as a MAP estimator in the context of decoding convolutionally encoded messages from a Markov source It has, however, been used in the problem of text recognition (Refs 5 and 6) Also, error bounds like the ones given here, for cases where the source has memory, do not seem to have been obtained, nor are there available comparisons between the MAP and ML estimator applications of the VA to decoding problems for sources with memory

II. The New Metric

A. Definition for a BSC

Consider a BSC with channel error or transition probability p_e and a convolutional code of constraint length K, where b bits are transferred at a time into the encoder and n symbols are output at a time (i e , a rate b/n code) Here, "at a time" means at each clock pulse There are bK bits in the encoder register

A Markov source, which we define below, is a simple example of a source with memory A Markov source of order S is defined as one having the property that the probability distribution of the n^{th} bit it outputs (for $n > S$) depends only on the values of the previous S bits output That is, if the sequence of bit output by the source is $\{u_1, u_2, \quad, u_n, \quad\}$, then for $n > S$, the conditional probability $p(u_n|u_{n-1}, \quad, u_1)$ can be expressed as

$$p(u_n|u_{n-1}, \quad, u_1) = p(u_n|u_{n-1}, \quad, u_{n-S}) \qquad (1a)$$

A symmetric first-order Markov source has

$$p(1|0) = p(0|1) \triangleq p_s \qquad (1b)$$

and

$$p(0|0) = p(1|1) \triangleq q_s = 1 - p_s \qquad (1c)$$

Here p_s is called the source transition probability In this paper, whenever we refer to a first-order Markov source, we mean this symmetric one

We first consider a Markov source of order $S \leq bK - 1$, and, for this case, we show that MAP decoding is achieved by using the Viterbi decoding algorithm with modified branch metrics M'_{mi} defined below Each branch defines a transition out of a state s involving $b(K - 1)$ bits to a new state t uniquely defined by the b incoming bits and the $b(K - 1)$ bits of state s Thus, if the Markov source memory extends over fewer than bK previous bits, there is a unique *a priori* probability p_{mi} of occurrence of each branch in the state diagram given by Eq (2b) below

If $S > bK - 1$, we can follow exactly the same decoding procedure with the metrics which we define below, with the exception that the state diagram and the trellis diagram for the decoder now have $2^{(S-b+1)}$ states, with each state represented by $(S - b + 1)$ bits rather than $2^{b(K-1)}$ states, each represented by $b(K - 1)$ bits (Each node will, as usual, have 2^b branches merging at it and 2^b branches emanating from it) However, since $S - b + 1 > b(K - 1)$ for $S > bK - 1$, this increases the decoder complexity So, if b is small, we might as well increase K, which increases the encoder complexity only slightly, but reduces BEP considerably Thus, it may often be worthwhile choosing b, K, S such that $S \leq bK - 1$ holds, if some other constraints are not violated in doing so If b is large, however, increasing K even by 1 increases the number of states by a factor of 2^b This may increase the decoder complexity much more than if we were to keep K fixed and have $2^{(S-b+1)}$ states in the decoder to take care of the source memory S being greater than $bK - 1$

The branch metric of conventional Viterbi decoding for the i^{th} branch of the m^{th} possible path through the trellis is $-d_{mi}$ where d_{mi} is the Hamming distance between the n-dimensional code subvector for the branch and the corresponding n-dimensional received subvector (see Ref 2) We define the new metric as

$$M'_{mi} = -d_{mi} + \frac{\ln p_{mi}}{\ln \dfrac{(1 - p_e)}{p_e}} \qquad (2a)$$

p_{mi} can be written as the conditional probability

$$p_{mi} = p(u_{mi}|u_{m(i-1)}, \quad, u_{m(i-S)}) \qquad (2b)$$

for an S^{th} order Markov source, where u_{mi} is the i^{th} bit of the m^{th} possible message of block length B Note that m runs from 0 to $2^B - 1$ We assume throughout that $B >> K$, and that the last $b(K - 1)$ bits transmitted are always 0

B. Definition for an Arbitrary Memoryless Channel

The conventional branch metric M_{mi} for the i^{th} branch of the m^{th} path is the logarithm of the conditional probability of the i^{th} received subvector (Ref 2)

$$M_{mi} = \ln p(\bar{y}_i|\bar{x}_{mi}) \tag{3}$$

where $\bar{x}_{mi}$ is the n-dimensional code subvector of the m^{th} message sequence for the i^{th} branching level, and $\bar{y}_i$ is the corresponding n-dimensional noisy received vector The modified metric in this case is

$$M'_{mi} = \ln p(\bar{y}_i|\bar{x}_{mi}) + \ln p_{mi} \tag{4}$$

where p_{mi} is defined in Eq (2b)

C. Derivation of New Metric

We now derive the new metric defined above for the case where the source memory is S

Let $\{u_{m1}, \quad , u_{mB}\}$ be the m^{th} possible message sequence of block length B Then the *a priori* probability of the sequence $\{u_{m1}, \quad , u_{mB}\}$ is

$$p(m) = p(u_{m1}, \quad , u_{mB})$$

$$= p(u_{mB}|u_{m(B-1)}, \quad , u_{m(B-S)})\, p(u_{m(B-1)}|u_{m(B-2)},$$

$$u_{m(B-S-1)}) \quad p(u_{m1}|u_{m0}, u_{m(-1)}, \quad , u_{m(1-S)})$$

$$= p_{mB} p_{mB-1} \quad p_{m1} \tag{5a}$$

where p_{mi} is defined as in Eq (2b), and we define

$$\{u_{m0}, u_{m(-1)}, \quad , u_{m(1-S)}\} = \{0, 0, \quad , 0\} \tag{5b}*$$

Then the MAP decoder should choose that B-bit block corresponding to message m that has the maximum *a posteriori* probability given by

$$p_{ap} = \prod_{i=1}^{B} p(\bar{y}_i|\bar{x}_{mi}) \frac{\{p(m)\}}{p(\bar{y})} \tag{6}$$

*Alternatively, we may take care of the initial bits by defining p_{m1}, , p_{mS} each to be 0 5

where $p(m)$ is given by Eq (5), $\bar{x}_{mi}, \bar{y}_i$ have the same meaning as in Eq (4), and $p(\bar{y})$ is the probability of receiving $\bar{y}$ This probability is constant for all messages m, and hence can be dropped from the maximization, or, equivalently, we can maximize the log of this probability (after dropping $p(\bar{y})$), i e ,

$$\ln p'_{ap} = \sum_{i=1}^{B} \ln \left\{ p(\bar{y}_i|\bar{x}_{mi}) \right\} + \ln \{p(m)\} \tag{7}$$

$$= \sum_{i=1}^{B} \left\{ \ln p(\bar{y}_i|\bar{x}_{mi}) + \ln p_{mi} \right\} \tag{8}$$

From this it follows that the branch metric for the i^{th} branch of the m^{th} message path is given by Eq (4) For a BSC with transition probability p_e, we can further simplify Eq (4) using the fact that (Ref 2)

$$p(\bar{y}_i|\bar{x}_{mi}) = p_e^{\,d_{mi}} (1 - p_e)^{n - d_{mi}} \tag{9}$$

Thus, Eq (4) becomes

$$M''_{mi} = \left\{ -d_{mi} \ln \left(\frac{1 - p_e}{p_e} \right) + n \ln (1 - p_e) + \ln p_{mi} \right\} \tag{10}$$

Or, dropping the $n \ln (1 - p_e)$, which is constant for all branches, and dividing by

$$\ln \left(\frac{1 - p_e}{p_e} \right)$$

we get

$$M'_{mi} = -d_{mi} + \frac{\ln p_{mi}}{\ln \left(\frac{1 - p_e}{p_e} \right)} \tag{11}$$

which establishes Eq (2a)

III. Error Probability Bounds With New Metric

We now derive upper bounds on the probability of error with the new metric in a manner paralleling the derivation of

Eq 4 4-8 of Ref 2, which is repeated as Eq R1 below

$$E[n_b(j)] \leqslant \sum_{i=1}^{\infty} \sum_{d=d_f}^{\infty} ia(d,i)Z^d \qquad \text{(R1)}$$

where $E[n_b(j)]$ is the expected number of bit errors caused by an incorrect path diverging at node j, $a(d,i)$ is the number of paths diverging from the all-zeros path (at node j) at distance d and with i "1's" in its data sequence over the unmerged segment, d_f is the minimum distance of any path from the correct one, called the free distance, and Z is defined in Eq (R2)

$$Z = \sum_{y} \sqrt{p_1(y)\,p_0(y)} \qquad \text{(R2a)}$$

Here $p_1(y)$, $p_0(y)$ are the probabilities of receiving a given value of a bit y when the corresponding transmitted bit is a 1 or a 0, respectively For the special case of a BSC, Z reduces to

$$Z = \sqrt{4\,p_e(1-p_e)} \qquad \text{(R2b)}$$

A Extension of the Bhattacharya Bound

We first extend the Bhattacharya bound to the case in which MAP detection occurs rather than ML detection

If $p_E(m \to m')$ denotes the probability that message m' is decoded when message m is sent and only two alternatives (m and m') exist, and if $\bar{x}_m$ is the signal vector sent and $\bar{y}$ the one received, and if $\bar{x}'_m$ is the other possible signal vector, then the Bhattacharya bound states (Eq 2 3 15 of Ref 2) that

$$p_E(m \to m') \leqslant \sum_{y} \sqrt{p(\bar{y}|\bar{x}'_m)\,p(\bar{y}|\bar{x}_m)} \qquad \text{(R3)}$$

We now extend this bound to the case of MAP detection We have

$$p_E(m \to m') = \sum_{\bar{y} \in \Lambda_{mm'}} p(\bar{y}|\bar{x}_m) \qquad \text{(12a)}$$

where

$$\Lambda_{mm'} = \left\{ \bar{y} \;\middle|\; \frac{p_{m'}\,p(\bar{y}|\bar{x}'_m)}{p_m\,p(\bar{y}|\bar{x}_m)} \geqslant 1 \right\} \qquad \text{(12b)}$$

or

$$\Lambda_{mm'} = \sum_{\bar{y}} f(\bar{y})\,p(\bar{y}|\bar{x}_m) \qquad (13)$$

where

$$f(\bar{y}) = \begin{cases} 1, & \text{for } y \in \Lambda_{mm'} \\ 0, & \text{otherwise} \end{cases} \qquad (14)$$

Now

$$f(\bar{y}) = \begin{cases} 1 \leqslant \sqrt{\dfrac{p'_m\,p(\bar{y}|\bar{x}'_m)}{p_m\,p(\bar{y}|\bar{x}_m)}}, & \text{for } y \in \Lambda_{mm'} \\ 0 \leqslant \sqrt{\dfrac{p'_m\,p(\bar{y}|\bar{x}'_m)}{p_m\,p(\bar{y}|\bar{x}_m)}}, & \text{otherwise} \end{cases} \qquad (15)$$

where the first part of the inequality follows from the definition of $\Lambda_{mm'}$ and the second is trivial

Thus, for all $\bar{y}$,

$$f(\bar{y}) \leqslant \sqrt{\frac{p'_m\,p(\bar{y}|\bar{x}'_m)}{p_m\,p(\bar{y}|\bar{x}_m)}} \qquad (16)$$

Using this in Eq (13) gives

$$p_E(m \to m') \leqslant \sum_{\bar{y}} \sqrt{\frac{p'_m}{p_m}\,p(\bar{y}|\bar{x}'_m)\,p(\bar{y}|\bar{x}_m)} \qquad (17)$$

Thus, the only difference between this inequality and the corresponding one for ML decoding (Eq R3), i e , the usual Bhattacharya bound, is the extra factor $\sqrt{p'_m/p_m}$ in Eq (17) This bound is tighter than the usual Bhattacharya bound whenever the decoded message m' is less probable than the one sent, m, i e , if

$$p'_m \leqslant p_m \qquad (17)'$$

B. MAP Decoding Error Bound

This bound is derived using the union bound and the extended Bhattacharya bound (Eq 17) The fact that the *a priori* probabilities of the various possible messages are unequal changes the locations of the MAP receiver decision

boundaries in signal space but the expression for the union bound is unchanged Thus, we get, for the message m actually being sent, that the total probability of error considering all other possible messages is

$$p_{Em} \leqslant \sum_{m' \neq m} p_E(m \to m') \tag{18}$$

$$\leqslant \sum_{\bar{y}} \sum_{m' \neq m} \sqrt{\frac{p'_m}{p_m} p(\bar{y}|\bar{x}_{m'}) p(\bar{y}|\bar{x}_m)} \tag{19}$$

after using Eq (17)

Now for memoryless channels we can show that (see Appendix)

$$p_E(m \to m') \leqslant \sqrt{\frac{p'_m}{p_m}} \left\{ \sum_y \sqrt{p_1(y) p_0(y)} \right\}^{w_{mm'}}$$

$$\triangleq \sqrt{\frac{p'_m}{p_m}} Z^{w_{mm'}} \tag{20a}$$

where $w_{mm'}$ is the Hamming distance between messages m and m', and $p_1(y)$, $p_0(y)$ are the probabilities of receiving a given value of a bit y given that the corresponding transmitted bit is a 1 or 0, respectively Here

$$Z \triangleq \sum_y \sqrt{p_1(y) p_0(y)} \tag{20b}$$

which, for the special case of a BSC, reduces to

$$Z = Z_{\text{BSC}} = \sqrt{4 p_e (1 - p_e)} \tag{20c}$$

We now apply these equations to the calculation of upper bounds on event and bit error probabilities We know that a necessary condition for an event error to begin occurring at node j is that an incorrect path diverging from the correct one at node j accumulates higher total metric than the correct one over the unmerged segment If we denote by Γ the set of all such incorrect paths when the input message is m, using the union bound as in Eq (18), we get, for the probability of an event error occurring at node j with m input,

$$p_j(e|m) \leqslant \sum_{m' \in \Gamma} \sqrt{\frac{p'_m}{p_m}} Z^{w_{mm'}}$$

$$\leqslant \sum_{m' \neq m} \sqrt{\frac{p'_m}{p_m}} Z^{w_{mm'}} \tag{21}$$

In the second inequality above, the summation is over all $m' \neq m$

We can bound the probability of bit error for the input message m, $p(b|m)$, by weighting each of the terms in the sum in Eq (21) by the number of bit errors $\iota_{mm'}$ occurring in choosing that incorrect path m', i e ,

$$p(b|m) \leqslant \sum_{m' \neq m} \sqrt{\frac{p'_m}{p_m}} \iota_{mm'} Z^{w_{mm'}} \tag{22}$$

Accounting for all possible transmitted messages m, the overall BEP is given by

$$p_b(\text{MAP}) = \sum_m p(b|m) p_m$$

$$\leqslant \sum_m \sum_{m' \neq m} \sqrt{p'_m p_m} \iota_{mm'} Z^{w_{mm'}} \tag{23}$$

Equations (22) and (23) can, in theory, be evaluated for a specific code, but, except for certain cases, as in those of Subsection III-F, are very cumbersome in practice

We cannot make further simplifications in Eqs (22) and (23), directly at least, as we can in the usual ML decoding case, because each sum in the bound in Eq (22) depends on the particular message m and the incorrect message m' For certain specific messages m it is possible to extend the generating function method (as we do in Subsection III-F) to obtain elegant expressions for $p(b|m)$, but that is not sufficient to enable calculation of the overall BEP $p_b(\text{MAP})$, since all messages do not have the same error probabilities

C. Comparison of MAP and ML Decoding Error Bounds

If the usual Viterbi or ML decoding were used for the same system, we would have, for the bit error probability given that message m is sent,

$$p(b|m) \leq \sum_{m' \neq m} Z^{w_{mm'}} \iota_{mm'} \tag{24}$$

where $w_{mm'}$ and $\iota_{mm'}$ are the same as in Eq (22) The overall BEP would be

$$p_b(\mathrm{ML}) = \sum_m p(b|m) p_m$$

$$\leq \sum_m \sum_{m' \neq m} p_m \iota_{mm'} Z^{w_{mm'}} \tag{25}$$

Now Eq (23) and Eq (25) both involve a double summation over all possible pairs of messages m, m' We compare these term by term Consider a pair of messages m_1 and m_2 with probabilities p_{m_1}, p_{m_2} Their contributions to the sums in Eqs (23) and (25) are

$$C_{\mathrm{MAP}} = Z^{w_{m_1 m_2}} \iota_{m_1 m_2} \left(\sqrt{p_{m_1} p_{m_2}} + \sqrt{p_{m_1} p_{m_2}} \right)$$

$$= 2 \sqrt{p_{m_1} p_{m_2}} Z^{w_{m_1 m_2}} \iota_{m_1 m_2} \tag{26}$$

and

$$C_{ML} = \left(p_{m_1} + p_{m_2} \right) Z^{w_{m_1 m_2}} \iota_{m_1 m_2} \tag{27}$$

Comparing Eqs (26) and (27), we see that

$$C_{\mathrm{MAP}} \leq C_{\mathrm{ML}} \tag{28}$$

for all p_{m1}, p_{m2}, with equality holding for $p_{m1} = p_{m2}$ Thus, we get

(MAP) error upper bound $\leq$ (ML) error upper bound (29)

Since the upper bounds in Eqs (23) and (25) are asymptotically tight, we expect from Eq (29) that, for low BEP where the bounds are close to the actual error probabilities, the new metric is better than, or as good as, the conventional one Also, on general principles, we know that MAP decoding is always at least as good as ML decoding

D. Approximate Magnitude of Improvement Expected From Upper Bound Expressions

From Eqs (23) and (25) we may obtain an order-of-magnitude estimate of the improvement in BEP using MAP decoding We assume a low enough BEP so that the actual BEP is replaceable by the upper bounds in Eqs (23) and (25) Since the BEP is low, we must have Z small, so that the terms in Eqs (23) and (25) with factors $Z^{w_{mm'}}$, where $w_{mm'}$ is greater than the free distance d_f of the code, are negligible compared to the terms with factors Z^{d_f} Thus, we may retain only these terms and have

$$\frac{p_b(\mathrm{ML})}{p_b(\mathrm{MAP})} \approx \frac{\sum_{mm' \in \Gamma} p_m Z^{d_f} \iota_{mm'}}{\sum_{mm' \in \Gamma} \sqrt{p_m p_{m'}} Z^{d_f} \iota_{mm'}}$$

$$= \frac{\sum_{mm' \in \Gamma} p_m \iota_{mm'}}{\sum_{mm' \in \Gamma} \sqrt{p_m p_{m'}} \iota_{mm'}} \tag{30}$$

where Γ is the set of path pairs m, m' with Hamming distance equal to d_f between them

Further simplification is possible only if we know the probabilities of the message pairs that are at the free distance from each other and this is specific to the code and the source

E. Further Approximation for First-Order Markov Source

In this section we make an order-of magnitude estimate of the improvement in BEP for the specific case of a first-order Markov source with low transition probability p_s For such a source with low p_s, there is a lot of redundancy in the message output, and we may expect the MAP method to be most useful in this case In making our estimate of the improvement in BEP in this section, we make the following assumptions

(1) We assume that the most probable message transmitted, m_1, has an *a priori* probability so close to 1 that the overall BEP p_b(MAP) may be closely approximated by the BEP given m_1, $p(b|m_1)$

(2) Given that an error is made in decoding this message m_1, we assume that the BEP given m_1 can be calculated by considering only those possible erroneously decoded messages that are closest in distance to m_1 In doing this, we are again using the arguments leading to Eq (30) in Subsection III-D

(3) Among these closest-distance erroneous messages, we further restrict our attention to the one that has the highest *a priori* probability There may be more than one such message possible but we ignore this small factor in getting our order-of-magnitude estimate

Thus, assumption (1) enables us to consider only one transmitted message m_1 and assumptions (2) and (3) enable us to narrow down the set of possible erroneously decoded messages (given that m_1 is sent) to only one message, which we call m_2

Since the first-order Markov source has a low transition probability p_s, the most probable messages it puts out will consist of long strings of zeros and long strings of ones with occasional (with probability p_s) transitions from one type of string to the other We now make the following assumption

(4) We assume that the most probable message m_1 has long enough runs of zeros and ones that we can replace it, for the purpose of calculating BEPs, by one with no transitions at all, say, the all-zero message

Now the messages closest to m_1 will differ from it in only a small number of bits (like 1 or 2 depending on the specific code) We can see that the most probable of these, i e , m_2, will have at least 2 transitions in it For instance, the relevant portions of m_1 and m_2 may be -000- and -010-, or -0000- and -0110- Thus, for the specific code discussed in Section IV, if an error occurs in decoding a portion -000- of a message, and if the erroneously decoded message is at the free distance from the correct one, it occurs because -000- is decoded as -010-

We may now calculate the improvement in BEP considering only the messages m_1 and m_2 For symmetry, we include in p_b(MAP), both $p(b|m_1)$ and $p(b|m_2)$, where the conditional bit error probability for each message is calculated assuming the other one as being the erroneously decoded message We do this using the method of Subsection III-D, and get

$$\frac{p_b\,(\mathrm{ML})}{p_b\,(\mathrm{MAP})} \approx \frac{p_{m1} + p_{m2}}{2\sqrt{p_{m1}\,p_{m2}}} \tag{31}$$

Defining

$$q_s = 1 - p_s \tag{32}$$

this becomes

$$\frac{p_b\,(\mathrm{ML})}{p_b\,(\mathrm{MAP})} \approx \frac{q_s}{2p_s} + \frac{p_s}{2q_s} \tag{33}$$

For instance, if $p_s = 10^{-3}$, we have from Eq (33),

$$\frac{\text{old BEP}}{\text{new BEP}} \approx 499.5 \tag{34}$$

Thus, there is about a factor of 500 improvement in BEP in this case using the new metric

F. Generating Function Method for Low p_S Case

In this section, we show how to calculate the improvement in BEP more exactly than we did in Subsection III-E The method to be described holds for all p_s if the only message considered is the all-zeros or the all-ones message and also possibly for certain specific messages depending on the code For low p_s, the most probable messages consist of strings of zeros and ones with occasional transitions between strings so that this analysis holds for most of the probable message sequences

We have for 2 messages m, m',

$$p_E(m \to m') \leqslant \sqrt{\frac{p_{m'}}{p_m}}\; Z^{w_{mm'}} \tag{20}$$

which differs from the corresponding equation for the conventional decoder only in the factor $\sqrt{p_{m'}/p_m}$ Here, p_m is the probability of the transmitted message sequence in consideration and p'_m is the probability of the erroneously decoded message m' We can express p_m and p'_m using Eq (5) for the special case of the first-order Markov source as

$$p_m = p_{mB}\,p_{m(B-1)} \quad p_{m1} \tag{35}$$

$$p_{m'} = p_{m'B}\,p_{m'(B-1)} \quad p_{m'_1} \tag{36}$$

where

$$p_{mJ} = p\left(u_{mJ}|u_{m(J-1)}\right) \tag{35a}$$

$$p_{m'_J} = p\left(u_{m'_J}|u_{m'(J-1)}\right) \tag{36a}$$

So we have

$$p_E(m \to m') \leqslant Z^{w_{mm'}} \sqrt{\frac{p_{m'B}}{p_{mB}} \quad \frac{p_{m'1}}{p_{m1}}} \tag{37}$$

We can then rewrite Eqs (21) and (22) as

$$p_I(e|m) \leqslant \sum_{m' \neq m} Z^{w_{mm'}} \sqrt{\frac{p_{m'B}}{p_{mB}} \frac{p_{m'1}}{p_{m1}}} \tag{21}'$$

$$p(b|m) \leqslant \sum_{m' \neq m} \iota_{mm'} Z^{w_{mm'}} \sqrt{\frac{p_{m'B}}{p_{mB}} \frac{p_{m'1}}{p_{m1}}} \tag{22}'$$

Now each of the factors $\sqrt{p_{m'_l}/p_{m_l}}$ in Eq (37) corresponds to a particular branch in the trellis If the input message is such (e g , the all-ones or the all-zeros message) that all possible incorrect paths can be accounted for by tracing varying numbers of loops on a diagram obtained by opening up the state diagram at some node, then we know that all the paths at various distances from the correct one can be expressed by terms of the series expansion of the generating function $T(D)$ (§4 3 of Ref 2) Here, D has the usual meaning that its exponent for any branch represents the distance of that branch from the corresponding code subvector of the input message In order to weight each of these terms by the factor $\sqrt{p_{m'_l}/p_{m_l}}$, all we need to do is to associate with each branch of the opened-up state diagram the appropriate factor $\sqrt{p_{m'_l}/p_{m_l}}$ and then evaluate the resulting generating function which we denote by $T_m(D)$ We then set $D = Z$ in the expression $T_m(D)$ to evaluate the bound in Eq (21)' Similarly, to get the bound in Eq (22)', we obtain the generating function $T_m(D,I)$, where I has the usual meaning that $I = 1$ for a given branch if its bit differs from the corresponding bit in the input message and $I = 0$ otherwise, and we set $D = 2$, $I = 1$ in $\partial T_m/\partial I\,(D,I)$ to evaluate the bound in Eq (22)' This generating function method allows us to take into account all possible erroneous paths and their error contributions rather than just one as in Subsection III-E

In the special case of the first-order Markov source, we get an even simpler expression for event and bit error probability bounds Each of the p_{m_l} and $p_{m'_l}$ is either p_s or q_s in this case So each term in the sums in Eqs (21)' and (22)' has a factor of M^k evaluated at $M = \sqrt{p_s/q_s}$, where k is an integer This integer can be determined as follows We first associate with each branch of the opened-up state diagram either M or 1 or M^{-1}, depending on whether $p_{m'_l}/p_{m_l} = p_s/q_s$ or 1 or q_s/p_s for the particular branch Thus, for the all-zeros or the all-ones message, we write M for branches corresponding to a transition in the message and 1 for branches with no transition, since in these cases, p_{m_l} is always equal to q_s and $p_{m'_l}$ can be either p_s or q_s We then evaluate the transfer function $T(D,M)$ (this takes the place of the transfer function $T_m(D)$ we had in the previous paragraph for the higher order Markov cases) and the transfer function $T(D,M,I)$ (to take the place of $T_m(D,I)$ of the previous paragraph) We can then see that the event error probability at any node, say, J, is given by

$$p_J(e|m) \leqslant T(D,M) \Big|_{\substack{M = \sqrt{\frac{p_s}{q_s}} \\ D = Z}} \tag{38}$$

and the BEP given m is given by

$$p(b|m) \leqslant \frac{\partial T}{\partial I}(D,M,I) \Big|_{\substack{D = Z \\ I = 1 \\ M = \sqrt{\frac{p_s}{q_s}}}} \tag{39}$$

It is not easy to generalize these results to get the overall BEP considering all possible messages, because the functions $T_m(D)$, $T_m(D,I)$ here are message-dependent unlike the usual Viterbi decoding case Thus, for non-repetitive messages, a general expression like those in Eqs (38) and (39) that identifies all other possible paths and their error contributions are not easy to obtain A slight generalization of one method is possible for repetitive messages like, say, 1000, 1000, 1000 for the code considered in the next section, by opening up, not just one node, but a path in the state diagram corresponding to the message unit repeated But even in this case, it is necessary to consider each possible erroneously decoded message individually and obtain its contribution to the BEP

As we have stated before, if p_s is low, then just considering the all-zeros or all-ones message should be good enough to obtain an estimate of the overall BEP

IV. Illustration With a Specific Code

A. The Code

We assume a BSC, a first-order Markov source with transition probability p_s and a specific $K = 3, b = 1, n = 2$ (rate 1/2) code The encoder is shown in Fig 1, and the state diagram is shown in Fig 2 Bits come in at the left in Fig 1 and the states (written in boxes at the nodes in Fig 2) are represented by the rightmost 2 bits of the encoder The dotted and solid lines in Fig 2 correspond to a 1 and a 0 input bit, respectively

B. Calculations

The state diagram with the 00 node opened up and the branches marked with the appropriate powers of D,I,M are shown in Fig 3 This diagram thus corresponds to the all-zeros input message

The generating function is

$$T(D,I,M) = \frac{D^5 IM^2}{1 - DI - DIM^2} \tag{40}$$

so that the BEP given $m =$ 00 is

$$p(b\,|m)|_{MAP} \leq \left.\frac{\partial T}{\partial I}\right|_{\substack{I=1 \\ M=\sqrt{\frac{p_s}{q_s}} \\ D=Z}}$$

$$= \left.\frac{D^5 M^2}{(1 - D - DM^2)^2}\right|_{\substack{M=\sqrt{\frac{p_s}{q_s}} \\ D=Z}} \tag{41a}$$

$$= D^5M^2 \{1 + 2D(1+M^2) + 3D^2(1+M^2)^2 + 4D^3(1+M^2)^3 + \}\Big|_{\substack{M=\sqrt{\frac{p_s}{q_s}} \\ D=Z}} \tag{41b}$$

For the case of the conventional ML decoder, we would obtain a similar expression with $M = 1$, i e ,

$$p(b\,|m)_{ML} \leq \left.\frac{D^5}{(1 - 2D)^2}\right|_{D=Z} \tag{42a}$$

$$\leq D^5 \{1 + 2D \cdot 2 + 3D^2 \cdot 2^2 + 4D^3 \cdot 2^3 + \}\Big|_{D=Z} \tag{42b}$$

The expansion of Eq (41b) shows that the path with minimum distance (=5) has 2 transitions and one bit error, corresponding to the term D^5M^2, of the two paths with distance 6, one has 2 transitions and the other 4, and each of these has 2 bit errors corresponding to the $2D^5 \cdot M^2 \cdot D(1 + M^2)$ term, and so on

From the expansions of Eqs (41b) and (42b), we see that if $M^2 < 1$, i e ,

$$p_s < 0\,5 \tag{43}$$

the bound of Eq (41b) is smaller than that of Eq (42b) by a factor of more then M^2, since each term in the brackets in Eq (41b) is smaller than the corresponding one in brackets in Eq (42b)

In our example, we assume $M^2 < 1$ If we assume the bounds in Eqs (41) and (42) to be close to the actual BEP because of our $p_s << 1$ assumption, there is an improvement in BEP by more than a factor of $M^2 = p_s/q_s$ Thus, for $p_s =$ 0 1, we have that the new BEP is lower than the old BEP by at least a factor of 1/9

For the all-ones input message, the 11 node can be opened up If the details are worked out, we obtain, as expected, exactly the same expression as in Eq (41)

C. The Simulations

We simulated the encoder and decoder for the code described above and ran several messages of 298-bit block lengths for various sets of parameters p_s and p_e, with both p_s, $p_e < 0\,5$ Initially, we checked the program with just a block of zeros or just a block of ones as input and, later, generated the input messages themselves within the program by including a simulation of the Markov source In this case the input messages are realistic ones and were found to consist of strings of zeros and ones as expected The simulations show that the BEP with the new metric is always lower (for p_s, $p_e < 0\,5$) than with the conventional metric But a larger number of simulations would be needed to obtain the exact amount of improvement, especially for the cases with low BEP However, the results shown in Table 2 clearly demonstrate the improvement We also see that for low enough p_e, the improvement in BEP is by a factor $> p_s/q_s$, as predicted by Eqs (41) and (42)

Another fact that was indicated by the simulations (see Table 1), but which again needs further verification, is that the decoder with the new metric needs a trellis truncation depth of at least 20 constraint lengths for negligible truncation error, as opposed to the 5 constraint lengths required for the old decoder (Ref 3) The truncation scheme we are talking about

here is the simple one described in §4 7 of Ref 2, in which, as each set of b bits enters the registers of each state, the b bits which entered 20K branches earlier are removed, after the decoder has made a final decision on these bits by setting them equal to the appropriate survivor bits of an arbitrary state In obtaining the results described in Table 2, we used a 40K truncation length rather than 20K, to be on the safe side

D. Channel Capacity Limitations

From the results of the simulations (Table 2) we see that for given p_s, if the probability of channel transition p_e is high, the BEP is high for both the new and the old decoding algorithm, and the ratio of the new BEP to the old BEP increases with p_e Similarly, for a given p_e, this ratio increases as p_s increases For the given source and channel, we can calculate the source entropy and the channel capacity, which are given, respectively, by

$$H(p_s) = -p_s \log_2 p_s - (1 - p_s) \log_2 (1 - p_s) \tag{44}$$

and

$$C(p_e) = 1 - H(p_e)$$

$$= 1 + p_e \log_2 p_e + (1 - p_e) \log_2 (1 - p_e) \tag{45}$$

Figure 4 shows the nature of these two curves, on the same plot for convenience

Since the channel capacity represents the upper limit on the reliable communication rate, we should expect that no scheme would allow any substantial reduction in BEP above channel capacity Thus, if we set

$$H(p_s) \leqslant C(p_e) \tag{46}$$

we can get the outer limits on the regions of p_e and p_s within which the new scheme can be expected to be useful

We need, from Eqs (44) through (46),

$$-p_e \log_2 p_e - (1 - p_e) \log_2 (1 - p_e) - p_s \log_2 p_s$$

$$- (1 - p_s) \log_2 (1 - p_s) \leqslant 1 \tag{47}$$

or

$$(p_e)^{p_e} (1 - p_e)^{(1-p_e)} (p_s)^{p_s} (1 - p_s)^{(1-p_s)} \geqslant 0\,5 \tag{48}$$

Some sets of parameters p_e and p_s satisfying this relationship with the equality sign are marked with an * in Table 2 Figure 5 shows a plot of old BEP, new BEP, and the ratio of new BEP to old BEP obtained from simulations with the Markov source model included in the program Two sets of curves are shown one set has $p_s = 0\,1$ and p_e varying, the other has $p_e = 0\,1$ and p_s varying Since an insufficient number of simulations were made, however, the shape of the curve is not very reliable But it does show an increase of the ratio of new BEP to old BEP as we approach and exceed channel capacity

E. Comparison of Calculations and Simulations

None of the simulations were made for the very low values of p_e (like 10^{-5} or 10^{-6}) that would be required for the upper bounds of Eqs (41) and (42) to be approached, since too many blocks of input would be required Even for the case of $p_s = 0\,1$ and $p_e = 0\,03$, which represents about the lowest data rate to channel capacity ratio in the simulations, there were 0 bit errors with the new decoder in the 10 blocks of 298 bits used and only 1 bit error with the conventional decoder in the same 10 blocks, corresponding to an old BEP of 0 000335, and an even lower new BEP Here the bounds of Eqs (41) and (42) give, respectively,

$$p_b(\mathrm{ML}) \leqslant 0\,046$$

$$p_b(\mathrm{MAP}) \leqslant 0\,001 \tag{49}$$

which are both much higher than the actual BEP obtained by simulation Hence direct verification of the bounds of Eqs (41) and (42) has not been performed in the simulations, but the bounds are probably very useful in calculating BEPs at rates well below capacity where too many simulations would be needed if computer calculation of BEPs were to be performed

V. Conclusions

We have shown that a simple modification of the metric used in the Viterbi decoding algorithm achieves MAP decoding for sources with memory It can cause a noticeable reduction in BEP for sources with strong correlation between bits (i e , low entropy) Analysis methods to obtain upper bounds on the BEP obtainable with the new metric have been given The simulations performed for a BSC and a first-order Markov source verify that an improvement occurs, but to obtain the exact ratio of improvement, more simulations are needed We can conclude, however, that the ratio of new BEP to old BEP for a first-order Markov source and a BSC with very low p_e is at least p_s/q_s and that the extent of improvement reduces as channel capacity is approached and exceeded Simulations also

indicate that a trellis truncation depth of 20 constraint lengths is probably needed for reliable results with the new metric

The modification of the metric required for the case of an arbitrary memoryless Gaussian channel is given The entire analysis given holds for such a Gaussian channel, but the simulations of the decoder have been performed only for the case of the BSC Except in cases where the first-order Markov source is specified, the analysis holds for any Markov source of arbitrary order More work is needed to extend the results to more realistic sources like video data sources Ultimately, the aim is to devise a reasonably simple modification of the Viterbi decoding algorithm that can make use of the correlation between neighboring pixels in video data of scenes to enable more efficient channel use than is possible with the normal Viterbi decoder

Acknowledgment

I would like to thank Dr Edward C Posner of the Jet Propulsion Laboratory, Pasadena, for suggesting the problem and for his valuable comments and encouragement throughout the work

References

1 Mark, J W , "Adaptive Trellis Encoding of Discrete-Time Sources with a Distortion Measure," *IEEE Trans Comm. Technol* , Vol COM-25, pp 408-417, 1977

2 Viterbi, A J , and Omura, J K , *Principles of Digital Communication and Coding*, McGraw-Hill, NY, 1979

3 Heller, J A , and Jacobs, I M , "Viterbi Decoding for Satellite and Space Communication," *IEEE Trans Comm Technol* , Vol COM-19, pp 835-848, 1971

4 Forney, G D , Jr , "The Viterbi Algorithm," *Proc IEEE*, Vol 61, pp 268-278, 1973

5 Neuhoff, D L , "The Viterbi Algorithm as an Aid in Text Recognition," *IEEE Trans Info Theory*, Vol IT-21, pp 222-226, 1975

6 Rosenberg, A E , and Schmidt C E , "Automatic Recognition of Spoken Spelled Names for Obtaining Directory Listings," *BSTJ*, Vol 58, pp 1797-1824, 1979

Table 1 Simulations described in Subsection IV-C to estimate effect of trellis truncation (all runs here have $p_s = 0\,1$, $p_e = 0\,4$)

Program	Truncation length, units	Number of 298-bit blocks	Conventional BEP	New BEP	Remarks
01	10K	1	0 4866	0 5336	Programs 01 through 04 show that 20K truncation length is needed
02	10K	1	0 4832	0 5537	
03	20K	1	0 4899	0 4698	
04	30K	1	0 4899	0 4698	Same sets of random numbers used for the source and channel in 04 as in 03, otherwise different sets used for different blocks of data for both source and channel simulations
05	30K	5	0 5080	0 4170	
06	40K	1	0 4765	0 2416	
07	40K	1	0 5101	0 4060	
08	40K	5	0 5000	0 3698	

Table 2 Simulations described in Subsection IV-C (all with truncation length 40K)

Program	p_s	p_e	Number of 298-bit blocks	Conventional BEP	New BEP	Ratio $\frac{\text{New BEP}}{\text{Conventional BEP}}$	Remarks
1	0 1	0 4	5	0 5000	0 3698	0 7396	All runs have different sets of random numbers for the source and different sets for the channel
2	0 1	0 3	3	0 4508	0 2573	0 5708	
3	0 1	0 2	3	0 3367	0 09396	0 2791	
4*	0 1	0 12	10	0 1117	0 02886	0 2583	
5	0 1	0 08	12	0 02041	0 005593	0 2740	
6	0 1	0 05	15	0 006714	0 0004474	0 0667	
7	0 1	0 03	10	0 000335	0	0	
8*	0 12	0 1	10	0 06146	0 013194	0 2147	
9	0 05	0 1	5	0 07651	0 01342	0 1754	
10	0 03	0 1	10	0 05570	0 002013	0 03614	
11*	0 2	0 04	10	0 003691	0 001678	0 4546	

*Means p_s, p_e for that program define operation at channel capacity

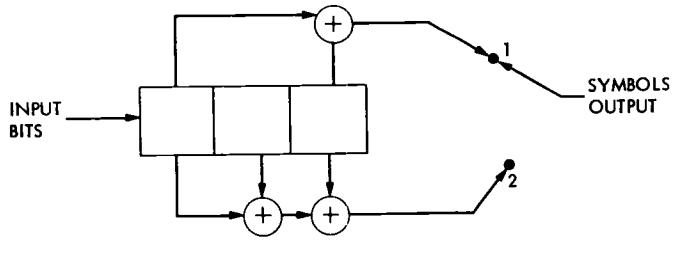

Fig 1 A $K = 3$ encoder

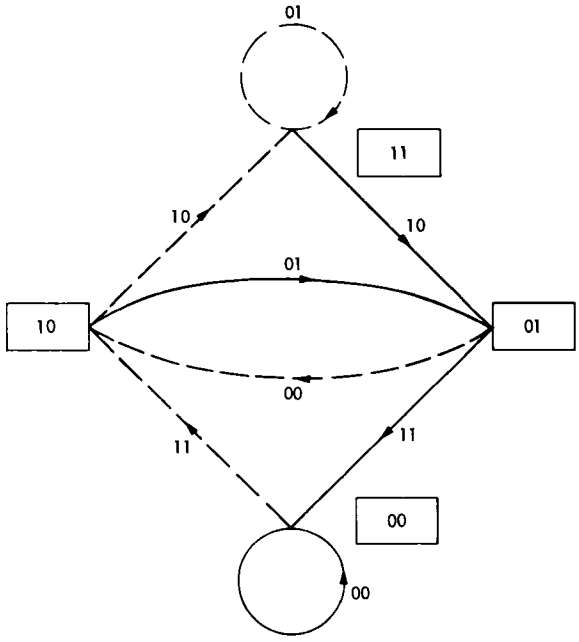

Fig 2 State diagram for encoder of Fig 1

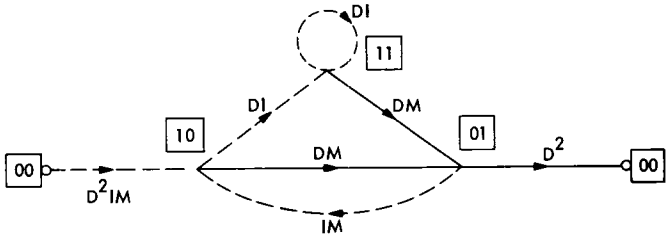

Fig. 3 State diagram labeled with distance, bit errors, and branch probability ratios relative to all-zeros input

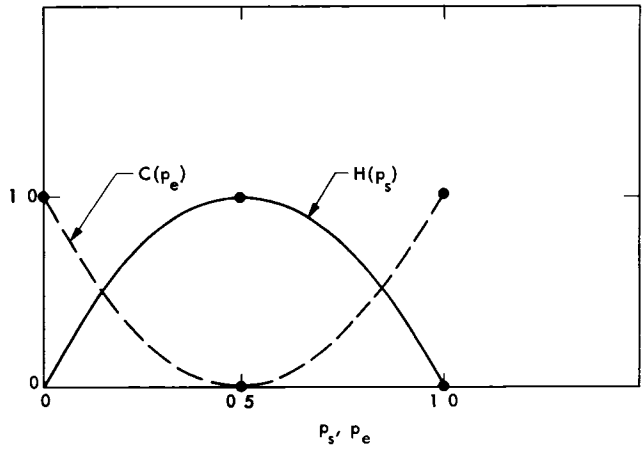

Fig 4 Source entropy vs p_s and channel capacity vs p_e

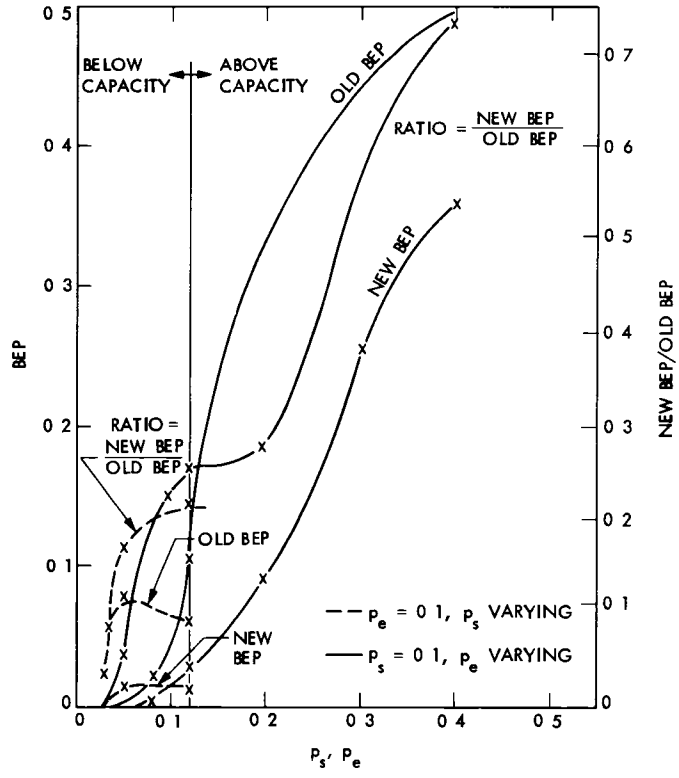

Fig 5 BEP with new and old metrics and their ratio vs p_e with p_s constant and vs p_s with p_e constant (from Table 2)

Appendix

Simplifying the Extended Bhattacharya Bound for Memoryless Channel

We show here the derivation of Eq (20) from Eq (17) for a memoryless channel The method used is similar to that in §2 9 of Ref 2 We have, from Eq (17), since $p(\bar{y}|\bar{x}_m)$ and $p(\bar{y}|\bar{x}_{m'})$ can be factored for a memoryless channel,

$$p_E(m \to m') \leqslant \sum_{\bar{y}} \sqrt{\frac{p_{m'}}{p_m} p(\bar{y}|\bar{x}_{m'}) p(\bar{y}|\bar{x}_{m'})} \tag{17}$$

$$= \sqrt{\frac{p_{m'}}{p_m}} \prod_{j=1}^{nB} \sum_{y} \sqrt{p(y|u_{mj}) p(y|u_{m'j})} \tag{A1-1}$$

where u_{mj}, $u_{m'j}$ are the input bits corresponding to the code subvectors $\bar{x}_{mj}$, $\bar{x}_{m'j}$, the sum in Eq (17) runs over all possible $\bar{y}$ vectors consisting of B n-dimensional subvectors, and the sum over y in Eq (A1-1) runs over the two possibilities 0 and 1 for each of these nB components

We have

$$p_E(m \to m') \leqslant \sqrt{\frac{p_{m'}}{p_m}} \prod_{j=1}^{nB} \sum_{y} \sqrt{p(y|u_{mj}) p(y|u_{m'j})} \tag{A1-1}$$

$$= \sqrt{\frac{p_{m'}}{p_m}} \prod_{j\, u_{m'j}=u_{mj}} \sum_{y} \sqrt{p(y|u_{mj}) p(y|u_{m'j})}$$

$$\cdot \prod_{j\, u_{m'j}=\bar{u}_{mj}} \sum_{y} \sqrt{p(y|u_{mj}) p(y|u_{m'j})}$$

(here, $\bar{u}_{mj}$ = logical complement of u_{mj}) This bound can be written as

$$p_E(m \to m') \leqslant \sqrt{\frac{p_{m'}}{p_m}} \prod_{j\, u_{m'j}=u_{mj}} \sum_{y} \sqrt{p(y|u_{mj}) p(y|u_{m'j})} \tag{A1-2}$$

since each sum in the first product in the previous equation is equal to 1

Thus, if the messages m, m' differ in $w_{mm'}$ bits, we get

$$p_E(m \to m') \leqslant \sqrt{\frac{p_{m'}}{p_m}} \left[\sum_{y} \sqrt{p(y|1) p(y|0)} \right]^{w_{mm'}}$$

$$\triangleq \sqrt{\frac{p_{m'}}{p_m}} \left[\sum_{y} \sqrt{p_1(y) p_0(y)} \right]^{w_{mm'}}$$

$$\triangleq \sqrt{\frac{p_{m'}}{p_m}} Z^{w_{mm'}} \tag{20}$$

Bibliography

Ananda, M P, "Lunar Gravity A Mass Point Model," *J Geophys Res*, Vol 82, No 20, pp 3049-3064, July 10, 1977

Anderson, J D, "Determination of Astrodynamic Constants and a Test of the General Relativistic Time Delay With S-Band Range and Doppler Data From Mariners 6 and 7," *Space Research*, Vol XI, pp 105-112, Akademie-Verlag, Berlin, 1971

Anderson, J D, et al, "Experimental Test of General Relativity Using Time-Delay Data From Mariner 6 and Mariner 7," *Astrophys J*, Vol 200, No 1, pp 221-233, Aug 15, 1975

Anderson, J D, et al, "Tests of General Relativity Using Astrometric and Radio Metric Observations of the Planets," *Acta Astronautica*, Vol 5, No 1-2, pp 43-61, Jan -Feb 1978

Barnum, P W, et al, *Tracking and Data System Support for the Mariner Mars 1971 Mission Orbit Insertion Through End of Primary Mission*, Technical Memorandum 33-523, Vol III, Jet Propulsion Laboratory, Pasadena, Calif, May 15, 1973

Barnum, P W, and Renzetti, N A, *Tracking and Data System Support for the Mariner Mars 1971 Mission Extended Mission Operations*, Technical Memorandum 33-523, Vol IV, Jet Propulsion Laboratory, Pasadena, Calif, Dec 15, 1973

Barton, W R, and Miller, R B, *Tracking and Data System Support for the Pioneer Project Pioneer 11–Prelaunch Planning Through Second Trajectory Correction to May 1, 1973*, Technical Memorandum 33-584, Vol II, Jet Propulsion Laboratory, Pasadena, Calif, Mar 15, 1975

Bartos, K P, et al, *Implementation of the 64-Meter-Diameter Antennas at the Deep Space Stations in Australia and Spain*, Technical Memorandum 33-692, Jet Propulsion Laboratory, Pasadena, Calif, Jan 15, 1975

Bathker, D A, *Predicted and Measured Power Density Description of a Large Ground Microwave System*, Technical Memorandum 33-433, Jet Propulsion Laboratory, Pasadena, Calif, Apr 15, 1971

Bathker, D A, Brown, D W, and Petty, S M, *Single- and Dual-Carrier Microwave Noise Abatement in the Deep Space Network*, Technical Memorandum 33-733, Jet Propulsion Laboratory, Pasadena, Calif, Aug 1, 1975

Bathker, D A, *Microwave Performance Characterization of Large Space Antennas*, JPL Publication 77-21, Jet Propulsion Laboratory, Pasadena, Calif, May 15, 1977

Beatty, R W, and Otoshi, T Y, "Effect of Discontinuities on the Group Delay of a Microwave Transmission Line," *IEEE Trans Microwave Theor Techniq*, Vol MTT-23, No 11, pp 919-923, Nov 1975

Benjauthrit, B, and Reed, I S, "Galois Switching Functions and Their Applications," *IEEE Trans Comput*, Vol C-25, No 1, pp 78-86, Jan 1976

Benjauthrit, B, and Reed, I S, "On the Fundamental Structure of Galois Switching Functions," *IEEE Trans Comput*, Vol C-27, No 8, pp 757-762, Aug 1978

Berlekamp, E R, et al, "On the Inherent Intractability of Certain Coding Problems," *IEEE Trans Inform Theor*, Vol IT-24, No 3, pp 384-386, May 1978

Berman, A L , and Rockwell, S T , *New Optical and Radio Frequency Angular Tropospheric Refraction Models for Deep Space Applications*, Technical Report 32-1601, Jet Propulsion Laboratory, Pasadena, Calif , Nov 1, 1975

Berman, A L , *The Prediction of Zenith Range Refraction From Surface Measurements of Meteorological Parameters*, Technical Report 32-1602, Jet Propulsion Laboratory, Pasadena, Calif , July 15, 1976

Born, G H , et al , "The Determination of the Satellite Orbit of Mariner 9," *Celest Mech* , Vol 9, No 3, pp 395-414, May 1974

Born, G H , and Mohan, S N , "Orbit Determination for Mariner 9 Using Radio and Optical Data," *J Spacecraft Rockets*, Vol 12, No 7, pp 439-441, July 1975

Butman, S , "Rate Distortion Over Band-Limited Feedback Channels," *IEEE Trans Inform Theor* , Vol IT-17, No 1, pp 110-112, Jan 1971

Butman, S , and Timor, U , "Interplex–An Efficient Multichannel PSK/PM Telemetry System," *IEEE Trans Commun* , Vol COM-20, No 3, pp 415-419, June 1972

Butman, S A , "Linear Feedback Rate Bounds for Regressive Channels," *IEEE Trans Inform Theor* , Vol IT-22, No 3, pp 363-366, May 1976

Butman, S A , et al , "Design Criteria for Noncoherent Gaussian Channels With MFSK Signaling and Coding," *IEEE Trans Commun* , Vol COM-24, No 10, pp 1078-1088, Oct 1976

Butman, S A , and Lesh, J R , "The Effects of Bandpass Limiters on *n*-Phase Tracking Systems," *IEEE Trans Commun* , Vol COM-25, No 6, pp 569-576, June 1977

Chadwick, H D , and Springett, J C , "The Design of a Low Data Rate MSFK Communication System" *IEEE Trans Commun Technol* , Vol COM-18, No 6, pp 740-750, Dec 1970

Chao, C -C , "Interstation Frequency Offset Determination Using Differenced 2-Way/3-Way Doppler Data," paper presented at the 1978 Spring Meeting of the American Geophysical Union, Miami, Florida, Apr 17-20, 1978

Christensen, C S , and Reinold, S J , "Navigation of the Mariner 10 Spacecraft to Venus and Mercury," *J Spacecraft Rockets*, Vol 12, No 5, pp 280-286, May 1975

Christensen, C S , et al , "On Achieving Sufficient Dual Station Range Accuracy for Deep Space Navigation at Zero Declination," paper presented at AAS/AIAA Astrodynamics Specialist Conference, Jackson Hole, Wyo , Sept 7-9, 1977

Christensen, E J , et al , "The Mass of Phobos from Viking Flybys," *Geophys Res Lett* , Vol 4, No 12, pp 555-557, Dec 1977

Clark, B G , et al , "High Resolution Observations of Compact Radio Sources at 13 cm," *Astrophys J* , Vol 161, pp 803-809, Sept 1970

Clauss, R , Flesner, L D , and Schultz, S , "Simple Waveguide Reflection Maser with Broad Tunability," *Rev Sci Instrum* , Vol 48, No 8, pp 1104-1105, Aug 1977

A Collection of Articles on S/X-Band Experiment Zero Delay Ranging Tests, Technical Memorandum 33-747, Vol I, Jet Propulsion Laboratory, Pasadena, Calif , Nov 1, 1975

Coyner, J V , Jr , *Radial Rib Antenna Surface Deviation Analysis Program*, Technical Memorandum 33-518, Jet Propulsion Laboratory, Pasadena, Calif , Dec 15, 1971

Curkendall, D W , and Stephenson, R R , "Earthbased Tracking and Orbit Determination—Backbone of the Planetary Navigation System," *Astronaut Aeronaut* , Vol 7, No 5, pp 30-36, May 1970

Curkendall, D W , "Planetary Navigation The New Challenges," *Astronaut Aeronaut* , Vol 7, No 5, pp 26-29, May 1970

Curkendall, D W , "Algorithms for Isolating Worst Case Systematic Data Errors," *J Guidance Contr* , Vol 1, No 1, pp 56-62, Jan -Feb 1978

Dickinson, R M , "The Beamed Power Microwave Transmitting Antenna," *IEEE Trans Microwave Theor Tech* , Vol MTT-26, No 5, pp 335-340, May 1978

Downs, G S , and Reichley, P E , "Observations of Interstellar Scintillations of Pulsar Signals at 2388 MHz," *Astrophys J* , Vol 163, No 1, Pt 2, pp L11-L16, Jan 1971

Downs, G S , et al , "Mars Radar Observation, A Preliminary Report," *Science*, Vol 174, No 4016, pp 1324-1327, Dec 24, 1971

Downs, G S , "Martian Topography and Surface Properties as Seen by Radar The 1971 Opposition," *Icarus*, Vol 18, No 1, pp 8-21, Jan 1973

Downs, G S , Reichley, P E , and Morris, G A , "Pulsar Detections at Frequencies of 8 4 and 15 1 GHz," *Astrophys J* , Vol 181, No 3, Part 2, pp L143-L146, May 1, 1973

Duxbury, T C , Johnson, T V , and Matson, D L , "Galilean Satellite Mutual Occultation Data Processing," *Icarus*, Vol 25, No 4, pp 569-584, Aug 1975

Edelson, R E (ed), *Telecommunications Systems Design Techniques Handbook*, Technical Memorandum 33-571, Jet Propulsion Laboratory, Pasadena, Calif , July 15, 1972

Edelson, R E , "An Observational Program to Search for Radio Signals From Extraterrestrial Intelligence Through the Use of Existing Facilities," Preprint IAF-A-76-033, Int Astronaut Fed XXVII Congress, Anaheim, Calif , Oct 10-16, 1976

Edelson, R E , and Levy, G S , "The Search for Extraterrestrial Intelligence Telecommunications Technology," *Proceedings of the 1976 National Telecommunications Conference,* Vol I, Dallas, Tex , Nov 29-Dec 1, 1976

Edelson, R E , "An Experimental Protocol for a Search for Radio Signals of Extraterrestrial Intelligent Origin in the Presence of Man-Made Radio Frequency Sources," paper presented at the XXVIIIth International Astronautical Congress, Prague, Czechoslovakia, Sept 25-Oct 1, 1977

Efron, L , and Solloway, C B , *Proceedings of the Conference on Scientific Applications of Radio and Radar Tracking in the Space Program*, Technical Report 32-1475, Jet Propulsion Laboratory, Pasadena, Calif , July 1, 1970

Esposito, P B , and Wong, S K , "Geocentric Gravitational Constant Determined from Mariner 9 Radio Tracking Data," paper presented at the International Symposium on Earth Gravity Models (American Geophysical Union, NASA), St Louis, Aug 1972

Estabrook, F B , and Wahlquist, H D , "Response of Doppler Spacecraft Tracking to Gravitational Radiation," *Gen Relat Grav* , Vol 6, No 5, pp 439-447, Oct 1975

Estacion Espacial de Madrid Madrid Space Station, Special Publication 43-26, Jet Propulsion Laboratory, Pasadena, Calif , Aug 31, 1975

Ferrari, A J , and Ananda, M P , "Lunar Gravity A Long-Term Keplerian Rate Method," *J Geophys Res* , Vol 82, No 20, pp 3085-3097, July 10, 1977

Fjeldbo, G , Kliore, A J , and Seidel, B L , "Bistatic Radar Measurements of the Surface of Mars with Mariner 1969," *Icarus*, Vol 16, No 3, pp 502-508, June 1972

Fjeldbo, G , "Radio Occultation Experiments Planned for Pioneer and Mariner Missions to the Outer Planets," *Planet Space Sci* , Vol 21, No 9, pp 1533-1547, Sept 1973

Fjeldbo, G , et al , "Viking Radio Occultation Measurements of the Martian Atmosphere and Topography Primary Mission Coverage," *J Geophys Res* , Vol 82, No 28, pp 4317-4324, Sept 30, 1977

Flanagan, F M , et al , *Deep Space Network Support of the Manned Space Flight Network for Apollo 1962-1968*, Technical Memorandum 33-452, Vol I, Jet Propulsion Laboratory, Pasadena, Calif , July 1970

Flanagan, F M , et al , *Deep Space Network Support of the Manned Space Flight Network for Apollo 1969-1970*, Technical Memorandum 33-452, Vol II, Jet Propulsion Laboratory, Pasadena, Calif , May 1, 1971

Fortenberry, J W , Freeland, R E , and Moore, D M , *Five-Meter-Diameter Conical Furlable Antenna*, Technical Report 32-1604, Jet Propulsion Laboratory, Pasadena, Calif , July 15, 1976

Freiley, A J , Batelaan, P D , and Bathker, D A , *Absolute Flux Density Calibrations of Radio Sources 2 3 GHz,* Technical Memorandum 33-806, Jet Propulsion Laboratory Pasadena, Calif , Dec 1, 1977

Gary, B , Olsen, E T , and Rosenkranz, P W , "Radio Observations of Cygnus X-3 and the Surrounding Region," *Nature Phys Sci* , Vol 239, No 95, pp 128-130, Oct 23, 1972

Georgevic, R M , *Mathematical Model of the Solar Radiation Force and Torques Acting on the Components of a Spacecraft*, Technical Memorandum 33-494, Jet Propulsion Laboratory, Pasadena, Calif , Oct 1, 1971

Goldstein, R M , et al , "Preliminary Radar Results of Mars," *Radio Sci* , Vol 5, No 2, pp 475-478, Feb 1970

Goldstein, R M , and Rumsey, H , "A Radar Snapshot of Venus," *Science*, Vol 169, Sept 1970

Goldstein, R M , "Radar Observations of Mercury," *Astron J* , Vol 76, No 10 pp 1152-1154, Dec 1971

Goldstein, R M , Holdridge, D B , and Lieske, J H , "Minor Planets and Related Objects XII Radar Observations of (1685) Toro," *Astron J* , Vol 78, No 6, pp 508-509 Aug 1973

Goldstein, R M , and Morris, G A , "Ganymede Observations by Radar," *Science,* Vol 188, No 4194, pp 1211-1212, June 20, 1975

Goldstein, R M , Green, R R , and Rumsey, H , Jr , "Venus Radar Images," *J Geophys Res* , Vol 81, No 26, pp 4807-4817, Sept 10, 1976

Goodwin, P S , et al , *Tracking and Data Systems Support for the Helios Project Project Development Through End of Mission Phase II*, Technical Memorandum 33-752, Vol I, Jet Propulsion Laboratory, Pasadena, Calif , July 1, 1976

Goodwin, P S , et al , *Tracking and Data Systems Support for the Helios Project DSN Support of Project Helios April 1975 Through May 1976,* Technical Memorandum 33-752, Vol II, Jet Propulsion Laboratory, Pasadena, Calif , Jan 15, 1977

Goodwin, P S , Jensen, W N , and Flanagan, F M , *Tracking and Data Systems Support for the Helios Project DSN Support of Project Helios May 1976 Through June 1977*, Technical Memorandum 33-752, Vol III, Jet Propulsion Laboratory, Pasadena, Calif , Mar 1, 1979

Gordon, H J , et al , *The Mariner 6 and 7 Flight Paths and Their Determination From Tracking Data*, Technical Memorandum 33-469, Jet Propulsion Laboratory, Pasadena, Calif , Dec 1, 1970

Gottlieb, P , et al , "Lunar Gravity over Large Craters from Apollo 12 Tracking Data," *Science*, Vol 168, No 3930, pp 477-479, Apr 1970

Gray, R M and Tausworthe, R C , "Frequency-Counted Measurements, and Phase Locking to Noise Oscillators," *IEEE Trans Commun Technol* , Vol COM-19, No 1, pp 21-30, Feb 1971

Gulkis, S , and Gary, B , "Circular Polarization and Total-Flux Measurements of Jupiter at 13 1 cm Wavelength," *Astron J* , Vol 76, No 1, pp 12-16, Feb 1971

Gulkis, S , et al , "Observations of Jupiter at 13-cm Wavelength During 1969 and 1971," *Icarus*, Vol 18, No 2, pp 181-191, Feb 1973

Gulkis, S , et al , "An All-Sky Search for Narrow-Band Radiation in the Frequency Range 1-25 GHz," paper presented at the 1976 U S National Commission, International Union of Radio Science, Amherst, Mass , Oct 10-15, 1976

Hachenberg, O , et al , "The 100-meter Radio Telescope at Effelsberg," *Proc IEEE*, Vol 61, No 9, pp 1288-1295, Sept 1973

Hall, J R , *Tracking and Data System Support for Lunar Orbiter*, Technical Memorandum 33-450, Jet Propulsion Laboratory, Pasadena, Calif , Apr 1970

Harris, A W , et al , "2290-MHz Flux Densities of 52 High-Declination Radio Sources," *Astron J* , Vol 81, No 4, pp 222-224, Apr 1976

Havens, W F , et al , *Scan Pointing Calibration for the Mariner Mars 1971 Spacecraft*, Technical Memorandum 33-556, Jet Propulsion Laboratory, Pasadena, Calif , Aug 1, 1972

Higa, W H , "Time Synchronization via Lunar Radar," *Proc IEEE*, Vol 60, No 5, pp 552-557, May 1972

Higa, W H "Spurious Signals Generated by Electron Tunneling on Large Reflector Antennas," *Proc IEEE*, Vol 63, No 2, pp 306-313, Feb 1975

Higa, W H , *The Superconducting Cavity-Stabilized Maser Oscillator*, Technical Memorandum 33-805, Jet Propulsion Laboratory, Pasadena, Calif , Dec 15, 1976

Holmes J K , "On a Solution to the Second-Order Phase-Locked Loop," *IEEE Trans Commun Technol* , Vol COM-18, No 2, pp 119-126, Apr 1970

Holmes, J K , "First Slip Times Versus Static Phase Error Offset for the First and Passive Second-Order Phase-Locked Loop," *IEEE Trans Commun Technol* , Vol COM-19, No 2, pp 234-235, Apr 1971

Holmes, J K , and Tegnelia, C R , *Digital Command System Second-Order Subcarrier Tracking Performance*, Technical Report 32-1540, Jet Propulsion Laboratory, Pasadena, Calif , Oct 1, 1971

Holmes J K , "Performance of a First Order Transition Sampling Digital Phase-Locked Loop Using Random-Walk Models," *IEEE Trans Commun* , Vol COM-20, No 2, pp 119-131, Apr 1972

Hunter, J A , "Orbiting Deep Space Relay Station, A Study Report," paper presented at AIAA Conference on Large Space Platforms, Future Needs and Capabilities, Los Angeles, Calif , Sept 27-29, 1978

Hurd, W J , and Anderson, T O , *Digital Transition Tracking Symbol Synchronizer for Low SNR Coded Systems*, Technical Report 32-1488, Jet Propulsion Laboratory, Pasadena, Calif , reprinted from *IEEE Trans Commun Technol* , Vol COM-18, No 2, pp 141-147, Apr 1970

Hurd, W J , "An Analysis and Demonstration of Clock Synchronization by VLBI," *IEEE Trans Instr Meas* , Vol IM-23, No 1, pp 80-89, March 1974

Jacobson, R A , McDanell, J P , and Rinker, G C , "Use of Ballistics Arcs in Low Thrust Navigation," *J Spacecraft Rockets*, Vol 12, No 3, pp 138-145, Mar 1975

Jordan, J F , Melbourne, W G , and Anderson, J D , "Testing Relativistic Gravity Theories Using Radio Tracking Data From Planetary Orbiting Spacecraft," *Space Research XIII*, pp 83-92, Akademie-Verlag, Berlin, 1973

Jurgens, R F , and Goldstein, R M , "Radar Observations at 3 5 and 12 6 cm Wavelength of Asteroid 433 Eros," *Icarus*, Vol 28, No 1, pp 1-15, May 1976

Jurgens, R F , and Bender, D F , "Radar Detectability of Asteroids," *Icarus*, Vol 31, No 4, pp 483-497, Aug 1977

Katow, M S , "Evaluating Computed Distortions of Parabolic Reflectors," *Record of IEEE 1977 Mechanical Engineering in Radar Symposium, Arlington, Virginia, Nov 8-10, 1977*, IEEE Publication 77CH 1250-0 AES, pp 91-93

Kellerman, K I , et al , "High Resolution Observations of Compact Radio Sources at 13 Centimeters," *Astrophys J* , Vol 161, No 3, pp 803-809, Sept 1970

Kliore, A J , et al , "Summary of Mariner 6 and 7 Radio Occultation Results on the Atmosphere of Mars," *Space Research*, Vol XI, pp 165-175, Akademie-Verlag, Berlin, 1971

Kliore, A J , et al , "Mariner 9 S-Band Martian Occultation Experiment Initial Results on the Atmosphere and Topography of Mars," *Science*, Vol 175, No 4019, pp 313-317, Jan 1972

Kliore, A J , et al , "The Atmosphere of Mars From Mariner 9 Radio Occultation Measurements," *Icarus*, Vol 17, No 2, pp 484-516, Oct 1972

Kliore, A J , et al , "S Band Radio Occultation Measurements of the Atmosphere and Topography of Mars with Mariner 9 Extended Mission Coverage of Polar and Intermediate Latitudes " *J Geophys Res* , Vol 78, No 20, pp 4331-4351, July 10, 1973

Kliore, A J , "Radio Occultation Exploration of Mars," *Exploration of the Planetary System* (IAU Symposium, No 65), pp 295-316, D Reidel Publishing Co , Dordrecht, Holland, 1974

Kliore, A J , Woiceshyn, P M , and Hubbard, W P , "Pioneer 10 and 11 Radio Occultations by Jupiter," *COSPAR Space Research*, Vol XVII, pp 703-710, Pergamon Press Ltd , Oxford, 1978

Kliore, A , et al , "The Polar Ionosphere of Venus Near the Terminator From Early Pioneer Venus Orbiter Radio Occultation," *Science*, Vol 203, No 4382, pp 765-768, Feb 23, 1979

Kuiper, T B H , and Morris, M , "Searching for Extraterrestrial Civilizations," *Science*, Vol 196, pp 616-621, May 6, 1977

Laeser, R P , et al , *Tracking and Data System Support for the Mariner Mars 1971 Mission Prelaunch Phase Through First Trajectory Correction Maneuver*, Technical Memorandum 33-523, Vol I, Jet Propulsion Laboratory, Pasadena, Calif , Mar 15, 1972

Layland, J W , and Lushbaugh, W A , "A Flexible High-Speed Sequential Decoder for Deep Space Channels," *IEEE Trans Commun Technol* , Vol COM-19, No 5, pp 813-820, Oct 1971

Layland, J W , "Buffer Management for Sequential Decoding," *IEEE Trans Commun* , Vol COM-22, No 10, pp 1685-1690, Oct 1974

Leavitt, R K , *The Least-Squares Process of MEDIA for Computing DR VID Calibration Polynomials*, Technical Memorandum 33-542, Jet Propulsion Laboratory, Pasadena, Calif , May 15, 1972

Lesh, J R , *Signal-to-Noise Ratios in Coherent Soft Limiters*, Technical Report 32-1589, Jet Propulsion Laboratory, Pasadena, Calif , Sept 15, 1973

Lesh, J R , "Signal-to-Noise Ratios in Coherent Soft Limiters," *IEEE Trans Commun* , Vol COM-22, No 6, pp 803-811, June 1974

Lesh, J R , "Sequential Decoding in the Presence of a Noisy Carrier Reference," *IEEE Trans Commun* , Vol COM-23, No 11, pp 1292-1297, Nov 1975

Levitt, B K , "Optimum Frame Synchronization for Biorthogonally Coded Data," *IEEE Trans Commun* , Vol COM-22, No 8, pp 1130-1134, Aug 1974

Levitt, B K , "Long Frame Sync Words for Binary PSK Telemetry," *IEEE Trans Commun* , COM-23, No 11, pp 1365-1367, Nov 1975

Levy, G S , et al , "Helios-1 Faraday Rotation Experiment Results and Interpretations of the Solar Occultations in 1975," *J Geophys* , Vol 42, No 6, pp 659-672, 1977

Levy, R , "Computer-Aided Design of Antenna Structures and Components," *Comput Struc* , Vol 6, Nos 4/5, pp 419-428, Aug /Oct 1976

Levy, R , and McGinness, H , *Wind Power Prediction Models*, Technical Memorandum 33-802, Jet Propulsion Laboratory, Pasadena, Calif , Nov 15, 1976

Levy, R , and Katow, M S , "Implementation of Wind Performance Studies for Large Antenna Structures," *Record of IEEE 1977 Mechanical Engineering in Radar Symposium, Arlington, Virginia, Nov 8-10, 1977*, IEEE Publication 77CH 1250-0 AES, pp 27-33

Levy, R , "Antenna Bias Rigging for Performance Objective," *Record of IEEE 1977 Mechanical Engineering in Radar Symposium, Arlington, Virginia, Nov 8-10, 1977*, IEEE Publication 77CH 1250-0 AES, pp 94-97

Lieske, J H , et al , "Simultaneous Solution for the Masses of the Principal Planets from Analysis of Optical Radar and Radio Tracking Data," *Celest Mech* , Vol 4, No 2, pp 233-245, Oct 1971

Lindsey, W C , and Simon, M K , "The Effect of Loop Stress on the Performance of Phase-Coherent Communication Systems," *IEEE Trans Commun Technol* , Vol COM-18, No 5, pp 569-588, Oct 1970

Lindsey, W C , and Simon, M K , "Carrier Synchronization and Detection of Polyphase Signals," *IEEE Trans Commun* , Vol COM-20, No 3, pp 441-454, June 1972

Lindsey, W C , and Simon, M K , "L-Orthogonal Signal Transmission and Detection," *IEEE Trans Commun* , Vol COM-20, No 5, pp 953-960, Oct 1972

Lindsey, W C , and Simon, M K , "On the Detection of Differentially Encoded Polyphase Signals," *IEEE Trans Commun* , Vol COM-20, No 6, pp 1121-1128, Dec 1972

Lindsey, W C , *Synchronization Systems in Communication and Control,* Prentice-Hall, Inc , Englewood Cliffs, N J , 1972

Lindsey, W C , and Tausworthe, R C , *A Bibliography of the Theory and Application of the Phase-Lock Principle,* Technical Report 32-1581, Jet Propulsion Laboratory, Pasadena, Calif , Apr 1, 1973

Lindsey, W C , and Simon, M K , *Telecommunication Systems Engineering,* Prentice-Hall, Inc , Englewood Cliffs, N J , 1973

Liu, A S , and Pease, G E , "Spacecraft Ranging From a Ground Digitally Controlled Oscillator," *J Spacecraft Rockets,* Vol 12, No 9, pp 528-532, Sept 1975

Lorell, J , et al , "Icarus Celestial Mechanics Experiment for Mariner," *Int J Sol Sys* , Vol 12, Jan 1970

Lorell, J , and Laing, P A , *Compilation of Lunar Orbiter Tracking Data Used for Long-Term Selenodesy,* Technical Memorandum 33-419, Jet Propulsion Laboratory, Pasadena, Calif , Feb 1, 1970

Lorell, J , "Estimation of Gravity Field Harmonics in the Presence of Spin-Axis Direction Error Using Radio Tracking Data," *J Astronaut Sci* , Vol XX, No 1, pp 44-54, Aug 1972

Ludwig, A C , et al , *Gain Calibration of a Horn Antenna Using Pattern Integration,* Technical Report 32-1572, Jet Propulsion Laboratory, Pasadena, Calif , Oct 1, 1972

Madrid, G A , et al , *Tracking System Analytic Calibration Activities for the Mariner Mars 1971 Mission,* Technical Report 32-1587, Jet Propulsion Laboratory, Pasadena, Calif , Mar 1, 1974

Martin, D P , *A Combined Radar-Radiometer With Variable Polarization,* Technical Memorandum 33-570, Jet Propulsion Laboratory, Pasadena, Calif , Oct 15, 1972

Martin, W L , and Zygielbaum, A I , *Mu-II Ranging,* Technical Memorandum 33-768, Jet Propulsion Laboratory, Pasadena, Calif , May 15, 1977

Melbourne, W G , "Planetary Ephemerides," *Astronaut Aeronaut* , Vol 7, No 5, pp 38-43, May 1970

Melbourne, W G , "Navigation between the Planets," *Sci Amer* , Vol 234, No 6, pp 58-74, June 1976

Miller, R B , *Tracking and Data System Support for the Pioneer Project Pioneers 6-9 Extended Missions July 1, 1972-July 1, 1973,* Technical Memorandum 33-426, Vol XII, Jet Propulsion Laboratory, Pasadena, Calif , March 1, 1974

Miller, R B, *Tracking and Data System Support for the Pioneer Project Pioneer 10–From April 1, 1972, Through the Jupiter Encounter Period, January 1974,* Technical Memorandum 33-584, Vol III, Jet Propulsion Laboratory, Pasadena, Calif, June 15, 1975

Miller, R B, et al, *Tracking and Data System Support for the Pioneer Project Pioneer 10–From January 1974 to January 1975, Pioneer 11–From May 1, 1973 Through Jupiter Encounter Period, January 1975,* Technical Memorandum 33-584, Vol IV, Jet Propulsion Laboratory, Pasadena, Calif, Dec 1, 1975

Moyer, T D, *Mathematical Formulation of the Double-Precision Orbit Determination Program (DPODP),* Technical Report 32-1527, Jet Propulsion Laboratory, Pasadena, Calif, May 17, 1971

Mudgway, D J, *Tracking and Data System Support for the Viking 1975 Mission to Mars Prelaunch Planning, Implementation, and Testing*, Technical Memorandum 33-783, Vol I, Jet Propulsion Laboratory, Pasadena, Calif, Jan 15, 1977

Mudgway, D J, and Traxler, M R, *Tracking and Data System Support for the Viking 1975 Mission to Mars Launch Through Landing of Viking 1*, Technical Memorandum 33-783, Vol II, Jet Propulsion Laboratory, Pasadena, Calif, Mar 15, 1977

Mudgway, D J, *Tracking and Data System Support for the Viking 1975 Mission to Mars Planetary Operations*, Technical Memorandum 33-783, Vol III, Jet Propulsion Laboratory, Pasadena, Calif, Sept 1, 1977

Mudgway, D J, *Tracking and Data System Support for the Viking 1975 Mission to Mars Extended Mission Operations December 1976 to May 1978,* Technical Memorandum 33-783, Vol IV, Jet Propulsion Laboratory, Pasadena, Calif, Dec 15, 1978

Muhleman, D O, et al, "Radio Propagation Measurements of the Solar Corona and Gravitational Field Applications to Mariner 6 and 7," in *Proceedings of the Conference on Experimental Tests of Gravitational Theories,* California Institute of Technology, Pasadena, Calif, Nov 1970

Muhleman, D O, Esposito, P B, and Anderson, J D, "The Electron Density Profile of the Outer Corona and the Interplanetary Medium From Mariner-6 and Mariner-7 Time-Delay Measurements," *Astrophys J*, No 211, No 3, Part 1, pp 943-957, Feb 1, 1977

Mulhall, B D, et al, *Tracking System Analytic Calibration Activities for the Mariner Mars 1969 Mission,* Technical Report 32-1499, Jet Propulsion Laboratory, Pasadena, Calif, Nov 15, 1970

Muller, P M, Sjogren, W L, and Wollenhaupt, W R, "Lunar Gravity Apollo 15 Doppler Radio Tracking," *The Moon,* Vol 10, No 2, pp 195-205, June 1974

Murray, B C, Gulkis, S, and Edelson, R E, "Extraterrestrial Intelligence An Observational Approach," *Science,* Vol 199, No 4328, pp 485-492, Feb 3, 1978

The NASA/JPL 64-Meter-Diameter Antenna at Goldstone, California Project Report, Technical Memorandum 33-671, Jet Propulsion Laboratory, Pasadena, Calif, July 15, 1974

Newburn, R L, Jr, et al, *Earth-Based Research on the Outer Planets During the Period 1970-1985,* Technical Report 32-1456, Jet Propulsion Laboratory, Pasadena, Calif, Mar 15, 1970

Ohlson, J E, "Polarization Tracking of a Partially Coherent Signal Using a Double Loop," *IEEE Trans Commun*, Vol COM-23, No 9, pp 859-866, Sept 1975

Ohlson, J E , and Reid, M S , *Conical-Scan Tracking With the 64-m-diameter Antenna at Goldstone,* Technical Report 32-1605, Jet Propulsion Laboratory, Pasadena, Calif , Oct 1, 1976

O'Neil, W J , et al , *Mariner 9 Navigation,* Technical Report 32-1586, Jet Propulsion Laboratory, Pasadena, Calif , Nov 13, 1973

Ong , K M , et al , "A Demonstration of a Transportable Radio Interferometric Surveying System With 3-cm Accuracy on a 307-m Base Line," *J Geophys Res*, Vol 81, No 20, pp 3587-3593, July 10, 1976

Otoshi, T Y , Stelzried, C T , and Yates, B C , "Comparisons of Waveguide Losses Calibrated by the DC Potentiometer, AC Ratio Transformer, and Reflectometer Techniques," *IEEE Trans Microwave Theor Tech*, Vol MTT-18, No 7, pp 406-409, July 1970

Otoshi, T Y , and Stelzried, C T , "A Precision Compact Rotary Vane Attenuator," *IEEE Trans Microwave Theor Tech*, Vol MTT-19, No 11, pp 843-854, Nov 1971

Otoshi, T Y , "Precision Reflectivity Loss Measurements of Perforated-Plate Mesh Materials by a Waveguide Technique," *IEEE Trans Instr Meas*, Vol IM-21, No 4, pp 451-457, Nov 1972

Otoshi, T Y , and Stelzried, C T , "Cosmic Background Noise Temperature Measurement at 13-cm Wavelength," *IEEE Trans Instr Meas*, Vol IM-24, No 2, pp 174-179, June 1975

Phillips, R J , et al , "Simulation Gravity Modeling to Spacecraft-Tracking Data Analysis and Application," *J Geophys Res*, Vol 83, No B11, pp 5455-5464, Nov 10, 1978

Posner, E C , "Random Coding Strategies for Minimum Entropy," *IEEE Trans Inform Theor*, Vol IT-21, No 4, pp 388-391, July 1975

Posner, E C , "Life Cycle Costing with a Discount Rate," *Utilitas Mathematica,* Vol 13, pp 157-188, 1978

Powell, R V , and Hibbs, A R , "An Entree for Large Space Antennas," *Astronaut Aeronaut*, Vol 15, No 12, pp 58-64, Dec 1977

Reed, I S , Truong, T K , and Benjauthrit, B , "On Decoding of Reed-Solomon Codes over GF(32) and GF(64) Using the Transform Techniques of Winograd," *Conference Record, 1978 National Telecommunications Conference,* Vol 2, Birmingham, Alabama, Dec 3-6, 1978

Reid, M S , et al , "Low-Noise Microwave Receiving Systems in a Worldwide Network of Large Antennas," *Proc IEEE,* Vol 61, No 9, pp 1330-1335, Sept 1973

Renzetti, N A , *Tracking and Data System Support for the Pioneer Project Pioneer VI Prelaunch to End of Nominal Mission,* Technical Memorandum 33-426, Vol I, Jet Propulsion Laboratory, Pasadena, Calif , Feb 1, 1970

Renzetti, N A , *Tracking and Data System Support for the Pioneer Project Pioneer VII Prelaunch to End of Nominal Mission,* Technical Memorandum 33-426, Vol II, Jet Propulsion Laboratory, Pasadena, Calif , Apr 15, 1970

Renzetti, N A , *Tracking and Data System Support for the Pioneer Project Pioneer VIII Prelaunch Through May 1968,* Technical Memorandum 33-426, Vol III, Jet Propulsion Laboratory, Pasadena, Calif , July 15, 1970

Renzetti, N A , *Tracking and Data System Support for the Pioneer Project Pioneer IX Prelaunch Through June 1969,* Technical Memorandum 33-426, Vol IV, Jet Propulsion Laboratory, Pasadena, Calif , Nov 15, 1970

Renzetti, N A , *Tracking and Data System Support for the Pioneer Project Pioneer VI Extended Mission July 1, 1966-July 1, 1969,* Technical Memorandum 33-426, Vol V, Jet Propulsion Laboratory, Pasadena, Calif , Feb 1, 1971

Renzetti, N A , *Tracking and Data System Support for the Pioneer Project Pioneer VII Extended Mission February 24, 1967-July 1, 1968,* Technical Memorandum 33-426, Vol VI, Jet Propulsion Laboratory, Pasadena, Calif , Apr 15, 1971

Renzetti, N A , *Tracking and Data System Support for the Pioneer Project Pioneer VII Extended Mission July 1, 1968-July 1, 1969,* Technical Memorandum 33-426, Vol VII, Jet Propulsion Laboratory, Pasadena, Calif , Apr 15, 1971

Renzetti, N A , *Tracking and Data System Support for the Pioneer Project Pioneer VIII Extended Mission June 1, 1968-July 1, 1969,* Technical Memorandum 33-426, Vol VIII, Jet Propulsion Laboratory, Pasadena, Calif , May 1, 1971

Renzetti, N A , *Tracking and Data System Support for the Pioneer Project Pioneers VI-IX Extended Missions July 1, 1969-July 1, 1970,* Technical Memorandum 33-426, Vol IX, Jet Propulsion Laboratory, Pasadena, Calif , Aug 15, 1971

Renzetti, N A , and Siegmeth, A J , *Tracking and Data System Support for the Pioneer Project Pioneers 6-9 Extended Missions July 1, 1971-July 1, 1972,* Technical Memorandum 33-426, Vol XI, Jet Propulsion Laboratory, Pasadena, Calif , May 1, 1973

Renzetti, N A , et al , *Tracking and Data System Support for the Mariner Mars 1969 Mission Planning Phase Through Midcourse Maneuver,* Technical Memorandum 33-474, Vol I, Jet Propulsion Laboratory, Pasadena, Calif , May 15, 1971

Renzetti, N A , et al , *Tracking and Data System Support for the Mariner Mars 1969 Mission Midcourse Maneuver Through End of Nominal Mission,* Technical Memorandum 33-474, Vol II, Jet Propulsion Laboratory, Pasadena, Calif , Sept 1, 1971

Renzetti, N A , Linnes, K W , and Taylor, T M , *Tracking and Data System Support for the Mariner Mars 1969 Mission Extended Operations Mission,* Technical Memorandum 33-474, Vol III, Jet Propulsion Laboratory, Pasadena, Calif , Sept 15, 1971

Renzetti, N A , *A History of the Deep Space Network From Inception to January 1, 1969,* Technical Report 32-1533, Vol I, Jet Propulsion Laboratory, Pasadena, Calif , Sept 1, 1971

Renzetti, N A , "Radio Communications at Planetary Distances," paper presented at the International Convention on Radio Communication, Rome and Bologna, Italy, Mar 1974

Rusch, W V T , *Applications of Two-Dimensional Integral-Equation Theory to Reflector-Antenna Analysis,* Technical Memorandum 33-478, Jet Propulsion Laboratory, Pasadena, Calif , May 1, 1971

Rusch, W V T , "Double Aperture Blocking by Two Wavelength-Sized Feed-Support Struts," *Electron Lett ,* Vol 10, No 15, pp 296-297, July 25, 1974

Siegmeth, A J , Purdue, R E , and Ryan, R E , *Tracking and Data System Support for the Pioneer Project Pioneers 6-9 Extended Missions July 1, 1970-July 1, 1971,* Technical Memorandum 33-426, Vol X, Jet Propulsion Laboratory, Pasadena, Calif , Aug 15, 1972

Siegmeth, A J, et al, *Tracking and Data System Support for the Pioneer Project Pioneer 10–Prelaunch Planning Through Second Trajectory Correction December 4, 1969 to April 1, 1972,* Technical Memorandum 33-584, Vol I, Jet Propulsion Laboratory, Pasadena, Calif, Apr 1, 1973

Simon, M K, "Nonlinear Analysis of an Absolute Value Type of an Early-Late Gate Bit Synchronizer," *IEEE Trans Commun Technol*, Vol COM-18, No 5, pp 589-596, Oct 1970

Simon, M K, "Optimization of the Performance of a Digital-Data-Transition Tracking Loop," *IEEE Trans Commun Technol*, Vol COM-18, No 5, pp 686-689, Oct 1970

Simon, M K, and Lindsey, W C, "Data-Aided Carrier Tracking Loops," *IEEE Trans Commun Technol*, Vol COM-19, No 2, pp 157-168, Apr 1971

Simon, M K, "On the Selection of an Optimum Design Point for Phase-Coherent Receivers Employing Bandpass Limiters," *IEEE Trans Commun*, Vol COM-20, No 2, pp 210-214, Apr 1972

Simon, M K, "On the Selection of a Sampling Filter Bandwidth for a Digital Data Detector," *IEEE Trans Commun*, Vol COM-20, No 3, pp 438-441, June 1972

Simon, M K, and Springett, J C, "The Performance of a Noncoherent FSK Receiver Preceded by a Bandpass Limiter," *IEEE Trans Commun*, Vol COM-20, No 6, pp 1128-1136, Dec 1972

Simon, M K, and Springett, J C, *The Theory, Design, and Operation of the Suppressed Carrier Data-Aided Tracking Receiver,* Technical Report 32-1583, Jet Propulsion Laboratory, Pasadena, Calif, June 15, 1973

Simon, M K, and Smith, J G, "Hexagonal Multiple Phase-and-Amplitude-Shift-Keyed Signal Sets," *IEEE Trans Commun*, Vol COM-21, No 10, pp 1108-1115, Oct 1973

Simon, M K, and Smith, J G, "Carrier Synchronization and Detection of QASK Signal Sets," *IEEE Trans Commun*, Vol COM-22, No 2, pp 98-106, Feb 1974

Simon, M K, *Data-Derived Symbol Synchronization of MASK and QASK Signals,* Technical Memorandum 33-720 Jet Propulsion Laboratory, Pasadena, Calif, Dec 15, 1974

Simon, M K, "A Generalization of Minimum-Shift-Keying (MSK) Type Signaling Based Upon Input Data Symbol Pulse Shaping," *IEEE Trans Commun*, Vol COM-24, No 8, pp 845-856, Aug 1976

Simon, M K, "An MSK Approach to Offset QASK," *IEEE Trans Commun*, Vol COM-24, No 8, pp 921-923, Aug 1976

Simon, M K, "The False Lock Performance of Costas Loops with Hard-Limited In-Phase Channel," *IEEE Trans Commun*, Vol COM-26, No 1, pp 23-34, Jan 1978

Simon, M K, "On the Calculation of Squaring Loss in Costas Loops with Arbitrary Arm Filters," *IEEE Trans Commun*, Vol COM-26, No 1, pp 179-184, Jan 1978

Simon, M K, "Tracking Performance of Costas Loops With Hard-Limited In-Phase Channel," *IEEE Trans Commun*, Vol COM-26, No 4, pp 420-432, Apr 1978

Sjogren, W L, "Lunar Gravity Estimate Independent Confirmation," *J Geophys Res*, Vol 76, No 29, Oct 10, 1971

Sjogren, W L, et al, "Lunar Gravity via Apollo 14 Doppler Radio Tracking," *Science,* Vol 175, No 4018, pp 165-168, Jan 14, 1972

Sjogren, W L , et al , "Gravity Fields," *IEEE Trans Geosci Electron* , Vol GE-14, No 3, pp 172-183, July 1976

Slade, M A , et al , "Alsep-Quasar Differential VLBI," *The Moon*, Vol 17, pp 133-147, 1977

Slobin, S D , "Beam Switching Cassegrain Feed System and Its Applications to Microwave and Millimeterwave Radioastronomical Observations," *Rev Sci Instr* , Vol 41, No 3, pp 439-443, Mar 1970

Spier, G W , *Design and Implementation of Models for the Double Precision Trajectory Program (DPTRAJ),* Technical Memorandum 33-451, Jet Propulsion Laboratory, Pasadena, Calif , Apr 15, 1971

Springett, J C , and Simon, M K , "An Analysis of the Phase Coherent-Incoherent Output of the Bandpass Limiter," *IEEE Trans Commun Technol* , Vol COM-19, No 1, pp 42-49, Feb 1971

Stelzried, C T , "Precision Microwave Waveguide Loss Calibrations," *IEEE Trans Instrum Measurement,* Vol IM-19, No 1, pp 23-25, Feb 1970

Stelzried, C T , *A Faraday Rotation Measurement of a 13-cm Signal in the Solar Corona,* Technical Report 32-1401, Jet Propulsion Laboratory, Pasadena, Calif , July 15, 1970

Stelzried, C T , et al , "The Quasi-Stationary Coronal Magnetic Field and Electron Density as Determined From a Faraday Rotation Experiment," *Sol Phys* , Vol 14, No 2, pp 440-456, Oct 1970

Stelzried, C T , "Operating Noise-Temperature Calibrations of Low-Noise Receiving Systems," *Microwave J* , Vol 14, No 6, pp 41-46, 48, June 1971

Stelzried, C T , et al , "Transformation of Received Signal Polarization Angle to the Plane of the Ecliptic," *J Spacecraft Rockets,* Vol 9, No 2, pp 69-70, Feb 1972

Tausworthe, R C , "Convergence of Oscillator Spectral Estimators for Counted-Frequency Measurements," *IEEE Trans Commun* , Vol COM-20, No 2, pp 213-217, Apr 1972

Tausworthe, R C , "Simplified Formula for Mean-Slip Time of Phase-Locked Loops With Steady-State Phase Error," *IEEE Trans Commun* , Vol COM-20, No 3, pp 331-337, June 1972

Tausworthe, R C , and Crow, R B , "Improvements in Deep-Space Tracking by Use of Third-Order Loops," *Proceedings of the 1972 International Telemetering Conference, Los Angeles, California, October 10-12, 1972*, pp 577-583

Tausworthe, R C , *Standard Classifications of Software Documentation,* Technical Memorandum 33-756, Jet Propulsion Laboratory, Pasadena, Calif , Jan 15, 1976

Textor, G P Kelly, L B , and Kelly, M , *Tracking and Data System Support for the Mariner Mars 1971 Mission First Trajectory Correction Maneuver Through Orbit Insertion,* Technical Memorandum 33-523, Vol II, Jet Propulsion Laboratory, Pasadena, Calif , June 15, 1972

Thomas, J B , et al , "A Demonstration of an Independent-Station Radio Interferometry System With 4-cm Precision on a 16-km Base Line," *J Geophys Res* , Vol 81, No 5, pp 995-1005, Feb 10, 1976

Timor, U, "Equivalence of Time-Multiplexed and Frequency-Multiplexed Signals in Digital Communications," *IEEE Trans Commun*, Vol COM-20, No 3, pp 435-438, June 1972

Toukdarian, R Z, *Final Engineering Report for Goldstone Operations Support Radar,* Technical Memorandum 33-800, Jet Propulsion Laboratory, Pasadena, Calif, Nov 1, 1976

Truong, T K, and Reed, I S, "Convolutions Over Residue Classes of Quadratic Integers," *IEEE Trans Inform Theor*, Vol IT-22, No 4, pp 468-475, July 1976

Truong, T K, and Reed, I S, "Convolutions over Quartic Integer Residue Classes," *Proceedings of the International Conference on Information Sciences and Systems,* Patras, Greece, Aug 19-24, 1976

Truong, T K, Liu, K Y, and Reed, I S, "Fast Number-Theoretic Transforms for Digital Filtering," *Electron, Lett*, Vol 12, No 24, Nov 1976

Truong, T K, et al, "X-Ray Reconstruction by Finite Field Transforms," *IEEE Trans Nucl Sci*, Vol NS-24, No 1, pp 843-849, Feb 1977

Truong, T K, Golomb, S W, and Reed, I S, "Integer Convolutions Over the Finite Field $GF(3 \cdot 2^n + 1)$," *SIAM J Appl Math*, Vol 32, No 2, pp 356-365, Mar 1977

Truong, T K, Reed, I S, and Liu, K Y, "Fast Algorithm for Computing Complex Number-Theoretic Transforms," *Electron Lett*, Vol 13, No 10, pp 278-280, May 12, 1977

von Roos, O H, Yip, K B W, and Escobal, P R, "A Global Model of the Earth's Ionosphere for Use in Space Applications," *Astronautica Acta,* Vol 18 (Supplement), No 3, pp 215-232, Aug 1974

Weber, W J, III, "Performance of Phase-Locked Loops in the Presence of Fading Communication Channels," *IEEE Trans Commun*, Vol COM-24, No 5, pp 487-499, May 1976

Weber, W J, III, Ackerknecht, W E, and Kollar, F J, *Viking X-Band Telemetry Experiment Final Report,* Technical Memorandum 33-794, Jet Propulsion Laboratory, Pasadena, California, Sept 1, 1976

Wong, J S L, et al, *Review of Finite Fields Applications to Discrete Fourier Transforms and Reed-Solomon Coding,* JPL Publication 77-23, Jet Propulsion Laboratory, Pasadena, Calif, July 15, 1977

Wong, S K, and Reinbold, S J, "Earth-Moon Mass Ratio From Mariner 9 Radio Tracking Data," *Nature,* Vol 241, No 5385, pp 111-112, Jan 12, 1973

Woo, R, and Ishimaru, A, "Remote Sensing of the Turbulence Characteristics of a Planetary Atmosphere by Radio Occultation of a Space Probe," *Radio Sci*, Vol 8, No 2, pp 103-108, Feb 1973

Woo, R et al, *Effects of Turbulence in the Atmosphere of Venus on Pioneer Venus Radio–Phase I,* Technical Memorandum 33-644, Jet Propulsion Laboratory, Pasadena, Calif, June 30, 1973

Woo, R, "Measurements of the Solar Wind Using Spacecraft Radio Scattering Observations," in *Study of Traveling Inter-Planetary Phenomena,* pp 81-100, D Reidel Publishing Co, Dordrecht, Holland/Boston, 1977

Woo, R, "Radial Dependence of Solar Wind Properties Deduced from Helios 1/2 and Pioneer 10/11 Radio Scattering Observations," *Astrophys J*, Vol 219, No 2, Part 1, pp 727-739, Jan 15, 1978

Woo, R T, "Observations of Turbulence in the Atmosphere of Venus Using Mariner 10 Radio Occultation Measurements," *J Atmos Sci*, Vol 32, No 6, pp 1084-1090, June 1975

Yuen, J H, "A Double-Loop Tracking System," *IEEE Trans Commun*, Vol COM-20, No 6, pp 1142-1150, Dec 1972

Yuen, J H, *A Practical Statistical Model for Telecommunications Performance Uncertainty*, Technical Memorandum 33-732, Jet Propulsion Laboratory, Pasadena, Calif, June 15, 1975

End of Document